ADVANCED ENERGY MATERIALS
www.advenergymat.de

# Unveiling the Potential of Covalent Organic Frameworks for Energy Storage: Developments, Challenges, and Future Prospects

*Prashant Dubey, Vishal Shrivastav, Tribani Boruah, Giorgio Zoppellaro, Radek Zbořil, Aristides Bakandritsos,* and Shashank Sundriyal**

**Covalent organic frameworks (COFs) are porous structures emerging as promising electrode materials due to their high structural diversity, controlled and wide pore network, and amenability to chemical modifications. COFs are solely composed of periodically arranged organic molecules, resulting in lightweight materials. Their inherent properties, such as extended surface area and diverse framework topologies, along with their high proclivity to chemical modification, have positioned COFs as sophisticated materials in the realm of electrochemical energy storage (EES). The modular structure of COFs facilitates the integration of key functions such as redox-active moieties, fast charge diffusion channels, composite formation with conductive counterparts, and highly porous network for accommodating charged energy carriers, which can significantly enhance their electrochemical performance. However, ascribing intricate porosity and redox-active functionalities to a single COF structure, while maintaining long-term electrochemical stability, is challenging. Efforts to overcome these hurdles embrace strategies such as the implementation of reversible linkages for structural flexibility, stimuli-responsive functionalities, and incorporating chemical groups to promote the formation of COF heterostructures. This review focuses on the recent progress of COFs in EES devices, such as batteries and supercapacitors, through a meticulous exploration of the latest strategies aimed at optimizing COFs as advanced electrodes in future EES technologies.**

## 1. Introduction

In recent years, highly porous organic polymers like hypercross-linked polymers (HCPs), porous aromatic frameworks (PAF), and conjugated microporous polymers (CMPs) have garnered profound attention as candidates in miscellaneous applications due to their unique features, such as tailored architecture, low density, and periodic porous network. Covalent organic frameworks (COFs) are such an emerging class of porous organic materials offering a wealth of benefits and have attracted substantial attention. COFs exhibit extended $\pi$-conjugated regions that are either stacked in-plane or perpendicularly, a large number of accessible sites for catalysis, sensing or electrochemical energy storage (EES), high structural diversity, intermolecular interactions, chemical functionalities within size-tailored cavities, and, importantly, a lightweight nature due to their low density.[1–5] Unlike the traditional crystalline porous solids such as zeolites

P. Dubey
Advanced Carbon Products and Metrology Department
CSIR-National Physical Laboratory (CSIR-NPL)
New Delhi 110012, India

V. Shrivastav
Institute of Physical Chemistry
Polish Academy of Sciences
Kasprzaka 44/52, Warsaw 01–224, Poland

The ORCID identification number(s) for the author(s) of this article can be found under https://doi.org/10.1002/aenm.202400521



**DOI: 10.1002/aenm.202400521**

T. Boruah
School of Chemistry
Cardiff University
Translational Research Hub, Maindy Road, Cathays, Cymru/Wales, Cardiff CF24 4HQ, UK

G. Zoppellaro, R. Zbořil, A. Bakandritsos, S. Sundriyal
Regional Center of Advanced Technologies and Materials
The Czech Advanced Technology and Research Institute (CATRIN)
Palacký University Olomouc
Šlechtitelů 27, Olomouc 779 00, Czech Republic
E-mail: a.bakandritsos@upol.cz; shashank.sundriyal@upol.cz

G. Zoppellaro, R. Zbořil, A. Bakandritsos
CEET
Nanotechnology Centre
VŠB—Technical University of Ostrava
17. listopadu 2172/15, Ostrava, Poruba 708 00, Czech Republic

and metal-organic frameworks (MOFs), COFs are purely organic structures, granting them several distinct advantages: 1) highly modular structure owing to the diverse organic chemistry, allowing for structure-property relationships tuning and thus higher efficiency in certain applications; 2) enhanced stability compared to MOF since the latter are often susceptible to degradation due to the labile coordination bonds, while COFs can be synthesized to remain stable under variable conditions and are typically more robust; 3) cost-effectiveness, owing to their straightforward synthesis and use of inexpensive precursors; 4) non-toxic and environment-friendly nature due to absence of metal ions.[6,7]

The synthesis of COFs can be traced back to 2005 when Yaghi et al. developed new organic frameworks by covalently linking organic molecules to form 2D extended structures, termed as COF-1 and COF-5.[4] These COFs were based on boronate ester linkages and provided a fundamentally new way of constructing ordered, crystalline, and porous organic materials from molecular building blocks using strong covalent bonds. The boronate ester linkages, used to construct the frameworks, are reversible under certain conditions, and thus were essential for facilitating error-correction mechanisms during the self-assembly process and achieving crystalline materials. The primary building elements of COFs are organic monomers composed of light atoms (C, H, O, N, Si, B). Commonly used organic reactive linkers include, apart from boronate esters are boronate anhydrides, hydrazines, imines, and nitriles, which react via cyclotrimerization.[8] The intriguing properties of COFs, including the high structural control, the micro and mesopores, the wide availability and variability of functional groups, and the possibility for tailored chemical modifications to tune spins, photoexcited energy carriers (excitons, polarons) have rendered them as highly attractive materials for numerous applications. The intricate and tunable structural and physicochemical suite of compelling properties of COFs underscore their potential across diverse applications in a broad spectrum of disciplines, spanning from sensing,[9,10] environmental remediation,[11,12] separation,[13] and EES[14–16] to advanced domains of photo-/electrocatalysis,[17] spintronics,[18] optoelectronics,[19] and biomedicine.[20]

COFs are emerging promising candidates as active materials in EES owing to their unique features arising by their framework which is rich in ordered in-plane or stacked $\pi$-conjugated motifs, stabilized by the organic linkers.[21] The key features rendering COFs attractive systems in EES embrace: a) the inherent and uniform porous architecture with ordered alignment, which provides a large specific surface area (SSA) and facilitates rapid ion transport pathways; b) the abundance of charge storage sites, such as pores and redox moieties; c) the enhanced mobility of the charge carriers is particularly promoted by the aromatic conjugated network, and ionic sites residing in side-functionalities of the linkers. The rich chemistry of COFs allows for precise tuning at the molecular level, enabling selective incorporation of various functional groups to enhance electroactive sites and optimize the charge storage process;[22–25] d) The high strength of the covalent bonds within COFs contributes to superior structural integrity, enabling them to withstand volume changes and structural deformation brought on by ion intercalation/deintercalation during cycling process; e) COFs predominantly consist of lightweight elements like C, N, and O, which may offer higher gravimetric capacitance compared to electrode materials that contain metals. These structural and functional features are crucial parameters for tailoring the properties of COFs, including charge storage capacity, electrochemical stability, and rate capability.[26,27] Therefore, COFs have generated extensive attention within the EES domain.

This review gives an insight on the latest advances in the growing domain of COF materials, the pivotal role of their architectural design, synthesis methods and the underlying physical and chemical properties. A notable aspect of this review lies in the exploration of the diverse structures exhibited by COFs, achieved through the utilization of distinct building blocks with varying symmetries, while also delving into the advantages and drawbacks associated with different synthesis approaches. Furthermore, this review sheds light on the recent progress of COFs in the EES landscape encompassing metal ion batteries, supercapacitors, and metal ion capacitors. Their role as hosts for post-lithium chemistries, as redox-active electrodes, solid-state ion conductors, polysulfide shuttling inhibitors, and electrode separators is also highlighted. Ultimately, this work concludes by addressing the existing challenges and promising future research directions in this emerging field. **Figure 1** shows the structural properties of COFs that are directly associated with the electrochemical properties targeting the EES applications.

## 2. Timeline of Advancements in the Field of COFs

During the 20th century, the remarkable improvements in our understanding of covalent bonding in organic molecules led to a shift from an empirical approach toward a more rational design of organic molecules. Thus, the synthesis of COF materials has evolved substantially during the past 20 years, with multiple noteworthy turning points (**Figure 2**).[28,29] With the successful synthesis of the first COF structure, known as COF-1, and the visionary work of Yaghi and his coworkers, a new era emerged.[4] Following this breakthrough, the research in this field witnessed the birth of an exciting family of previously unexplored materials with an extraordinary opportunity of structural diversity and modulation. The groundbreaking structure of COF-1, based on benzene rings connected by atoms of boron and oxygen, laid the groundwork for further developments. By 2007, scientists showcased a wide range of COF structures through the use of different organic building blocks, demonstrating the growth possibilities of the COF family.[30] The field evolved as a result of these advancements, unlocking a wide range of organic framework architectures. The synthesis of imine-linked COFs, such as COF-5, was accomplished in 2009 by Furukawa et al. These compounds demonstrated improved stability and promising properties for use in gas storage and separation.[31] In 2011, a milestone discovery signaled a change in the field of COFs related to the synthesis of covalent triazine frameworks (CTFs).[32] COFs based on CTFs captured the attention of scientists with their outstanding thermal stability and broad potential in fields like gas storage/capture, and catalysis.[33–36] The COF landscape evolved further by the synthesis of extended $\pi$-conjugated COFs in 2013 by Yaghi et al., which introduced interesting new applications in optoelectronics and sensing.[37] Novel device designs and sensing platforms were made possible by the remarkable electrical characteristics demonstrated by these COFs with extended $\pi$-conjugated areas. The effective synthesis of dynamic

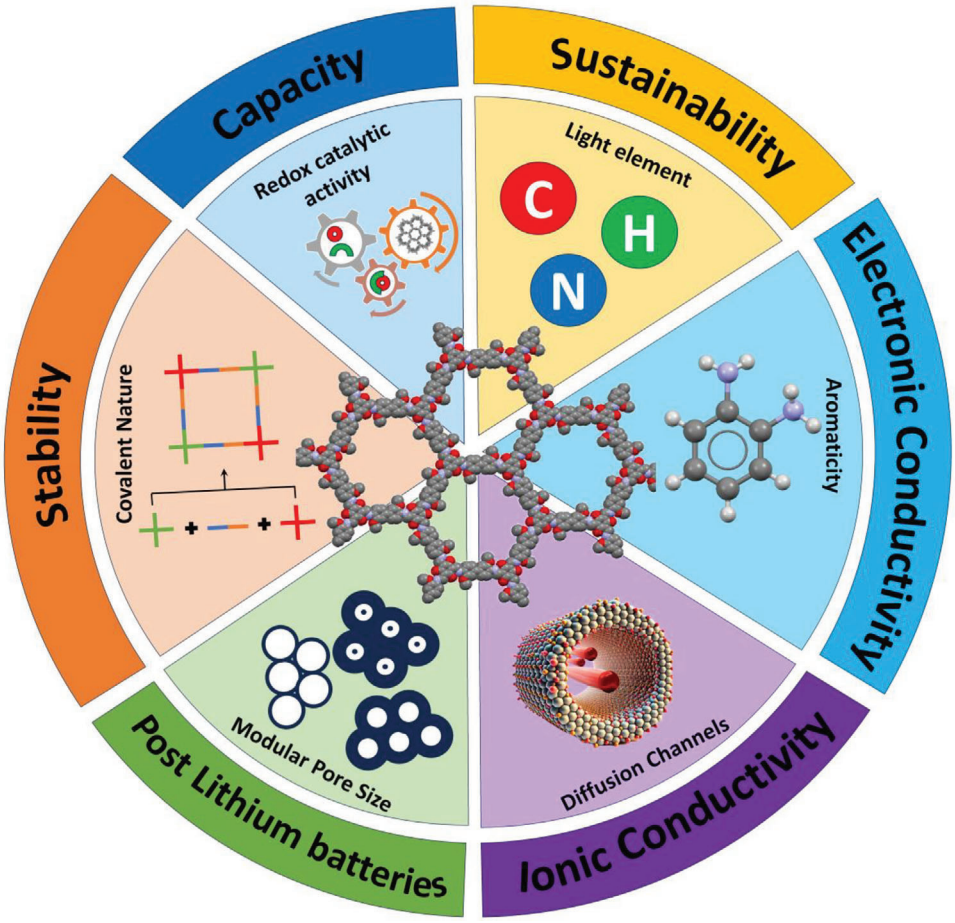


**Figure 1.** The distinct properties of COFs associated with the corresponding structural and physical properties targeting the EES applications.

COFs, which are capable of reversible structural alterations, was another achievement in 2016. By creating novel materials that respond to stimuli, these adaptive COFs enabled the creation of tunable frameworks.[38–40] Synthesizing COF single crystals and thin films with regulated and extended crystallinity and orientation in 2018 was another milestone.[41,42] Following a two-step process, nanoscale seeds of boronate ester-linked 2D COFs were grown into micrometer-scale single crystals by using a solvent that suppresses the nucleation of additional nanoparticles, which otherwise mainly lead to amorphous powders. The extended crystalline solids displayed superior charge transport compared with that observed in conventional powders. This discovery increased the potential applications of COFs across a range of industries by making it easier to incorporate them into electrical devices and

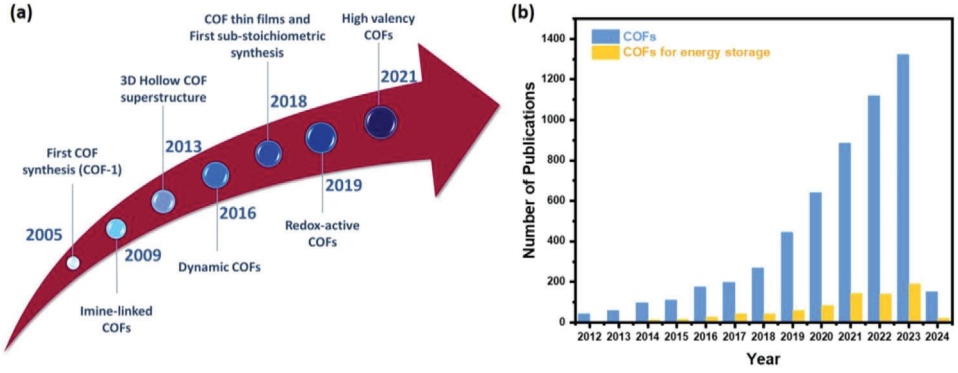


**Figure 2.** a) Timeline of the advancements in the COFs field; b) Number of publications investigating research on COFs in the last 12 years, as of Feb 2024 (as per Web of Science).

membranes. In 2018, free aldehyde synthesis of COF has been reported to lead to the opening of sub-stoichiometric synthesis capable of yielding either free amine or free aldehyde groups in imine-linked COFs.[43] Coupled with opportunities for functionalization, such as post-synthetic modification of frustrated groups, this method has facilitated the utilization of these networks in water harvesting, gas adsorption, and separation, as well as in various applications of photocatalysis.[44] Furthermore, the sub-stoichiometric approach was another recent development in COFs chemistry which typically results in unconventional topologies with free and active functional groups within the pores of these materials that are not present in the case of COFs with fully linked network nodes.[45] The production of redox-active COFs in 2019 which have the ability to store and release charge introduced new prospects for electrochemical and energy storage uses. Their applicability in sustainable energy technologies has been successfully demonstrated by these redox-active COFs.[25,46–48] A significant advancement in COF synthesis was achieved in 2021 when high-valency COF structures were successfully synthesized with extended connectivity of the building units.[49] These structures, based on multivalent polycubane linkers expanded the possible topologies for COFs by surpassing the previous valency limits of 3 and 4, dictated by the reliance on the $sp^2$ and $sp^3$ hybridization of carbon chemistry. This created new possibilities for applications in fields including drug delivery, sensing, and catalysis by providing enormous surface areas and customizable architectures.

## 3. Engineering Aspects Governing the Design of COF-Driven Electrode Materials

### 3.1. Architectural Design Strategies

Generally, the morphology, dimensions, and configuration play a critical role in determining the structure of COFs. Utilizing topological diagrams, one can effectively predict the growth mechanism of COFs.[8] The core growth of the COF is depicted in the topological schematic of **Figure 3a**, which indicates the sequential formation of covalent links within the propagating polymer chain. For the directional control of bond formation, the monomers—or foundational building blocks—are engineered with rigid backbones. These backbones include reactive functional units in a geometrically predefined arrangement, facilitating the precision construction of the COF architecture. The assembly of planar monomers culminates in a well-defined polymeric architecture, terminating at a specific juncture to yield 2D atomic layers, each exhibiting distinct topologies.[50–55] These 2D layered structures are marked by an alignment of $\pi$-conjugated blocks affixed onto the atomic planes, predominantly arising through $\pi$–$\pi$ stacking interactions.[7] In such an arrangement, interlayer non-covalent interactions promote structural stability, whereas the robust intra-layer covalent bonds secure the framework's integrity.

COFs exhibit significant advantages connected to their diverse skeleton designs and rich porous networks, which give rise to a great variety of COF architectural motifs, including, but not limited to, imine-linked COFs, hydrazone-linked COFs, and keto–enol-linked COFs.[56,57] Primarily, ordered 1D channels are created by the covalent assembly of 2D COFs, which are 2D polymers in the x and y directions that stretch and aggregate in the *z*-direction. The interlayer interactions in these 2D polymers eventually lead to the formation of a layered structure[51,58]. The intrinsic growth mechanism of COFs facilitates their uniform propagation in a specified direction, contributing to the high crystallinity and lattice precision often observed in these materials. Due to the layered configuration, each monomeric unit is superimposed over two adjacent monomeric units, further promoting the overall stability and dictating the orientation of neighboring layers.

Conversely, the construction of 3D COFs involves the multidirectional extension of the polymeric backbone, leveraging a synthesis strategy that combines chain folding with layer-overlapping methodologies. This expansion is not merely spatial but also functional, providing these materials with a dimensional versatility that enables their application in a broad field of technological frontiers. This functional adaptability confers upon these materials a dimensional versatility that is pivotal for their integration into a wide spectrum of technological applications, from gas storage and separation to catalysis, sensing, and drug delivery.[59–63]

### 3.2. Structural Diversification: Building Units

The topology diagram serves as the blueprint for engineering intricate frameworks within 2D or 3D COFs. These frameworks consist of interconnected lattices formed by assembling building block units, resulting in periodically arranged knots and linkers. The strategic selection of aromatic monomers, known for their versatile geometries, allows for the topologically guided synthesis of COFs. In this context, it is crucial to identify the symmetry components, particularly the rotational symmetry associated with the relevant monomers. This can be achieved by determining the rotational axes of the monomers.

Aromatic rings, recognized for their rigid structures, are favored as the fundamental units for supporting well-ordered growth pathways within both 2D and 3D architectures. To leverage the inherent order dictated by the topology and to maintain the planarity of extended COF structures, the integration of rigid building blocks is a common strategy in COF construction. Their rigidity is conducive to the formation of coordination bonds, guiding the linear and planar extension of the COF backbone in a spatially organized manner. Various building blocks, including but not limited to extended $\pi$-conjugated systems, macrocyclic structures, and nitrogen or sulfur-rich components, have been synthesized enriching the toolkit for structural and functional control. According to the topological map, these COFs exhibit an extensive array of skeletal topologies and pore configurations.

The diversity of 3D COFs heavily relies on the choice of monomeric units, which not only dictates the framework's topology but also its functionality. Despite the constraints imposed by the pursuit of Td-symmetry or orthogonal termini, these units offer a valuable pool for structural variation. The backbone of COFs can adopt an array of configurations, ranging from basic geometries from benzene and heterocyclic motifs to macrocycles like octahedra, as well as different configurations such as C2, C3, C4, and Td. Moreover, monomeric units extend beyond their role in shaping the COF structure; they also

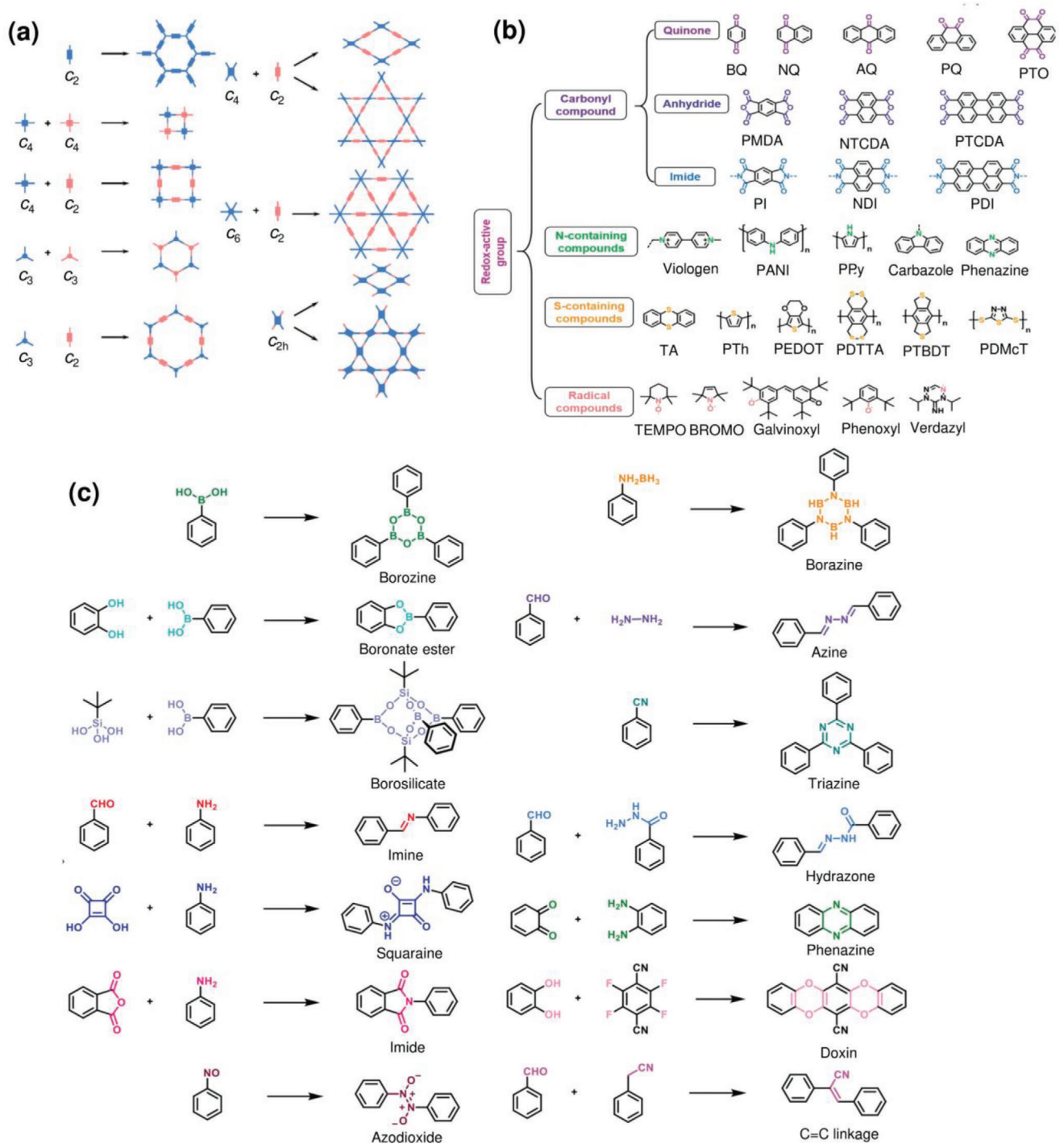


**Figure 3.** a) Topology diagram of COFs with different structures and building blocks, b) redox-active groups used in COFs, and c) Different linkers and bond formation leading to COF synthesis. Reproduced with permission.[25] Copyright 2021, John Wiley & Sons.

endow the framework with a plethora of additional features. These features encompass the provision of docking sites for guest molecules, the introduction of active sites for catalysis, the creation of chiral centers for enantioselective applications, and the integration of photosensitive elements for energy and sensing applications.

### *3.2.1. COFs in the 2D Architectural Domain*

The domain of 2D COFs is distinguished by a wide range of architectural configurations. These structures can be engineered to exhibit both isotropic and anisotropic polygonal skeletons, with each configuration dependent on a carefully chosen array of

linkers and building blocks. Typically, each design relies on a significant number of linkers and construction blocks. By employing diverse monomer geometries within the topological framework, various skeletal and pore configurations can be achieved, resulting in distinct 2D frameworks with diverse arrangements of pores and skeletons (Figure 3a,b).[24,50,52,64–66]

For instance, COF engineering can involve the utilization of C2, C3, C4, and C6 symmetric linkers as the knots for fabricating 2D COFs with rhombic, trigonal, tetragonal, hexagonal, and kagome geometries. By linking C2-symmetric units to other C2 or C3-symmetric counterparts as knots, in combinations such as [C3 + C3], [C2 + C2 + C2], and [C3 + C2], hexagonal two-dimensional COFs with distinct pore size distributions, arrangements, and spacing between pores can be synthesized. Conversely, tetragonal COFs, characterized by four-sided geometries, can be synthesized using [C4 + C2] and [C4 + C4] linkages.[67–72] Additionally, the synthesis of triangular and rhombic crystal lattices, featuring dual pore networks and symmetric termini, is achievable.[73] In comparison to other C2-symmetric knots that form rhombic polygons, the use of C2-symmetrical knots with larger aromatic systems and the incorporation of C3-symmetric macrocycles can facilitate strong interactions, often leading to the formation of kagome-type geometries. For example, the use of C3-symmetric macrocyclic can produce kagome COF with six triangular apertures on the periphery, and a dodecagonal aperture in the center (Figure 1a). However, the final morphology of a single COF crystal can be influenced by factors such as the dimensions and strength of the inter-layer interfaces, as well as the overall bulkiness and steric effects of the knot unit.[74,75]

#### *3.2.2. COFs in the 3D Architectural Domain*

The design of 3D COFs requires at least one building unit with tetrahedral or orthogonal geometry. These fundamental geometries are pivotal as they enable the polymer chains to propagate into an extensive covalently bonded 3D network (Figure 3b). Furthermore, by integrating tetrahedral or orthogonal nodes, 3D COFs can be architecture to allow the twisting and interlacing of polymer chains in multiple dimensions, culminating in the formation of intricate 3D skeletal structures and porosity (Figure 3b).[51,66,76–78] For example, the combination of Td + C3 symmetries can produce skeletal networks with dramatically improved surface areas.[79–81] Conversely, the interplay between Td and C2 symmetries can yield [Td + C2] and [Td + Td] layouts, which offer a diverse range of 3D COF structures due to the inclusion of linker units possessing C2 symmetry.[82–84] In these cases, tailored configurations of polymer backbones and the strategic interlacing of polymer chains are harnessed to engineer one-dimensional channels. These channels typically exhibit pore diameters ranging from 0.7 to 1.5 nm, classifying them within the microporous regime. The [Td + C2] and [Td + C4] layouts are employed to construct appropriate network nodes resulting in two-fold interpenetrated 3D COFs (using two C2- or C4-symmetric units with four reactive sites).[77,85,86] For example, 3D COF-505 illustrates a helical structure that integrates an orthogonal Cu(II) complex with phenanthroline moieties acting as the knot, interconnected by C2-symmetrical linkers.[76]

Despite the advancements in 3D COF design, the current topological models cannot precisely predict the fold multiplicity or control the folding patterns within a given COF, rendering predesigned and synthetically programmable 3D COFs a rarity. Consequently, regulating the ultimate properties of COFs by anticipating the degree of interpenetration and folding patterns remains a formidable challenge. Nevertheless, these complexities present a fertile ground for innovation, particularly at the nexus of computational design and artificial intelligence.

### 3.3. Diversification of Linkage

In the realm of COFs, the diversification of linkage groups plays a pivotal role in dictating their structural and functional attributes. Predominantly accessible linkage groups include boroxine, boronate-ester, borosilicate, imine, hydrazone, borazine, squaraine, azine, phenazine, and imide, with C═C, azine, hydrazone, boronate-ester, imine, and boroxine (Figure 3c) being the most frequently employed.[87,88] These linkages are central to the synthesis of COFs, often leveraging reversible covalent bonds to impart distinct properties, such as high crystallinity via dynamic covalent chemistry.[89] For example, pre-organizing monomers using a reversible and removable covalent linkage. This method produced highly crystalline imine COFs with increased porosity, ascribing to the obtained COF superior charge carrier transport, and photocatalytic hydrogen evolution. The synthesis of COFs substantially relies on the solvent medium, typically a combination of polar and nonpolar solvents. Strategic choice of solvents and combinations facilitates the manipulation of solubility parameters, crucial for enabling optimal conditions for bond formation. Moreover, the thermodynamics of the synthesis is influenced by several key factors: the nature of solvent interactions, the presence and type of catalysts, solvent effects on catalytic organic bond formation, the reaction temperature, and the duration of the synthesis. Each of these elements plays a vital role in steering the reaction towards the desired product. Furthermore, the ability to fine-tune the synthesis conditions allows control over additional aspects, since by adjusting the combination and ratios of the linkages, COFs' crystallinity, porosity, and overall composition can be tailored. This versatility in synthesis underscores the potential of COFs as modular materials with attractive functionalities and applications in diverse scientific fields.

## 4. Synthesis Methods for COFs

A multitude of synthesis methods have been developed for the creation of COFs, including solvothermal, microwave, mechanochemical, and room temperature approaches, among others[90] (**Figure 4**). It is crucial to understand the influence of the synthesis method on the physical and chemical properties of COFs, as this knowledge is essential for tailoring the qualities of COFs for specific applications. For example, the synthesis of COFs relies on the dynamic covalent chemistry (DCC) approach, because it is well known to produce extremely crystalline and thermally stable structures.[8] The porous nature of COFs arises from their organic chemical constituents, enabling the precise integration of organic building components, enables the precise

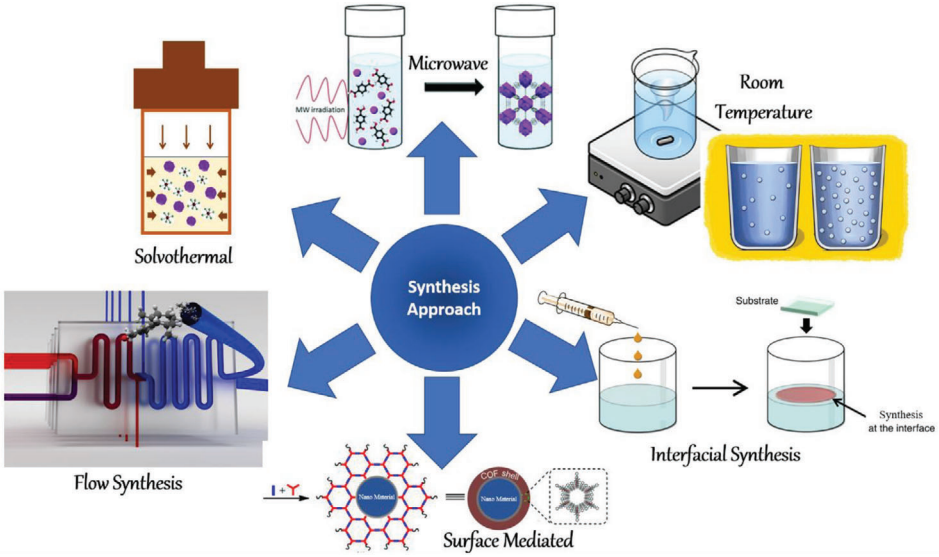


**Figure 4.** Different approaches for the synthesis of COFs (solvothermal and microwave, reproduced with permission,[115] Copyright, 2015, Royal Society of Chemistry; room temperature, and interfacial synthesis, reproduced with permission,[116] Copyright 2015, Springer Nature; surface mediated, reproduced with permission,[117] Copyright 2017, Royal Society of Chemistry; and flow synthesis, reproduced with permission,[118] Copyright 2015, John Wiley & Sons).

integration of organic building components, which is essential for optimizing their performance in energy storage devices. In 2005, Yaghi and his team successfully synthesized the first COF by molecular dehydration of 1,4-benzene diboronic acid.[4] Since then, extensive research has been conducted to explore novel methods of COF synthesis. COFs of diverse morphologies, including sheet, fibrous, petal, and spherical COFs, as well as intricate topologies, such as rhombic and hexagonal, quadrangular, and trihexagonal COFs, can be produced using a wide range of organic monomers and functional groups.[91,92] Various synthesis techniques can be employed to combine such 2D and 3D topological COFs, often modified with side functional groups.[93] In addition, the well-organized or crystalline structure of COFs can be pre-designed by adjusting the proportions of constituent molecules and linkages, altering reaction conditions, or selecting alternative monomers as organic building blocks. The architecture, size, and porosity of COFs can be further adjusted by modifying the molecular geometry and concentration of the building blocks. Different synthesis methods offer unique opportunities to control the morphology, structure, and properties of COFs to meet the material requirements for energy storage applications. In terms of material requirements for energy storage applications, synthesized COFs should possess specific characteristics such as i) high surface area to provide ample active sites for charge storage, ii) porosity and crystallinity for efficient electrolyte penetration and ion diffusion, iii) stability to withstand the electrochemical stresses encountered during charge-discharge cycles, iv) conductivity to facilitate electron transport within the material, and v) tunable morphology and structure to optimize performance for different types of energy storage devices (e.g., capacitors, batteries).

For instance, the solvothermal method allows for the precise control of reaction conditions, resulting in highly crystalline COFs with well-defined structures. These COFs typically possess high surface areas and tailored pore structures, making them suitable for applications requiring efficient electrolyte penetration and ion.[30,94,95] On the other hand, microwave-assisted synthesis offers advantages in terms of efficiency and speed, which can be beneficial for scaling up the production of COF materials for energy storage devices. However, keeping high crystallinity is one of the major concerns in the microwave synthesis method which is critical for the effective exploitation of the porous network to attain the fast insertion/de-insertion of ions. Regarding this, Cooper et al. discovered that adding a catalyst during microwave synthesis could improve the crystallinity of the product.[96] In the general microwave synthesis of covalent triazine frameworks (CTF), $CF_3SO_3H$ was used as a catalyst which drastically improved the crystallinity. The efficiency and speed of microwave synthesis can be advantageous for scaling up the production of COF materials for commercial applications. The mechanochemical synthesis approach allows for the synthesis of COFs under ambient conditions, offering simplicity, scalability, and environmental friendliness by omitting harmful organic solvents.[97] The mechanism underlying mechanochemical organic synthesis is still not fully understood, although it is hypothesized that the formation of low-melting eutectic intermediate phases may facilitate covalent bond formation during the process.[98] The main downside of the mechanochemical synthesis is the very low SSA and crystallinity of the COF than that of other methods (70-100 $m^2\ g^{-1}$).[99,100] However it has been reported that mechanochemical synthesis could exfoliate the COF layers down to 10–30 layers, improving the ionic conductivity.[101] Moreover, mechanochemical synthesis methods conducted at room temperature provide mild conditions for COF formation, potentially leading to the production of COFs with enhanced stability. The ionothermal synthesis can produce highly crystalline COFs, but this method is mainly suitable for some CTFs.[102] By tailoring the synthesis method and conditions,

research endeavors aim to control the properties of COFs to meet the requirements in terms of structural features and physicochemical properties which are appropriate for enhancing their performance in energy storage applications. Additionally, ongoing research into novel synthesis techniques and functionalization strategies are anticipated to further expand the range of COF materials available for energy storage technologies.

### 4.1. Solvothermal Synthesis

The synthesis of COFs has predominantly relied on the solvothermal synthesis method,[103] a technique that involves high-temperature and high-pressure reactions between the monomers dissolved in a solvent (typically non-aqueous), in a sealed environment.[104,105] This method, pivotal in COF production, is instrumental in determining the resultant COF's structural, physical, and chemical attributes. Typically, the monomer dissolved in a solvent is contained in a pyrex tube for a specific amount of time at a specific temperature to produce the COF product as a precipitate.[106] Key parameters such as reaction temperature, duration, pressure, and solvent choice significantly influence the structure, and thus the physical and chemical properties of the resulting COFs. Most COFs can be synthesized within a temperature range of 85–120 °C, depending on the reactivity of the organic monomers.[107] However, certain COFs, utilizing Schiff-base chemistry, require higher temperatures and longer reaction times, spanning from two to nine days.[3] Generally, in most synthesis methods for COFs, a minimum of three days is required for the completion of reactions and obtaining the product with a high yield.[95,108,109] For the production of thin films, the general experimental procedure involves immersing the appropriate substrate in the solvothermal reaction mixture.

Han et al. used solvothermal processes to synthesize novel imine-linked chiral COFs, and used them for the separation of racemic alcohols.[110] However, the presence of a catalyst (acetic acid) led to the formation of amorphous polyimine sediments, thereby impeding the growth and nucleation of COFs. To bypass this, recently, Zhao et al. proposed a modified synthetic method for producing imine-linked COFs, utilizing the *tert*-butyloxycarbonyl (Boc) as a protective agent for the amine group to prevent the formation of amorphous polyimine.[111] Similarly in another report, Wang et al. reported the synthesis of COF-LZU1 using a solvothermal method by submerging a substrate into a reaction mixture containing an amine-protecting compound, 4-(tert-butoxy-carbonyl amino)-aniline (NBDPA).[112] The resulting thin films exhibited aligned structure and consistent thickness, composed of highly homogeneous protonated COF crystals interconnected by imine groups. Characterization of the produced COF thin films with the highly aligned structure showed a consistent thickness of 190 nm, which could be tailored by varying the monomers concentrations in the reaction mixture, the solvents, and the immersion duration. These studies demonstrated that this technique is quite effective for growing COFs with high crystallinity and orientation. Additionally, solvothermal methods were employed to synthesize a highly porous COF (TpPa-1) and its application as hydrophilic material for N-linked glycopeptides enrichment.[113] Additionally, COF-5 was produced by polymerizing 2,3,6,7,10,11-hexahydroxytriphenylene (HHTP) and 1,4-phenylenebis (boronic acid) (PBBA) in a pyrex capillary tube using dioxane and mesitylene as a solvent.[114] The reaction mixture was heated for 72 h at 100 °C to produce the COF as a powder.

Recent studies have demonstrated the significant influence on the development of COFs of suitable growth substrates with good adhesive properties. One promising candidate for facilitating COF growth is single-layered graphene (SLG), known for its intriguing photoelectric properties. SLG can serve as an effective interface between COF and other substrates, improving the growth quality. Notably, Colson et al. achieved highly oriented COF growth over SLG and observed further enhancement of the orientation when using substrates such as Cu, SiC, and $SiO_2$.[119,120] Specifically, the solvothermal condensation of 2,3,6,7,10,11-hexahydroxytriphenylene (HHTP) and phenylene bis(boronic acid) (PBBA) at 90 °C in a solution of mesitylene and dioxane over SLG/Cu substrate was used to grow COF-5. The produced COF-5 film exhibited hexagonal lattice grains parallel to the SLG. When SLG was used as a thin coating for other substrates, such as transparent fused $SiO_2$, the substrate still significantly impacts the quality of thin films, affecting parameters such as thickness and uniformity. Thicker films were produced on the SLG/Cu substrate compared to the SLG/$SiO_2$ substrate, although the growth reaction was performed for the same time. Using the SLG/Cu substrate, thin films ranging from 30–37 nm of HHTP-DPB COF and a series of Zn phthalocyanine (ZnPc) COFs were successfully grown.

In an interesting report, Medina et al. demonstrated that $\pi$–$\pi$ interactions within the COF material are not necessary for the formation of oriented COF thin films over substrates.[121] A thiophene-based BDT-COF was successfully produced over an indium-doped tin oxide (ITO) and NiO/ITO coated glass substrates, with a thickness of 150 nm, and a highly crystalline nature, as demonstrated from the high-intensity diffraction peaks in XRD. Analysis of the diffractogram verified that the obtained COF thin film structure corresponded to a hexagonal unit cell with a lattice constant of a = b = 36.9Å. This study confirmed that COF thin films can be produced on polycrystalline inorganic substrates (such as glass covered with NiO/ITO) without compromising the film quality. Ding et al. validated this finding by producing a TTF-COF over a Si/$SiO_2$ substrate and ITO-coated glass employing the solvothermal synthesis method.[122]

In addition to the other factors, the chemical stability of COFs, especially in water and acidic environments, remains a critical consideration, particularly for energy storage applications. Previous studies have demonstrated that COFs linked by b-ketoenamine bonds exhibit high stability in aqueous and acidic environments.[123] By leveraging these findings, DeBlase et al. disclosed a modified solvothermal synthesis for the production of a COF based on ketoenamine-linked anthraquinones (DAAQ–TFP COF).[124] Instead of immersing the substrate in the reaction mixture, they achieved the formation of a disordered thin film with a thickness of 300–400 nm by adding triformylphloroglucinol (TFP) to a solution of 2,6-diaminoanthraquinone (DAAQ), which was prior deposited on an Au substrate. The starting concentration of the reaction monomers was varied to achieve control over the film's thickness. The b-ketoenamine COF (DAB-TFP COF) thin films were also successfully produced using various substrates (indium tin oxide, fluorine-doped tin oxide, silicon,

and platinum). This COF, synthesized through the condensation of p-phenylenediamine (DAB) with 1,3,5-triformylphlorogluciol (TFP), was grown solvothermally and formed oriented thin films.[125] Two strategies were developed to fabricate well-defined metal/COF multi-layered structures and to pattern the obtained COF thin films. The first strategy involved alternating physical deposition of metal and chemical deposition of COF, while the second strategy utilized photolithography and reactive ion etching techniques.

### 4.2. Microwave Synthesis

Typically, microwave synthesis refers to the application of microwave irradiation during the reactions performed for COF synthesis. Microwaves promote the reaction rate and lead to the reaction products in shorter times.[126,127] Microwave irradiation during synthesis can be also applied in synergy with solvothermal techniques, considerably decreasing the time and enhancing the yield. To exploit the microwave irradiation, the reaction mixture must contain a polar solvent. Cooper and his group pioneered on the microwave synthesis of boronate ester-linked COFs (COF-5 and COF-102).[109,128] These COFs were produced about 200 times faster than they would have by conventional solvothermal synthesis. It was discovered that the COF-5 produced using the microwave method had a significantly larger SSA than the COF-5 produced using the traditional solvothermal process. Similarly, Wei et al. produced a 2D enamine-linked COF-TpPa using a microwave synthesizer.[129] The microwave-assisted solvothermal method resulted in a COF with a highly ordered crystalline structure, while synthesized rapidly. This was combined with superior stability, maintaining its structural integrity under nine different solvents and enhancing its practical applications. COF-TpPa displayed as well an SSA of 724 $m^2\ g^{-1}$, and a high $CO_2$ capacity combined with adsorption selectivity for $CO_2$ over $N_2$. In this regard, the utilization of the microwave-assisted solvothermal method in COF synthesis emerges as a highly advantageous approach offering notable structural benefits, combined with rapidity, affordability, and simplicity. Consequently, it holds significant promise for facilitating the large-scale manufacturing of COFs at a reduced cost. It is worth noting that the microwave synthesis method has not yet been widely employed for synthesizing a diverse range of COF structures. It should be noted, however, that precise calibration of reaction parameters is of utmost importance when aiming to achieve controlled synthesis of COFs. This necessitates conducting elaborate and multiple experiments to fine-tune the conditions.

### 4.3. Room-Temperature Synthesis

Despite the excellent thermal and acid-base stability exhibited by room-temperature synthesized COFs, their applications remain limited, and only a few reports have been published to date.[130] The formation of COFs generally involves the reaction of organic building blocks that must undergo specific bond-forming reactions, such as condensation or nucleophilic substitution, to create the covalent bonds that hold the framework stable. Usually, these reactions require an activation energy, which is typically provided by heating. Therefore, achieving controlled and efficient assembly of COF structures under room temperature conditions has been challenging. In 2005, Yang et al. proposed a straightforward solution-phase synthesis approach for the room-temperature formation of COF(TpBD).[131] Following straightforward synthesis steps, the produced COF exhibited improved thermal stability, but the yield and crystallinity were low. In another report, Lin et al. reported the synthesis of COFs at ambient temperature for the extraction of proteins from biological samples.[132] The COFs were obtained via the reaction between 1,3,5-tris(4-aminophenyl) benzene and terephthaldicarboxaldehyde, and were stable in water, organic solvents like methanol and THF, 10 mM HCl, and 1 mM NaOH at room temperature overnight, demonstrating the good chemical stability due to the strong C═N covalent bond formed, resulting to a polyimine-linkage skeleton. The same group also demonstrated the room-temperature synthesis of COFs by using 1,3,5-triformylbenzene (Tb) and benzidine (BD) as ligands.[133] It is interesting to note that these COFs were synthesized on the surface iron oxide magnetic nanoparticles, which facilitated the magnetic separation of the COFs after the biological separation processes. Nevertheless, the metal centers on the surface of the magnetic nanoparticles could possibly play a crucial role in catalytic bond formation of the COF linkages at room temperature. Medina et al. established a modified method for the preparation of COFs at room temperature involving the conversion of the reaction mixture via a vapor-assisted approach.[121] This method allowed the control of various physical aspects of the COF. Changing the linker composition facilitated the control of periodicity/crystallinity, while droplet volume and solution concentration affected the thickness, porosity, and grain boundaries. To demonstrate this, BDT-COF and COF-5 based on benzodithiophene were prepared. The benzodithiophene diboronic acid (BDTBA), HHTP, dry acetone, and pure EtOH were all subjected to ultrasonication before being passed through a syringe filter in a concentration ratio of 0.025 mmol: 0.017 mmol. The 150 µL of BDTBA/HHTP filtered mixture was then applied to a glass substrate using the drop-casting technique, followed by exposure of the glass substrate to mesitylene and dioxane vapors in a vacuum desiccator. After 72 h, this resulted in the growth of a 7.5 µm thick dark green organic thin film. By reducing the droplet volume and solution concentration, the thickness of the resulting film could be adjusted. For example, using the same concentration but with a reduced droplet volume of 60 µL, a 2 µm thick film could be produced, while using 60 µL of a droplet with one-third of initial concentration, a thin film of 300 nm was produced. This highly effective technique can also be used to synthesize other COFs. While room temperature synthesis methods offer unique advantages such as simplicity and environmental friendliness, they are limited by the solubility of building monomers and the inability to synthesize a wide range of COF linkages and structures. Temperature plays a crucial role in the synthesis of COFs, allowing the introduction of new monomers and facilitating the combination of COFs with other materials. Despite the limitations, these reports highlight the promising potential of room-temperature synthesis methods in various research areas, paving the way for future investigations of room-temperature-derived COFs.

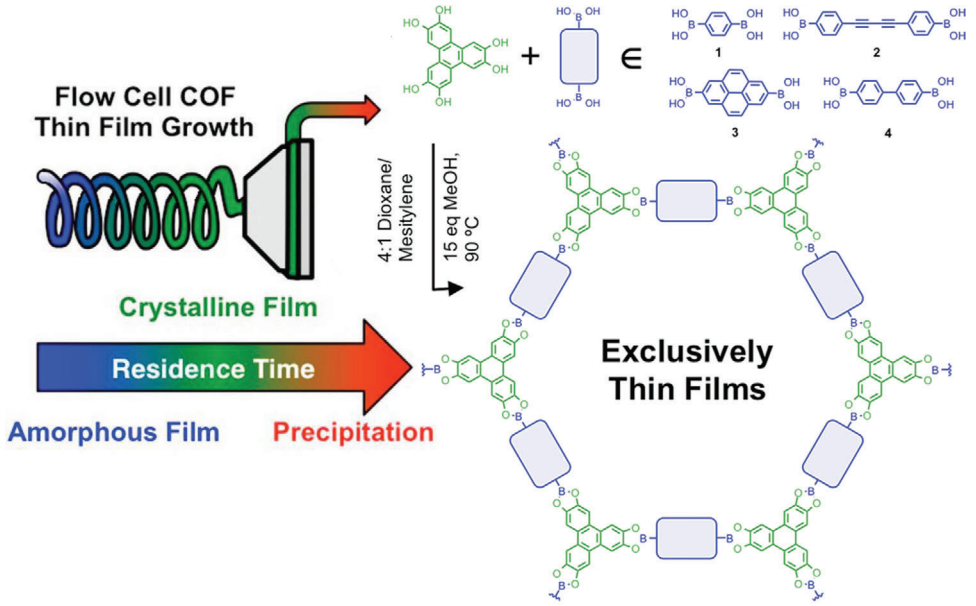


**Figure 5.** Schematic of flow setup designed with variable induction period for the formation of 2D COFs and their general structure of the 2D COFs formed from HHTP condensed with linear bis(boronic acids) (structures 1–4). Reproduced with permission.[135] Copyright 2016, American Chemical Society.

### 4.4. Synthesis Under Continuous Flow Conditions

Continuous flow synthesis of COFs has been developed to overcome the drawbacks of the standard solvothermal synthesis. These drawbacks include i) the blockage of COF pores due to the presence of unreacted monomers, unwanted reactant byproducts, and oligomers, ii) the requirement of harsh conditions that could degrade the sensitive precursors, substrates, or even the covalent bonds of the framework, and iii) the lack of effective, affordable, and efficient methods to control the nucleation or growth of COF thin films. The constraints imposed by solvothermal technologies can be overcome in a number of ways.[134] For instance, Bisbey et al. produced highly homogeneous and crystalline 2D COF thin films using the continuous flow method, which exploited the constant mass deposition rate to tune the thickness and crystallographic properties with high precision.[135] They used a flow cell to produce the modified 2D COF-5 film, during the continuous flow of the HHTP and various bis(boronic acid) (such as PBBA) monomers. Initially, the monomers reacted slowly at ambient temperature, and when the temperature increased to 90 °C, the COF-5 crystal formed within 2 min of the induction period. Reservoirs containing the reaction mixture were used for heating, and the reaction mixture was then fed into a flow cell consisting of a substrate and a quartz crystal microbalance to monitor the film thickness (**Figure 5**). The thickness, shape, crystallinity, and rate of formation of the COF thin films can be controlled by the physical properties of the reaction mixture, such as temperature, residence time, reaction mixture composition, and flow rate.[136] The residence time can be used to control the polymerization mechanism that takes place over the substrate in the flow cell. In particular, large monomer species can reach the substrate at higher residence times, whereas smaller oligomers and monomers can only do so at lower residence times. Therefore, the flow cell configuration enables the study of the reaction conditions for thin film formation. In addition to the synthesis of COF-5, the suitability of this synthetic approach in a flow cell has been demonstrated for numerous other boronate ester-linked COFs (mainly DPB-COF, TP-COF, and COF-102).[137]

### 4.5. Interfacial Synthesis

To date, several types of interfacial synthesis methods have been reported embracing liquid/liquid, liquid/air, and solid/liquid interfaces. The interfacial synthesis method can effectively control the thickness of the grown COFs can be controlled effectively. In this method, the reaction between monomers takes place at a thin interface. Depending on the two phases forming the interface, different methods are used to limit the growth of COF's film thickness.

#### *4.5.1. Liquid–Air Interface Synthesis*

The liquid–air interface synthesis route involves the formation of COFs at the interface between a liquid phase and the surrounding air. Typically, a precursor solution containing the organic building blocks and a catalyst is applied to a liquid subphase, such as water or an organic solvent. As the solvent evaporates at the air–liquid interface, the organic building blocks self-assemble into a 2D layer. Subsequently, a crosslinking reaction takes place, resulting in the formation of a COF film. The COF film can be transferred onto various substrates. Monomers can also be confined in a Langmuir monolayer at the interface.[138] By manipulating the precursor concentration, solvent evaporation rate, and deposition time, precise control over the thickness of the COF film can

be achieved. The synthesis of 2D COF polymers is quite straightforward with this approach, however, the synthesis of monolayer COFs is challenging. In the early studies, the imine linker-based monomer was reacted in a Langmuir trough producing a free-standing film with a thickness similar to that of a single layer.[139] However, it was unclear whether the resulting COF thin film was amorphous or crystalline in nature. In the modified version of this synthesis, a single layer of surfactant was placed at the liquid/air interface and only one type of building block monomer was added, resulting in the building block/surfactant intimate interaction.[140,141] This resulted in the formation of a compact and structured Langmuir layer at the liquid/air interface. Subsequently, with the addition of the second building block, the reaction took place between the second building block and the preexisting layer of the first building block. Recently, Feldblyum et al. reported on a novel synthesis technique involving simple nucleation and control of the COF thickness.[142] Bis-aldehyde was used as a surfactant in the synthesis of poly-TB-COF by selecting tris(4-aminophenyl) amine (TAPA) and 2,6-dicarbaldehyde-4,8-dioctyloxybenzo di-thiophene (BDTA) as the building blocks. In this process, BDTA and TAPA reacted for two days in a closed Petri dish at the liquid/air interface, forming a thin, highly reflective film. However, it was found that the COF thin film produced by this process was far too rough to be used further in pertinent applications, since COF films must have a smooth surface in order to be successfully employed for device fabrication. Hence, for attaining COF films with a smooth surface, the interfacial method can be modified by using a filtered solution. Using this method, it was found that the film's average roughness was 0.2 nm, and importantly, the thickness of the films could be controlled by adjusting the incubation time. For instance, Dai et al. created a monolayer of COF thin film via dynamic imine chemistry.[139] Terephthalaldehyde and 1,3,5-trihexyl-2,4,6-tris(4-aminophenyl) benzene monomers were chosen to grow COF thin films. These monomers were ideal for the liquid/air interface synthesis due to the three hydrophobic n-hexyl groups. The product showed few defects owing to the emergence of self-correction and healing effects promoted by the reversible imine bonds. The appropriate monomers were first diluted in chloroform, then dispersed on the water/air interface and left overnight, to form a smooth, free-standing monolayer film with a thickness of 0.7 nm. However, achieving high reproducibility in terms of film quality, thickness, and structure remains challenging, as the solvent evaporation rate, humidity, and temperature can significantly influence the self-assembly process, requiring careful optimization and control.

#### 4.5.2. Liquid–Liquid Interface Synthesis

The liquid–liquid interface synthesis route involves the creation of an interface at the junction between two immiscible liquids. It is similarly attractive to the air/liquid interface synthesis, and it is versatile, however it is not favorable for producing monolayer COFs.[143] The primary advantage of this method is the ability to produce free-standing thin films. The confinement of the building blocks and catalysts (which are key components in the formation of COFs) has been shown to be particularly successful through the appropriate selection of immiscible solvents. For example, Dey et al. produced a large number of COF thin films (50–200 nm) at the interface of two immiscible liquids.[144] The precursor concentration can be optimized to control the thickness of the COF thin films. To improve crystallinity, the researchers introduced a salt-mediated technique using p-toluene sulfonic acid amine salt (PTSA) instead of free amine and aldehyde. The presence of the PTSA slows down the diffusion rate of precursors at the interface, promoting thermodynamically controlled crystallization. This strategy allowed the synthesis of four different COF thin films with distinct pore sizes at room temperature. Additionally, COF thin films were successfully transferred to a variety of substrates, including glass, holey grids, and metallic wires, without compromising their crystallinity. In another work, terephthalaldehyde (PDA) and 1,3,5-tris(4-aminophenyl)benzene were polymerized using the liquid–liquid interface approach to create an imine-linked TAPB-PDA COF (TAPB).[145] The Lewis acid catalyst $Sc(OTf)_3$, which has a higher solubility in the aqueous phase than in the organic phase, was used to limit the polymerization at the interface, thus facilitating the imine production and setting reaction limits.

Site-selective polymerization for the creation of thin films at the organic–water interface can assist in the spatial segregation of COF monomers. The size of the reaction vessel, the concentration of the building block monomers, and the volume of the organic phase can all be modulated to alter the lateral dimensions of the thin film, the thickness, and other structural features. Another key benefit of this technology is its versatility in transferring thin films to different substrates without affecting their physical structure.

#### 4.5.3. Liquid–Liquid–Gel Tri-Phase System

The third type of synthesis process is based on the liquid–liquid–gel interface.[146] By incorporating a hydrogel into the oil, a unique synthesis environment can be created. At the interface between the hydrogel and the oil, a super-spreading water layer can be developed by adding a small amount of water to the system. In this process, the amine monomer, dissolved in the hydrogel, and the aldehyde monomer, dissolved in the organic phase, engage in a reaction at the hydrogel–organic solvent interface, resulting in the formation of a COF film. The hydrogel layer plays a crucial role in moderating the diffusion rate of the amine monomers, thereby facilitating a controlled and gradual progression of the reaction at the interface. Concurrently, the monomer concentration within the hydrogel can be precisely manipulated to regulate the film's thickness, which can be varied between 5 and 100 nm. Several films of COFs can be produced at the interface by mixing one monomer with the oil and the other with the hydrogel.[147] Li et al. utilized acetic acid as the third liquid to modulate the interaction rate between two distinct solutions containing different monomers. Acetic acid creates a distinct layer between v and a mixture of dichloromethane and *N*,*N*-dimethylformamide. Owing to its higher density, the latter phase gradually descends through the acetic acid layer, ensuring a controlled contact with the dichloromethane solution at the bottom. At this juncture, the amine and aldehyde monomers undergo a reaction at their interface, culminating in the formation of a COF film. This innovative approach strategically slows down monomer diffusion

at the interface, thereby facilitating a more stable and sustained monomer reaction at the interface.[148] In another example, 2D COF thin films were produced, also using the superspreading water layer on a hydrogel immersed in oil as a reactor. By introducing amine and aldehyde monomers into the hydrogel and oil phases respectively, the reactants diffuse into the thin superspreading water layers, forming the homogeneous COF thin films. The imine-based ultrathin COF films showed high crystallinity with a specific orientation, as well as impressive mechanical properties, with a Young's modulus of ≈25.9 GPa. The synthesis strategy was extended to other COFs and the crystalline zeolitic imidazolate framework-8 (ZIF-8) thin film systems, demonstrating its broad applicability.[149] These thin film COFs show promising potential for attractive applications, particularly in the preparation of structurally stable thin film freestanding membranes as nanofilters, and photoelectrochemical sensors for selective detection of ruthenium ions.

### 4.6. Surface-Mediated Synthesis

Single-layer COFs with tunable structural design can be precisely formed on solid surfaces via template-assisted methods. Ultrahigh vacuum (UHV) or liquid conditions can be utilized for on-surface mediated synthesis, with the choice depending on specific reaction requirements.[150,151] These two synthetic methods can be dictated by the phase of the used precursors. Factors such as synthesis conditions, chemical and physical properties of the precursor, and the intended final application play a major role in the selection of the substrate. $SiO_2$, single-layer graphene (SLG), metals (such as Ag (111), Au (111), or Cu (111), among others), are the most widely used substrates and may also play a decisive role in the reactions by acting as catalytic surfaces or by influencing the developed dynamics and interfacial interactions.[152] For example, it was found that the COF formed a hexagonal lattice with a periodicity of 2.5 nm on graphite (001), a rectangular lattice with a periodicity of 3.1 nm on Cu (111), and a distorted hexagonal lattice with a periodicity of 2.8 nm on Ag(110). Furthermore, the substrate temperature has a significant impact on the final composition and coverage of the substrate's surface by the grown COF.

Single-layered COFs can be created on metallic surfaces via on-surface mediated synthesis under UHV conditions in an ultraclean environment.[153] This method offers an advantage over solution synthesis by allowing the use of extremely high temperatures without oxidizing or degrading the solvent. It also enables the use of stiff molecules with sublimation potential, which facilitates the production of COFs even with organic molecules which are insoluble, and thus impossible to use for COF synthesis via wet chemistry methods. However, a fundamental drawback of this approach is the continuous desorption of reaction byproducts, particularly water molecules. These desorbed water molecules hamper the vacuum condition and render the reactions irreversible, limiting the ability to achieve long-range order. Zwaneveld et al. used this technique to synthesize surface COFs (SCOFs) layers using boronate-based chemistry.[154] Particularly, under UHV conditions, sublimated 1,4-benzene di-boronic acid (BDBA) over Ag (111) surface was intermolecularly dehydrated forming the first SCOF-1. Similarly, successful was the esterification reaction of HHTP and BDBA to form another SCOF (SCOF-2). For this, a monolayer of HHTP was initially deposited on the Ag (111) substrate at room temperature in order to prevent the self-condensation of the BDBA precursor. Once covalent bonds were formed between the precursors, the substrate was heated in order to remove any extra HHTP and water molecules. SCOF-1 and SCOF-2 with hexagonal structure and pore size of 15 and 29 Å, respectively, were formed, which was in good agreement with DFT calculations. The SCOF-2 network displayed fewer defects at the atomic level compared to SCOF-1. The authors attributed this difference to the more favorable kinetic path of the bimolecular reaction in dioxaborole formation and the increased rigidity of the triphenylene group. Chen et al. recently showed the synthesis of porphyrin-containing single-layer COFs with a square lattice.[155] In this case, 5 dimethoxybenzene-1,4-carboxaldehyde (DMA) and 5,10,15,20-tetrakis (4- aminophenyl) porphyrin (TAPP) undergoes Schiff-base condensation reaction on a clean Au (111) surface resulting in the growth of 2.5 nm COFs single layers. Under UHV conditions, a distinct polymerization process may also occur, relying on the addition of halogenated precursors through radical reactions. Lackinger et al. created a covalent network of 3,5-dibromophenylboronic acid (DBPBA) which further underwent cyclo-condensation under UHV.[156] First, 1,3,5-tris(3,5-dibromophenyl)-boroxine (TDBPB) molecules were deposited on an Ag (111) substrate to produce the more reactive form of triphenylene-boroxine hexaradicals (TPBHR), and the substrate was then annealed at moderate temperatures to produce the final networks. The substrate plays an important role in the growth of COFs, often acting as a catalyst promoting specific reaction intermediates. In this particular case, it is indicative that the use of graphite (001) was found to be inefficient when used in place of Ag (111).

In contrast to on-surface synthesis under UHV conditions, on-surface synthesis under liquid conditions involves the growth of COFs on substrates using thin liquid films where the reactants are dissolved. The reaction in solution promotes dynamic covalent chemistry and the formation of reversible covalent bonds due to the co-presence of water as a byproduct from the condensation of reactants. These dynamic equilibrium conditions enable the formation of long-range-ordered surface-supported COFs and allow for the healing of defects. However, a significant drawback of this synthesis method is the difficulty in controlling the stoichiometry in multicomponent reactions. The method involves first dissolving the precursors in an organic solvent (such as carboxylic acids or aliphatic alcohols) before transferring for the polymerization onto the substrate.[157] In this course, Xu et al. conducted a room-temperature Schiff-base reaction between several aromatic diamine and benzene-1,3,5-tricarbaldehyde on a HOPG surface, yielding COF films covering almost completely the substrate's surface.[158] Specifically, COF structures with pore diameters varying from 1.7 to 3.5 nm were obtained, which could be controlled by the length of the selected amine. The method was modified by Liu et al., who used the surface of HOPG to grow two imine-based SCOFs.[159] Their method was initiated by drop-casting the trigonal precursor onto the substrate, followed by adding $CuSO_4 \cdot 5H_2O$ (as a thermodynamic regulation agent) and the second precursor in the closed reactor, and then the temperature was increased. In particular, tris(4-aminophenyl) benzene (TAPB) and terephthal-di-carboxaldehyde (TPA) were

used in one example, while 1,3,5-triformyl benzene (TFB) and p-phenylenediamine (PPDA) were used in the second case, leading to SCOF-IC1 and SCOF-LZU1, respectively. The released $H_2O$ from $CuSO_4{\cdot}5H_2O$ promotes the reversibility of the aldehyde-amine coupling reaction.

## 5. COF as Electrode Components: Working Fundamentals

The charge storage mechanism in COFs having electroactive organic functionalities relies on their controlled and reversible modulation of their charge state.[160] Organic electrode materials used in these frameworks (like quinones or thiophenes), can be categorized into two groups during redox reactions: n-type and p-type organic materials.[161] p-Type organic compounds (e.g., tetrathiafulvalene-containing COFs) go through oxidation to form positively charged species like cations, whereas n-type organic materials (e.g., naphthalene diimide derivatives) are reduced to produce negative charges like anions. It has been observed that a large number of COFs behave as n-type systems. When COFs are used in lithium-ion batteries (LIBs), their charge/discharge mechanism is accomplished via reversible redox reactions. The movement of $Li^+$ inside COFs results in the simultaneous balancing of the negatively charged species and the reduction of functional groups of COFs. The movement of $Li^+$ ions into the electrolyte is accompanied by oxidation of the functional groups on COFs to restore their neutral state. For decades, carbonyl compounds have been thoroughly investigated as n-type electrode materials.[162] There are four typical organic carbonyl electrode materials that are widely used in metal-organic batteries: quinone, carboxylates, anhydrides, and imides.[163–165] During the discharge/charge mechanism, carbonyl compounds experience a reversible cleavage and formation of C═O bonds. During discharge, carbonyl compounds undergo a reduction reaction involving the cleavage of the C═O double bond, forming a single bond and an additional bond to a hydrogen atom or another substituent. During charging, the C═O double bond is reformed through an oxidation reaction. Therefore, a crucial stage in the redox mechanism is enolization, where a nucleophile addition takes place at the carbonyl carbon of the C═O functionality.[166,167] A remarkable Li storage capacity was attained by a network of COFs based on the poly-arylimide (PAI) redox entity. Wang et al. created a crystalline 2D-PAI@CNT through the polycondensation reaction involving tris(4-amino phenyl) amine (TAPA) and 1,4,5,8-naphthalenetetracarboxylic dianhydride (NTCDA) in the presence of carbon nanotubes (CNTs).[168] Through carbonyl reduction to lithium enolate, the imide functional units are assumed to be involved in the storage of Li. In addition to the carbonyl compounds, the presence of C═N bond linkage in the structure COFs has also attracted considerable attention.[14] For instance, Wang et al produced imine-based 2D COFs on CNTs surface having rich C═N and C−C bonds in planar benzene functional units. The composite showed a high Li storage capacity of 1536 mAh $g^{-1}$.[169] As a result, adding redox units to the framework offers a practical method to engineer COFs for EES applications.

The structural customizability such as high surface area and tailored pore networks make them versatile materials for enhancing energy storage performance. In LIBs, COFs can serve as both anode and cathode materials. As an anode material, COFs can provide a high surface area and stable structure for accommodating lithium ions during charging and discharging cycles.[170] The porous structure of COFs facilitates the insertion and extraction of lithium ions, leading to enhanced capacity and cycling stability.[171] As cathode materials, COFs can offer abundant redox-active sites and electrolyte accessibility necessary for efficient lithium-ion storage. It has been observed that 2D COFs are most explored as cathodes for LIBs.[172,173] Wu et al. designed a 2D COF with a high concentration of active groups (C═O and C═N), delivering 502 mAh $g^{-1}$ of capacity as a cathode for LIBs.[174] The greater the number of active sites, the more capacity can be delivered from the COF structure. In one report, a four-carbonyl-group-based 2D COF was produced to support 4 electron transfer redox reaction.[175] The tailored pore networks of COFs enable fast diffusion of lithium ions, leading to high energy density and long-term stability. In batteries using COF as electrode material, the ion transport mechanism is a complex interplay of various factors governing the movement of ions within the electrode materials during charging and discharging cycles. At the heart of this mechanism lies the structural design and charged chemical functionalities of COFs, which influence the diffusion kinetics and overall performance of the battery.[176] Upon charging, lithium ions or other ions (such as sodium, potassium, or metal ions in different battery chemistries) migrate from the electrolyte solution to the COF anode electrode material. For instance, a COF anode with 0.5 nm of pore size delivered much better capacity retention upon cycling compared to a respective COF with 1.5 nm pore size due to differences in interaction energies developed in the cavities when one or more metal ions were incorporated.[177] The high surface area and dense porous network of COFs provide ample active sites for ion adsorption and intercalation, facilitating the ion transport process. The ordered pore networks within COFs offer pathways for ions to travel through the electrode material, minimizing diffusion barriers and allowing for rapid transport. Ion transport is promoted by directional channels, abundant ion-hopping sites (through carbonyl, cyano-groups, and others), functional diversity, and structural robustness.[102] Moreover, the stability of COFs under electrochemical conditions ensures the long-term integrity of the electrode material, allowing for sustained ion transport and cycling stability over multiple charge-discharge cycles.[175]

In Li–S batteries, COFs play multiple roles to address challenges such as the shuttle effect and low conductivity of sulfur. COFs can serve as hosts for sulfur, providing multiple interaction sites (cyanide, carbonyl groups, and polysulfide chains) and a porous structure to accommodate sulfur and its intermediate products during cycling.[178] The confinement of sulfur within the pores of COFs is usually based on a selective ion-sieving effect by regulating the dynamic behavior of polysulfide anions and $Li^+$. Cationic COFs produced via cycloaddition can also provide ordered channels and strong interaction between quaternary ammonium cations and polysulfide anions.[179] In SIBs and PIBs, COFs exhibit similar advantages as in LIBs, providing high surface area, stable structures, and tailored pore networks for efficient ion storage.[180] The tunable porosity of COFs allows for the optimization of electrode materials tailored to the specific requirements of large atomic size of sodium and potassium ions. As separators, COFs with charged ionic structure through

anionic and cationic monomers offer selective and fast ion transport.[181] In supercapacitors, COFs can serve as electrodes due to their high surface area, accessible pore network, and reversible redox activity, allowing for efficient charge storage via pseudocapacitance or double-layer capacitance mechanisms.[182]

## 6. COFs for Battery Applications

There are different battery chemistries, each having benefits and drawbacks in terms of cost-effectiveness, capacity, energy density, stability (life cycle), safety, or charging rates, for example. The capacity of a battery significantly depends on the electrode materials and electrolytes used, because they influence the mechanisms of charge storage and parameters thereof.[183,184] Two common methods of charge storage are ion implantation inside the crystal structure (usually called intercalation type chemistry), or the formation of solid-state solutions (insertion chemistries), both accompanied by redox reactions. Due to this, the electrode materials undergo substantial structural changes during charging–discharging. The conventionally used transition metal oxides or hydroxides and carbon/graphite electrodes have some limits related to their ability to accommodate the structural changes with the insertion of ions. Additionally, electrode material cannot be used for other battery chemistries than the one originally designed for, due to the strong dependence of diffusion phenomena and coordination preferences, on the type of the ions and electrode materials. In regard to this, COFs have attracted profound interest due to their highly crystalline/ordered and porous nature (promoting diffusion pathways), high connectivity, structural stability, ability for accommodation of positively charged cations, open pore channels, tunable porosity tailored for different size of ions, and presence of a pi-conjugated skeleton enabling fast electron transfer and redox cycles.

### 6.1. COFs for Metal Ion Battery Electrode Materials

Until recently, COFs have been employed as electrode components in EES and energy conversion including supercapacitors, batteries, catalysis, and solar cells, emphasizing the significance and potential of COFs in key enabling technological domains.[88,185–188] The use of COFs in LIBs, sodium-ion batteries (SIBs), and other post-lithium chemistries is highlighted in this section.

#### *6.1.1. COFs for Li-Ion Batteries*

*COFs as Cathode Materials*: A broad variety of organic (macro)molecular systems, such as conducting polymeric materials,[189,190] sulfur-containing organic linkers,[191,192] organic radical intermediates, and compounds with carbonyl functional units[193–195] have drawn the interest as cathode components in LIBs. This is mainly attributed to the benefits emerging from the homogeneously and evenly distributed functional chemical moieties, controllable molecular geometries, and 3D architectures, promoting the properties that are critical for storage capacity. For instance, Yang et al. reported structure-modulated naphthalimide-based crystalline COFs, synthesized from 1,3,5-triformylphloroglucinol (Tp), 1,3,5-triformylbenzene (Tb), and 2,7-diaminobenzo[*lmn*][3,8] phenanthroline-1,3,6,8(2*H*,7*H*)-tetraone (DANT) (Tp-DANT/COF & Tb-DANT/COF),[196] and were used as cathodes for LIBs. The Tb-DANT/COF delivered initial discharge capacity of 144.4 mAh $g^{-1}$ at 0.34 C (50 mA $g^{-1}$) and also retained a reversible capacity of 71.7 mAh $g^{-1}$ after 600 cycles at a particularly high rate of 7.5C. Switching the linker from Tp to Tb significantly enhanced the conjugated backbone of Tb–DANT-COF with open nanopores, which is advantageous for facilitating charge transport and avoiding the dissolution of organic active molecules. As a result, during the first few cycles, Tb–DANT–COF electrodes have a larger reversible capacity than Tp–DANT–COF. This shows that by modifying the architectures of organic electrode materials, electrochemical performance may be tuned and enhanced. Research endeavors are focused on addressing some aspects of COFs, including low conductivity, insufficient chemical inertness, and stability, or solubility in organic electrolytes, which may expand further their application potential.

*Redox and Exfoliated COFs@Hybrids as Cathode*: In order to optimize the performance of the active material within an electrode, it is imperative to achieve a uniform and readily accessible distribution of reactive sites for electrolyte ions. Additionally, the framework must possess the capability to accommodate the volumetric changes during the insertion and extraction of charged species. It is also essential that the redox sites are present in the COF structure and accessible by the electrolyte ions. Nevertheless, it has been observed that densely packed layered structures present challenges in providing easy access to all redox-active sites. Moreover, polymeric-based amorphous electrodes have an architecture that limits the influx of electrolyte ions and accessibility to active sites. To address this issue, the growth of low-dimensional crystalline structures or few-layered materials can provide a solution to these matters. It is indicative that exfoliation of COF layers may be a successful method to substantially improve the capacity of the electrode materials. The versatility of the initial COF architecture which allows exfoliation, enables superior ion diffusion and charge transfer processes. Indicatively, Wang et al. demonstrated a novel technique for producing 2D few-layered nanosheets by synthesizing and delaminating redox-active COFs[197] as rechargeable battery cathode materials. Compared to pristine COFs, exfoliated COFs (ECOF) showed shorter $Li^+$ diffusion paths, higher redox site utilization efficiencies, and faster lithium storage dynamics. It was unveiled that charge transfer predominates redox processes in ECOFs as compared to bulk COF structures. The ECOF displayed rapid charge–discharge characteristics (74% retention at 500 mA $g^{-1}$ vs 20 mA $g^{-1}$ for the bulk COF electrode) and improved rechargeability (98% capacity retention over 1800 cycles). In another study, a new porous charge transfer (CT) complex (PCT-1) with a pseudo-hexagonal hybrid dendritic architecture was synthesized using hexahydroxytriphenylene and 1,4,5,8,9,12-hexaazatriphenylene-2,3,6,7,10,11-hexacarbonitrile precursors.[198] The structure has redox-activity originating from the mixed-stacked CT complexes integrated into the porous crystal structure. Its redox-active components and high porosity contributed to the increased capacity of 288 mAh $g^{-1}$ at 500 mA $g^{-1}$, as a cathode-electrode material in a lithium-ion rechargeable battery.

The efficiency of battery performance is significantly influenced by the dynamics of electron transport, as well as the prevalence and activity of redox-active sites. Integration of conductive coatings or additives has proven effective methods for enhancing electron transfer.[199,200] For instance, the utilization of a microporous carbon-based COF as a cathode for LIBs produced by in-situ polymerization over a graphene surface showed excellent performance for Li storage.[201] The use of CNTs and graphene-based additives along with controlled incorporation of polymeric materials has also been pursued to provide conducting pathways. Similarly, DeBlase et al. developed COF structures synthesized with functionalized polyimide (PI) units.[202] This approach included lowering the number of COF stacked layers by exfoliation to obtain readily accessible active redox surface sites and then incorporating reduced graphene oxide (rGO) to significantly enhance the conductivity. Such superstructure contributed to improving the exposure of the redox active sites and promoting charge transfer efficiencies. The enhanced electrochemical performance of the electrode material is ascribed to the shorter lithium diffusion channels and improved conductivity. In another report, triazine-based COFs were synthesized to construct exfoliated hybrids with carbon nanotubes (coded as E-CIN-1 and E-SNW-1).[203] The thin-layered 2D architectures of the exfoliated E-CIN-1@CNT and E-SNW-1@CNT offered increased ion/electron transport and redox-active sites. Li storage in these hybrids involved redox processes taking place on the organic functional units (particularly triazine or benzene aromatic rings) leading to 6-Li-ion accumulation. Such exfoliated E-CON@CNT composite materials exhibited superior cycling performance compared to prior COF-related active materials, and large reversible potentials (E-CIN-1 having a capacitance of 1005 mAh $g^{-1}$ and E-SNW-1 a capacity of 920 mAh $g^{-1}$ for 250 cycles at 100 mA $g^{-1}$). The lithium-storage mechanism involved 11 and 16 electron redox reactions, associated with the triazine, piperazine, and benzene rings, as well as with the presence of C═N and −NH− groups.

Meanwhile, the long-term stability of COFs as electrodes in LIBs remains a challenge. Agglomeration of the electrode COF materials is one of the elements that influence cyclic stability. Therefore, retaining the COF sheets separated can be pursued by intercalating molecular entities into the layered structure of COFs acting as pillars and avoiding the agglomeration of COF layers during charging/discharging. This strategy may ascribe long-term stability to the electrode materials. In this context, and inspired from the stability of imine-based 2D TFPB-COF, Chen et al. produced exfoliated-TFPB/COF & exfoliated-TFPB/COF@$MnO_2$ composites by electrochemical stripping.[204] The two electrode materials were endowed with fast ionic and electronic transport channels due to conjugated $\pi$ electrons from benzene rings in the COF, while the emergence of intricate organic redox-active centers contributed to the effective storage of large amounts of lithium. The nanosized $MnO_2$ embedded in the COF demonstrated a synergistic effect to the action of the organic redox centers and served as the "spacer" to prevent the agglomeration of the exfoliated COF sheets, offering exceptional cycling capabilities, and achieving 1359 mAh $g^{-1}$ (over 300 cycles) reversible capacity. On the other hand, the $MnO_2$-free TFPB/COF system delivered 968 mAh $g^{-1}$, while the non-exfoliated analog displayed a dramatically lower capacity.

Comparing redox COFs and ECOFs with each other in the context of their suitability for commercialization as cathode materials for Li-ion batteries, both exhibit promising characteristics. Redox COFs offer well-defined crystalline structures with integrated redox-active sites, providing high specific capacities and stable cycling performance. However, currently, their limited ion diffusion kinetics and electron conductivity often hinder their further application into commercial devices. On the other hand, ECOFs demonstrate shorter $Li^+$ diffusion paths, higher redox site utilization efficiencies, and faster lithium storage dynamics due to their thin-layered 2D architecture offering freely available surface. Moreover, the incorporation of additives, such as CNTs, graphene, and other conductive nanomaterials enhances their conductivity and electrochemical performance. Exfoliated COFs also offer superior cycling performance compared to their bulk counterparts by mitigating the encountered structural stress. Therefore, considering their enhanced properties and performance, exfoliated COFs appear to be promising for commercialization as cathode materials in LIBs. However, further research and development are needed to optimize their synthesis, scalability, and stability to meet the stringent requirements for large-scale commercial applications.

*Functionalized COFs as Cathodes*: Functional groups play a crucial role in attaining high specific capacity and stability, and could also inhibit the dissolution of product in the electrolyte solution. However, if the functional groups are electrochemically inactive, this could increase the dead mass of the cathode material leading to the lower specific capacities. Therefore, Wu et al. minimized the inactive functional groups and produced the COF structure with maximum active groups.[174] A 2D BQ1-COF with abundant redox sites (C═O and C═N) was synthesized with multiple electroactive functional sites, such as six C═O and twelve C═N groups forming stable chelate rings (C—N—Li—O—C) and enabling multiple electron redox reactions for high-capacity lithium storage, leading to a reversible capacity of 502.4 mAh $g^{-1}$ at 0.05 C. Interestingly, BQ1-COF was resistant to the common disintegration or dissolution in the electrolytes and exhibited a cycle lifetime over 1000 cycles (with 81% capacity retention after 1000 cycles) as a result of its relatively effective 2D conjugated structure that restricted its dissolution in the electrolyte. The BQ1-COF exhibited outstanding rate performance, maintaining a specific capacity of 170.7 mAh $g^{-1}$ even at an ultrahigh current density of 10C (7.73 A $g^{-1}$).

To address stability issues, Yang et al. used ionothermal condensation to create nanostructured fluorinated covalent quinazoline networks (F-CQNs) from fluorinated aromatic aminonitrile precursors (**Figure 6**a–c).[205] The structure displayed 23.5 wt% of nitrogen content, extended $\pi$-conjugated architecture, and bipolar combination of benzene and tricycloquinazoline (TCQ). During the ionothermal process, the cleavage of C—F bonds resulted into a high surface area of 1581 $m^2$ $g^{-1}$ and pore volume of 0.73 $cm^3$ $g^{-1}$. Interestingly, the introduction of fluorine species consistently lead to improved charge storage performance. The simultaneous involvement of electro-deficient TCQ units and electron-rich benzene rings endowed F-CQN-1-600 with a large working potential window (1.5–4.5 V versus $Li/Li^+$) with both p-doped and n-doped regions, while the porous morphology contributed to the fast ion-transport and the insertion/extraction of both anions

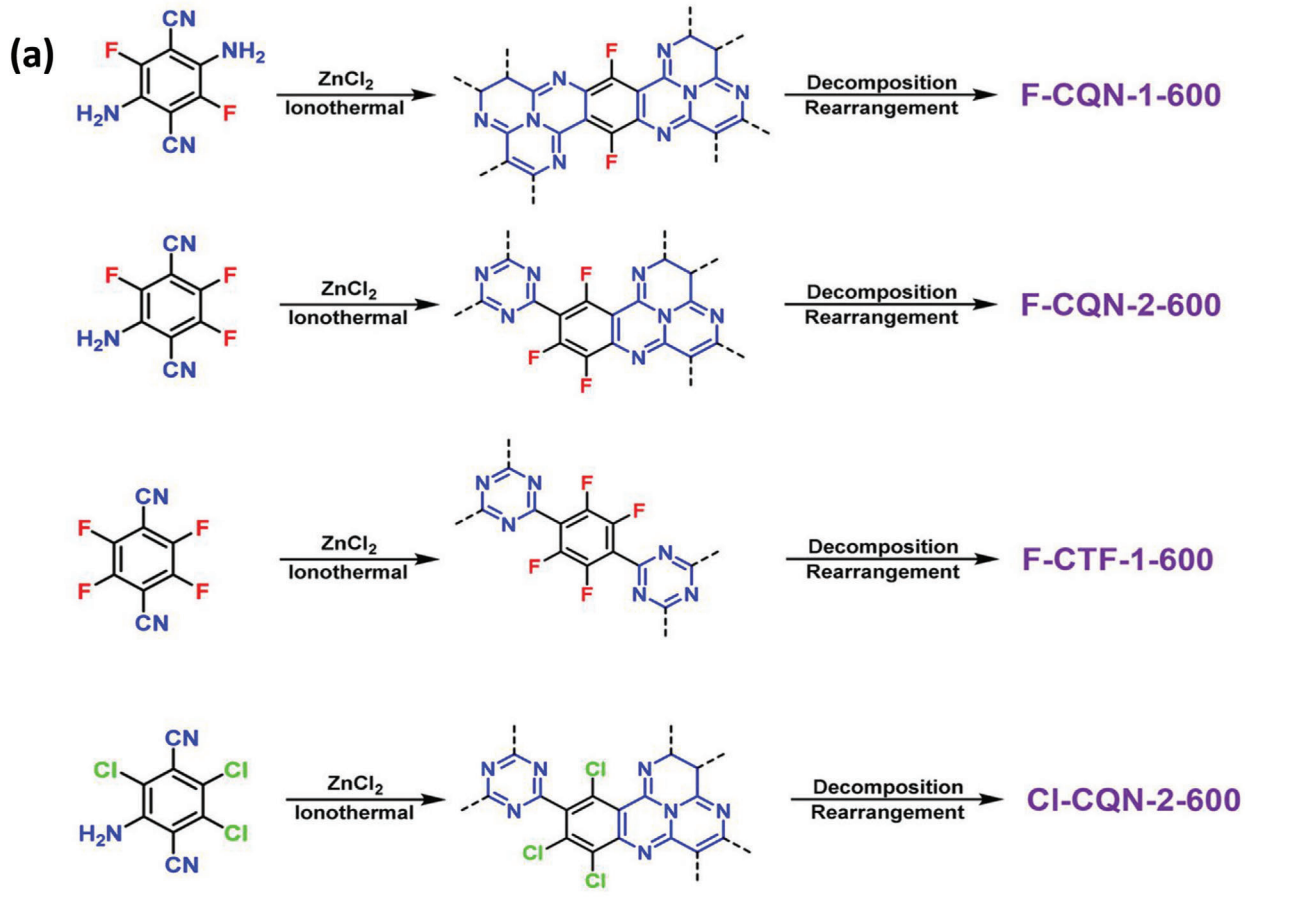


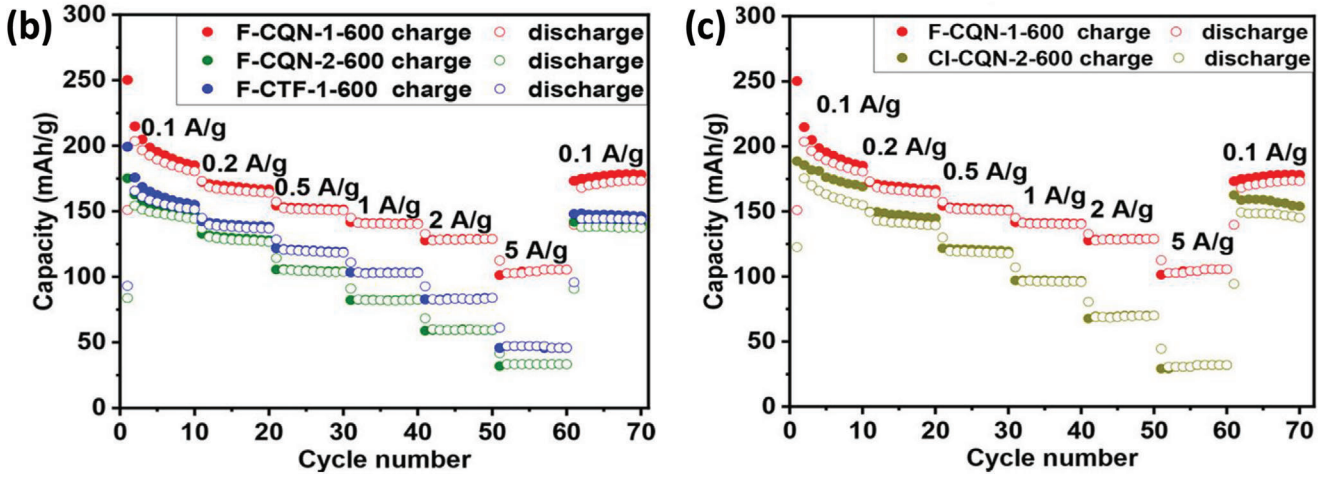


**Figure 6.** a) Synthesis of different fluorinated COF structures, b,c) rate performance of different fluorinated COF and chlorinated COF. Reproduced with permission.[205] Copyright 2020, American Chemical Society.

and cations during charge/discharge processes. Due to these exceptional qualities, the cathode material outperformed many organic cathode materials, as well as chlorinated COFs in terms of capacity (250 mAh $g^{-1}$ at 0.1 A $g^{-1}$), swift kinetics (105 mAh $g^{-1}$ at 5.0 A $g^{-1}$), and remarkable cycle stability (95.8% capacity retention over 2000 cycles and 99.95% of coulombic efficiency).

*Composites@COFs as Cathodes*: Covalent triazine frameworks, a form of COF, have been explored with great interested due to the n, p doping mechanism that they offer and which endows such materials with substantial lithium ion storage properties.[58,206–208] Their particularly small micropores and low conductivity, however, prevent counter-ion transfer, allowing

for capacities bellow the theoretical predictions. Growing CTFs with variable dimensionalities on carbon-based conductive materials or other conducting scaffolds, like MXenes, have been thus considered as promising routes to address this matter. Furthermore, the development of hierarchical pore architectures may further enhance electron conduction and ion transport routes. In this regard, 2D rGO & CTF have been studied for such synergistic integration, demonstrating features such as superior structural functionality and potent planar intermolecular conjugation. Zhang et al. integrated rGO with CTF using an in-situ polymerization process.[209] The composite exhibited considerable surface area of 1357 $m^2\ g^{-1}$, a high capacity (235 mAh $g^{-1}$ after 80 cycles at 0.1 A $g^{-1}$), and remarkable stability (127 mAh $g^{-1}$ sustained after 2500 cycles). Additionally, the extended and hierarchical pore architecture enhanced the $Li^+$ adsorption. During CTF's operation as cathode persistent bipolar-redox reactions take place over a broad voltage range, enabled by the reversible n/p-doping mechanisms. The covalent triazine-based frameworks were reduced and regulated by $Li^+$ cations as a consequence of the n-doping technique, as illustrated in the equation:

$$C_3N_3 + xe^- + xLi^+ = \left[C_3N_{3-x}\left(Li^+\right)_x\right] \quad (1)$$

In another report, poly(imide-benzoquinone), a 2D microporous COF that was synthesized by in-situ crosslinking on graphene (PIBN-G), was tested as a cathode component for LIBs.[201] The integration of graphene with PIBN enhanced the charge transfer phenomena which further allowed the electrons and $Li^+$ to immediately access the redox-active carbonyls. Consequently, reversible specific capacities of 271.0 and 193.1 mAh $g^{-1}$ were achieved at 0.1 and 10 C, respectively, while retention of more than 86% was achieved after 300 cycles. The process of discharging and charging involved the exchange of 8 $Li^+$ and 2 $Li^+$ between the carbonyls of the imide and quinone units, respectively.

Moreover, electroactive molecules can be grafted on conducting backbones,[210] converted into a salt,[211] or insoluble polymeric materials, which is crucial for preventing the dissolution of such small molecules in the electrolytes.[212] Polymeric materials are beneficial backbones since their molecular building blocks can be chemically modified leading to diverse architecture selected to enhance performance.[213] Polymerization also helps to reduce active material breakdown during cycling. Such polymeric electrodes retain their capacity better than monomers containing conjugated carbonyl groups.[214] For instance, a microporous poly-arylimide COF and CNT composite was developed using an in-situ polymerization process, which demonstrated an impressive 99.5% capacity retention over 8000 cycles.[168] Gao et al. presented additional results where rGO was used to create PIXCOF (where PI is polyamide and X is the concentration of rGO) composite materials through in-situ polycondensation method, and were evaluated as redox-active cathode electrode materials for LIBs.[215] Through this synthetic strategy, the PI-COF displayed small particle size, and thus increased exposed electroactive surface area. This facilitated swift transfer of electrons and $Li^+$ ion migration to the redox-active sites consisting of carbonyl groups. The composites, consequently, showed enhanced specific capacities, with PI50 having the highest, of 172 mAh $g^{-1}$ at 500 mA $g^{-1}$. The involvement of C═O double bonds in the redox process was demonstrated by FT-IR spectroscopy, which revealed their participation in the redox reactions. Similarly, in another report, the conjugated porous framework (CPFs), IEP-11 was reported comprising different conductive constituents, including MWCNTs, SWCNTs, and rGO. This COF structure exhibited redox-active anthraquinone building blocks, while the addition of nanocarbon (rGO and SWCNTs/MWCNTs) during the polymerization step led to the production of thick bucky-paper electrode having high mass loading (60 mg $cm^{-2}$) and active material content (80 wt%) (**Figure** 7a–d).[216] The development of self-supported, binder- and metal current collector-free, as well as high-mass-loading electrodes was possible by the incorporation of SWCNTs, which provided interconnected channels and mechanical stability. The high-mass-loading electrode demonstrated an unparalleled areal capacity of 6.3 mAh $cm^{-2}$ at 0.03C and a gravimetric capacity of 83.7 mAh $g^{-1}$. In another example, a new redox-active conjugated microporous polymer (RCMP) was introduced based on anthraquinone moieties (IEP-11), synthesized through a novel two-step pathway combining miniemulsion and solvothermal techniques with solvothermal treatment through Sonogashira cross-coupling reaction. This method resulted in polymer nanostructures that were easier to disperse in solvents and fabricate electrodes. EP-11 exhibited a dual porosity, combining micro and mesopores, with a specific surface area as high as 2200 $m^2\ g^{-1}$, one of the highest values reported for RCMPs. When tested as a cathode in Li-ion batteries, the electrode delivered gravimetric capacities around 100 mAh $g^{-1}$ and extraordinary rate capability, retaining 76% of discharge capacity when charged and discharged in just 12 minutes (5C). Additionally, the insoluble and robust conjugated porous structure of IEP-11 provides unprecedented cycling stability, retaining ≈90% and 60% of its initial capacity after 5000 and 80 000 cycles, respectively.[217] When RCMP was treated for a longer time under hydrothermal conditions, the electrodes could be effectively compressed, leading to a density three-fold higher than the EP-11 electrode. Therefore, the compressible electrode displayed dramatically higher volumetric capacity. Moreover, the insoluble and robust conjugated porous structure imparted unprecedented stability, retaining 90% of the initial capacity after 5000 cycles at 2 C.

In another report, a surface-controlled synthesis methodology was developed employing a pseudo-capacitive active anthraquinone-built COF (AQ-COF) composite with CNTs in a coaxial architecture.[218] AQ-COF was polymerized on the surface of CNTs to improve their dispersibility, processability, and electrochemical characteristics. The sample showed outstanding rate and cycle efficiency (100% capacity retention after 3000 charge/discharge cycles) attributed to the rapid surface-controlled redox processes, in conjunction with the conducting channels created by the presence of CNTs, favorable for the superior charge-transfer capabilities. COF structures have been also developed to harness the advantages of nickel-enriched layered metal oxides cathodes (e.g. NCM811) due to their exceptional capacity for lithium storage (200 mAh $g^{-1}$),[219] which however, are limited by low structural stability and restricted life cycle, owing to the strong Li cation interaction and mismatch with the metal oxide crystals. To address this issue, a pyrazine-2D COF surface coating for the nickel-enriched layered metal oxides (NCM811) was designed.[220] The 2D planar structure and conjugated bond orientation of pyrazine not only shielded NCM811 against

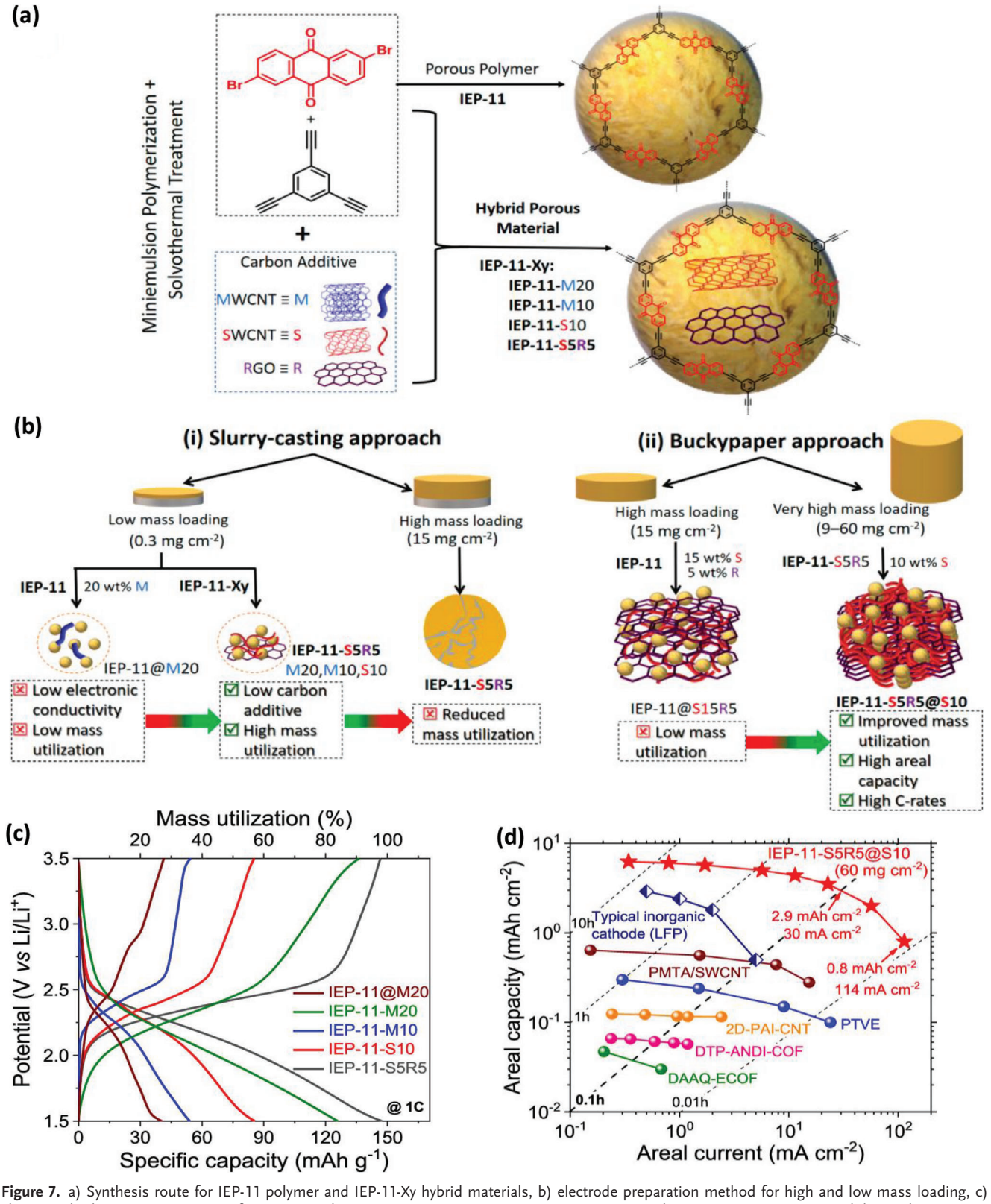


**Figure 7.** a) Synthesis route for IEP-11 polymer and IEP-11-Xy hybrid materials, b) electrode preparation method for high and low mass loading, c) charging/discharging comparison of IEP-11-XY (where, X is MWCNTs(M), SWCNTs(S), RGO(R), and Y is wt% composition), and d) aerial capacity vs aerial current for different COF samples. Reproduced with permission.[216] Copyright 2020, American Chemical Society.

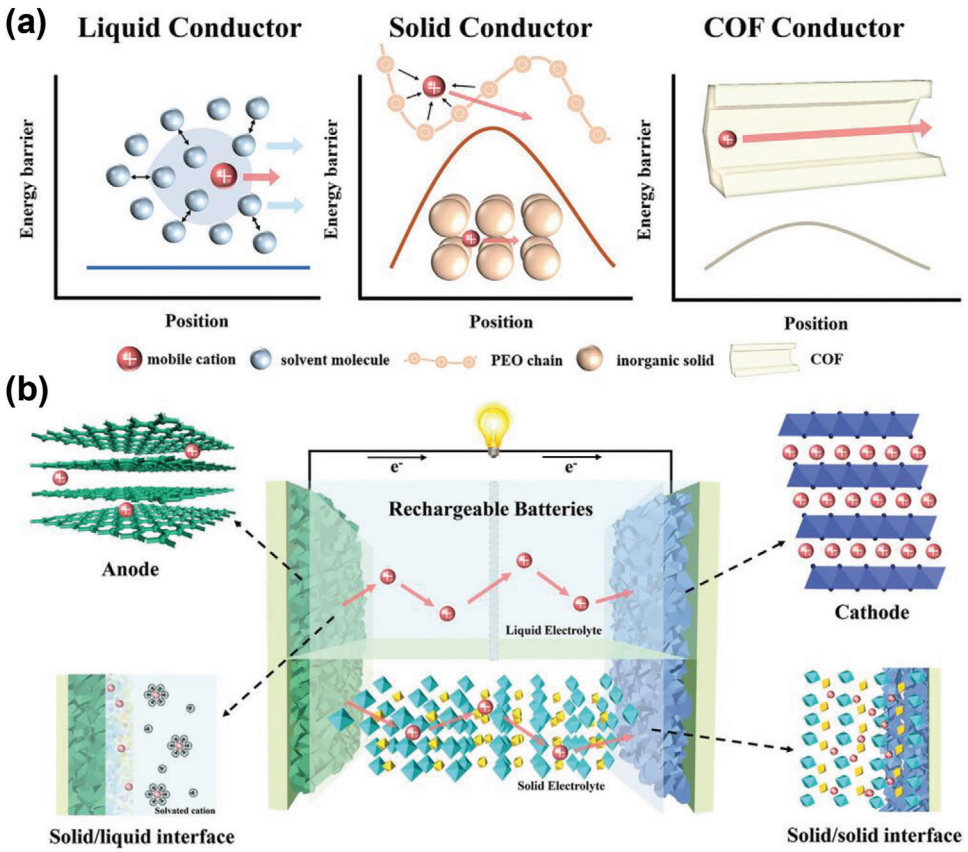


**Figure 8.** a) Diagrams illustrating the ion-conducting behavior and diffusion energy barrier in liquid, conventional solid, and COF conductors, respectively. b) Diagrams depicting the ion transport pathway in solid or liquid rechargeable batteries. Reproduced with permission.[102] Copyright 2022, John Wiley & Sons.

transition metal diffusion, but also generated a metal cation blended layer that prevented irreversible intercalation of Li cations.

The integration of COFs@composites with various materials, such as graphene, nanocarbon, and conjugated microporous polymers, has shown promising results in enhancing the performance of cathode materials for LIBs. The use of hierarchical pore architectures improves $Li^+$ adsorption and enables bipolar-redox reactions over a wide voltage range whereas, incorporating graphene/CNTs like structure into COFs enhanced charge transfer, facilitates electron and $Li^+$ access to redox-active sites, leading to improved cycling stability. Comparatively, the incorporation of graphene and nanocarbon into COF structures shows promise in achieving enhanced conductivity and charge transfer, while surface-controlled synthesis methodologies offer opportunities to improve structural stability, making them attractive avenues for further research and development in the field of composite COFs as cathode materials for LIBs.

*Solid State Li-Ion Conducting COFs as Cathode*: Solid-state lithium batteries are considered advanced EES technologies and are therefore studied extensively.[221,222] Prior research has focused on polymeric-based ion conductors[223] and inorganic sulfides-oxides.[224–226] Aside from these materials, COFs[227,228] and MOFs[229,230] with high porosity and ionic conductivity have also attracted interest in the area of solid-state batteries. Generally, the mechanism of action between solid-state electrolytes (SSE) and electrode materials in batteries involves several key processes that facilitate ion transport, charge transfer, and overall battery performance. Compared to liquid electrolytes, the diffusion energy barrier for SSE is considerably higher, as the liquid electrolyte has lower viscosity allowing for the fast exchange of ions and solvent molecules, which are not as tightly bound on a fixed lattice structure as they are in solids (**Figure 8a**).[224] One fundamental mechanism is ion migration through the periodic crystalline solid or chains of polymers and get stored in anode or cathode (Figure 8b).[231] In this scenario, SSE must exhibit high ionic conductivity, allowing ions (e.g., $Li^+$, $Na^+$, etc.) to move freely between the electrodes/SSE during charge and discharge cycles. The lattice structure and chemical composition of SSE influence ion mobility, where materials featuring open frameworks or interconnected pathways facilitate faster ion diffusion. Similar to the case with liquid electrolytes, a stable interphase layer, generally called the SEI, is formed at the electrode-electrolyte interface. The formation and stability of the SEI layer are influenced by factors such as electrolyte composition, electrode surface chemistry, and operating conditions.[232] Additionally, the SSE/electrode interaction affects charge transfer kinetics at the electrode interface. SSE with intimate contact with

the electrode surface promotes rapid electron transfer between the active material and the current collector, minimizing internal resistance and voltage losses. Tailoring SSE properties, such as elastic modulus and thermal expansion coefficient, can enhance compatibility and ensure the long-term stability of the battery system.[233] In the case of using COF as an SSE, the porous and crystalline structure of COFs serves as a pathway for ion migration, allowing ions to diffuse through the framework during charge and discharge processes.[234] This ion transport mechanism is governed by the interactions between the electrolyte ions and the functional groups within the COF lattice. For instance, the presence of triazine groups within the skeleton of COF provides lone pair electrons through N atoms which attract the positively charged $Li^+$ ions.[235] This uniform distribution of triazine groups throughout the CTF structure generates conductive paths enabling fast lithium diffusion or homogeneous $Li^+$ flux and deposition. Furthermore, the presence of 3D organized nanopores with densely packed functionalities enhances the interaction between ions and functional groups, facilitating ion hopping from one site to another (i.e., diffusion pathways) and enhancing ion mobility. The density of functional groups within these nanospaces directly influences the number of available interaction sites for ions, ultimately impacting the overall ionic conductivity. Unlike traditional inorganic or polymer solid conductors, COFs offer a unique advantage for ion transport through nanochannels, where ions hop between predefined pathways with significantly lower energy barriers.[236] COFs are endowed with an extensive free space, minimizing the energy required for ions to move,[237] in contrast to inorganic solid conductors.[224] Similarly, in polymeric solid conductors, the transfer path is influenced by the frustrated packing of linear polymers, which is heavily dependent on the degree of crystallinity and the glass transition temperature.[238] Further, COFs possess built-in pathways specifically designed to facilitate ion movement. This contrasts with polymer conductors, where the intertwined polymer chains create a complex and temperature-dependent path for ion diffusion.[239] Therefore, COFs combine the advantages of ample space and active pathways to offer superior ionic conductivity and stability for solid-state battery applications.

Recently, incorporating Lewis acidic structures into porous crystalline ion conductors was proposed as a means to enhance the diffusion of $Li^+$ ions.[181,183,185] In this direction, Chen et al. introduced a solvent-free cationic COF that utilized Li salt as an ion reservoir.[181] Nevertheless, the limited interaction between the cationic framework and the free anions resulted in an inadequate supply of $Li^+$ ions (61%). On the other hand, anionic frameworks with a higher $Li^+$ content (80%) required the use of organic solvents to ensure stable ionic conductivity, albeit at the expense of undesired interfacial side reactions.[186–188] The persistence of the uncontrolled growth of Li dendrites in a solid state makes the challenge greater.[240] Hence, it becomes imperative to develop advanced single Li-ion conductors that eliminate the presence of freely mobile anions and solvents. Jeong et al. synthesized lithium sulfonated COF (TpPa@$SO_3$Li) with the aim of establishing precisely defined ion pathways, achieving a high concentration of Li ions, and firmly anchoring anion ligands through covalent bonds.[234] Theoretical analysis unveiled the occurrence of unidirectional Li-ion transport in this material. As a result of the architecture, in combination with the absence of negatively charged mobile ions, TpPa-$SO_3$Li exhibited phenomenal charge transport properties (ionic conductivity = $2.7 \times 10^5$ S $cm^{-1}$, lithium ion transference number of 0.9 at room temperature and an activation energy of 0.18 eV), without additionally incorporating lithium salts and organic solvents. Such ion transport allowed the reversible and stable lithium plating/stripping on lithium metal electrodes.

An interesting aspect of most quinone-based redox compounds is the ability to receive only two electrons despite having several redox-active carbonyl groups. Truxenones, which consist of one core benzene aromatic ring fused by fluorenones have been considered that can boost the overall theoretical capacity of the electrode. For instance, Yang et al. reported COF@TRO based on truxenone as the cathodic material for solid-state LIBs.[241] The higher-density carbonyl substituents supported reversible redox reactions. This led to an excellent specific capacity of 268 mAh $g^{-1}$ which is 97.5% of the projected theoretical capacity.

*Pristine COFs as Anode Materials for Li Ion-Batteries*: The very first report of COF utilization in LIBs as an anode involved the use of a conjugated COF due to the high electrical conductivity and unusually high SSA, which lead to an outstanding stability and capacity.[242] Specifically, two COFs were synthesized through a condensation reaction of aldehyde and amine under solvothermal conditions. They displayed a uniform porous structure with stacking patterns. In this direction, Chen et al. reported conductive and conjugated PA-COF and TB-COF using imine linkers which delivered 401 mAh $g^{-1}$ and 379 mAh $g^{-1}$ of capacity, respectively, with excellent rate performance.[171] Both COF structures showed low charge transfer resistance, even after 500 cycles of charging discharging. In another report, Jiang et al. integrated the redox active sites of bicarbazole groups (with a pyrrole ring and conjugated aromatic carbon rings) in the pore channels of COFs to improve the specific capacity.[243] The material showed 628 mAh $g^{-1}$ of capacity when used as an anode for LIBs. COF structures have been also modified with carboxyl and nitride groups, which improved the overall conductivity, active redox sites, and hindered the dissolution of the active material in the electrolyte through the pi-pi interactions.[244] The presence of N═N and C═O groups was found to improve the electrochemical performance through the redox reactions/interactions. The large number of active sites, the presence of conjugated bonds, and overall geometry, surface area, and $Li^+$ transit channels, the COF anode components demonstrated improved electrochemical efficiency and morphological integrity. The respective LIBs retained 306 mAh $g^{-1}$ of capacity after 3000 cycles. In-situ FTIR and Raman spectroscopies showed the decrease of C═O and N═N vibrations indicating the formation of Li-O- and Li-N- during the charging steps (**Figure 9**a,b). The two-step potential change in the discharging curve verified that the binding of Li ions occurred with the COF subunit at the C═O and N═N linkages, based on the potential values of the observed steps (Figure 9c,d). The development of COF architectures with diverse sets of building units is certainly essential in identifying and optimizing chemical motives appropriate for boosting their energy storage properties. In this direction, Yu et al. developed polyoxometalate functionalized organic frameworks (CPOF), using both inorganic and organic structural components, that were joined by reversible covalent bonds.[245] The synthetic COF displayed exceptional stability, persistent porosity, and a diamondoid topology. When used

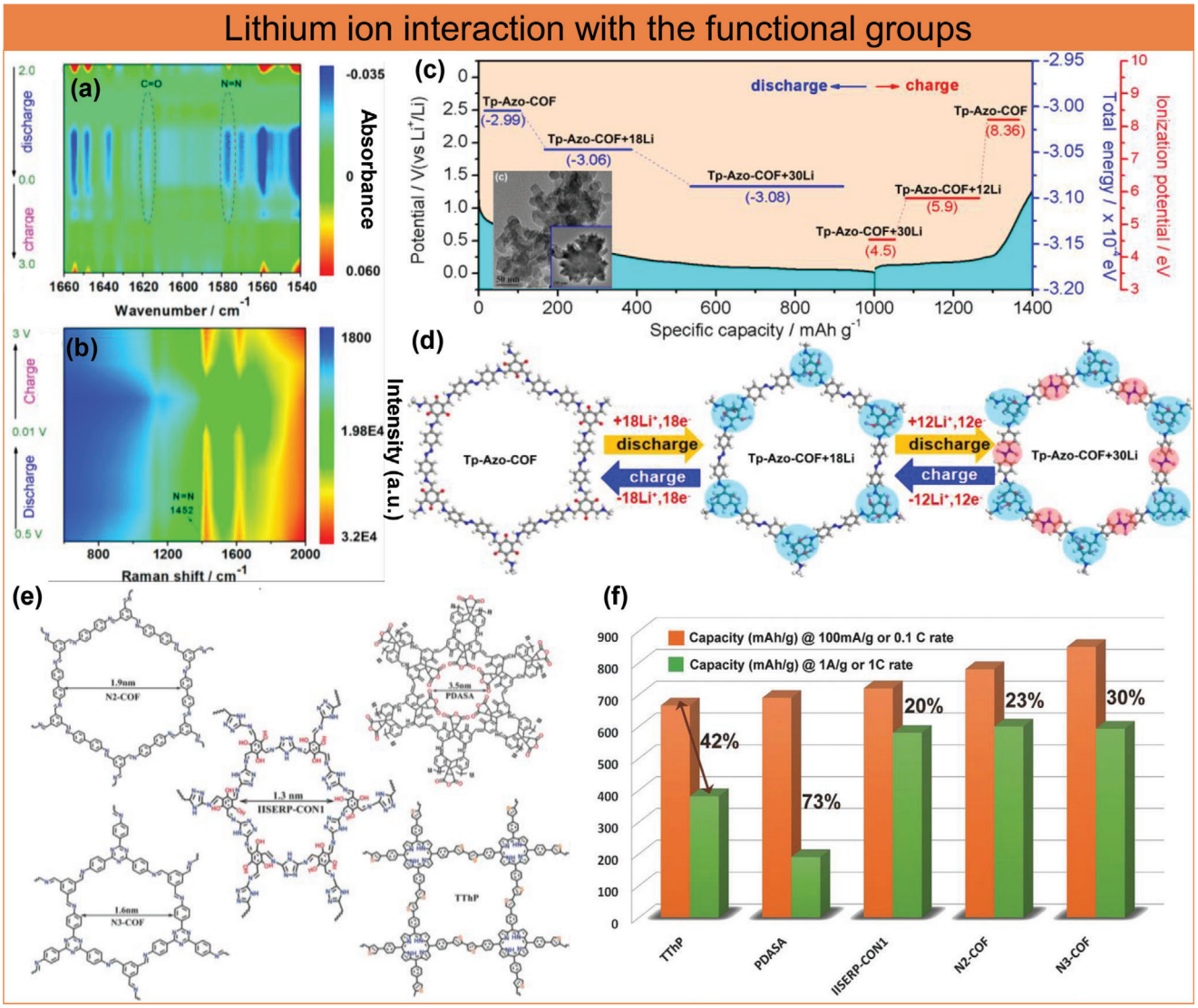


**Figure 9.** Role of chemical functionalities in storing $Li^+$: a,b) in situ FTIR and RAMAN plot of Tp-Azo-COF during charging-discharging indicating the role of C═O and N═N in $Li^+$ storage, c) discharge curve of Tp-Azo-COF showing the number of $Li^+$ transfer at different stages (inset; FESEM image of Tp-Azo-COF), d) lithium interaction sites in Tp-Azo-COF. Reproduced with permission.[244] Copyright 2020, American Chemical Society. e,f) Structure and electrochemical performance of different COF units. Reproduced with permission.[247] Copyright 2017, John Wiley & Sons.

as anode in LIBs the material exhibited 550 mAh $g^{-1}$ of capacity with cyclic stability of up to 500 cycles. The highly conjugated framework allowed quick electron transport and facilitated the buildup of $Li^+$. A COF built with dehydrobenzoannulene (DBA) unit has been reported to exhibit reversible redox reactions.[246] The self-exfoliated COF (PDASA) with triazole and phloroglucinol redox-active groups was also successfully synthesized[247] and employed as a LIB anode. The COF underwent exfoliation, breaking into small nanosheets. This process shortened the diffusion pathways for lithium ions, resulting in a notable capacity of 720 mAh $g^{-1}$. The high capacity was attributed to the presence of two redox-active groups capable of reversibly binding lithium ions, along with the increased redox sites following exfoliation. Upon further investigation into the charge storage mechanism, it was discovered that the short linker in the PDASA COF generated nanospaces with densely packed functionalities (as depicted in Figure 9e). In addition to this, PDASA COF contained functionalities that also enhanced the capacity retention of the material (Figure 9e,f). The functional group within PDASA acted as a Lewis acid, allowing it to form weak bonds with $Li^+$ ions.

In another report, Buyukcakir et al. developed a unique rCTF COF containing triazine, benzene, and anthraquinone sites to sustain multiple redox reactions in the structure (shown in **Figure 10**a–c).[248] The strong triazine linkages of rCTF provided a robust polymeric framework with outstanding electrochemical durability through the creation of a conjugated framework. More readily, accessible redox-active sites are produced because of the gradual structural deformation of rCTF during activation. The anode exhibited a specific capacity of up to 1190 mAh $g^{-1}$ at 0.5C at a current density of 300 mA $g^{-1}$ after 500 cycles. The

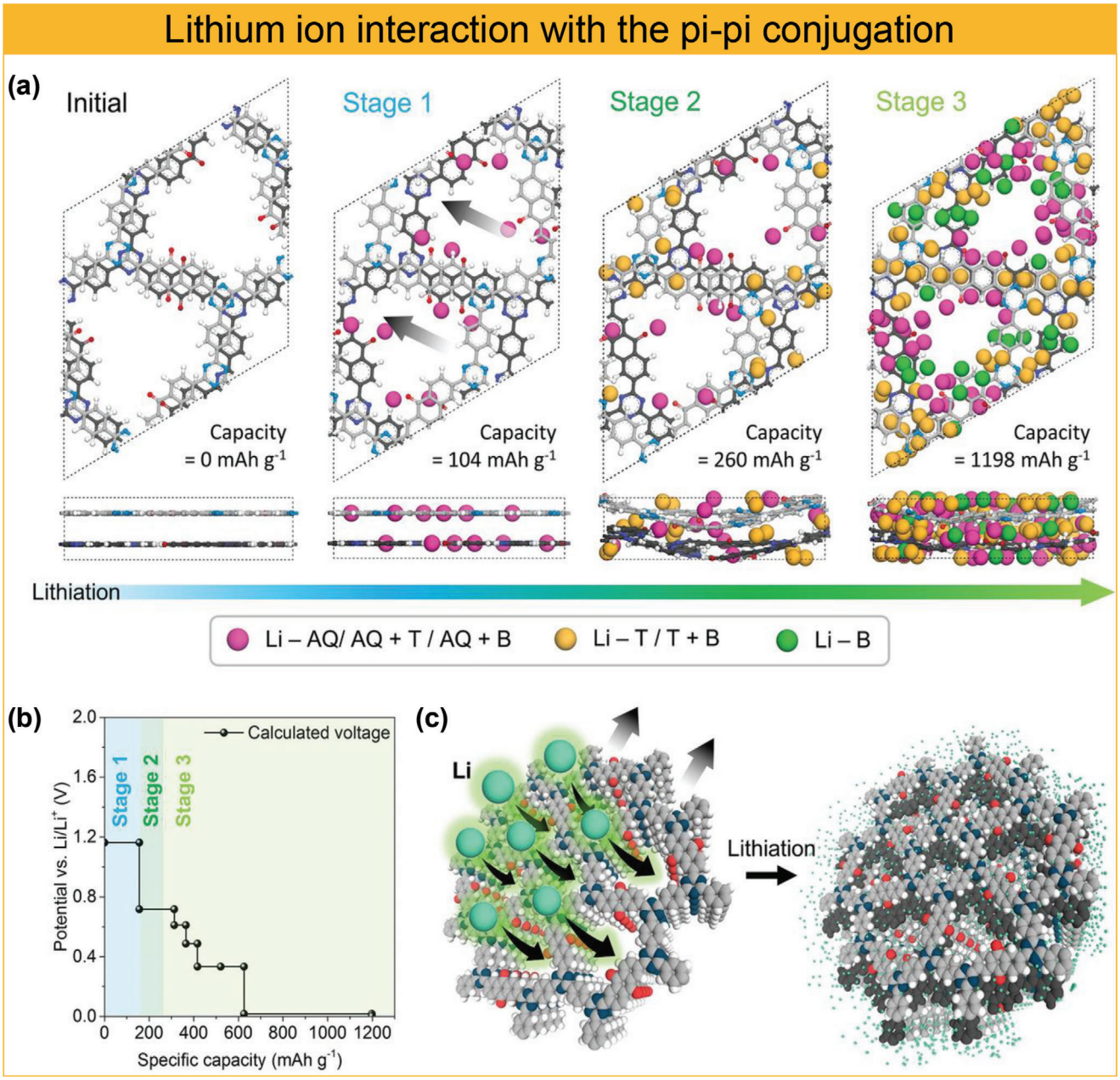


**Figure 10.** a,b) Different lithiation stages in rCTF COF, and c) scheme of lithiation in rCTF structure. Reproduced with permission.[248] Copyright 2020, John Wiley & Sons.

presence of several functional groups and the small particle size of the COFs facilitated the $Li^+$ migration and electrolyte diffusion, leading to an astounding rate capability of over 500 mAh $g^{-1}$ at 20C. The charge storage mechanism was studied by DFT calculations showing the participation of the quinone linkages (1 $Li^+$ per C═O) in the first stage of the reaction. In the second stage, $Li^+$ started to react with the nitrogen groups of the triazine rings. With the insertion of more lithium, structural changes started to take place, as highlighted in the stage 3, which generated new active sites such as C═O, C═N, C═C, and the conversion of benzene carbons to $sp^3$ hybridization. In the final stage, a subunit of the rCTF was capable of storing up to 23 $Li^+$ ions. These findings are valuable not only for the better understanding of the EES mechanism in COF-based LIB electrodes, but also to highlight the potential of such frameworks as high-performance LIB electrode materials.

Recent studies have explored lithium bis-(trifluoromethanesulfonyl) imide (LiTFSI) as a solvent for the synthesis of COFs. For instance, Zhou et al. used a novel method to synthesize the CTF-1 system using LiTFSI under ionothermal conditions.[249] It was discovered that LiTFSI not only served as a promoter, but also helped to create LiF particles in situ and distribute them uniformly throughout the framework. In the context of lithium-based anodes, the hierarchical

framework formed by CTF-LiF on the anode surface exhibited remarkable properties. These included strong lithiophilicity, excellent interfacial stability, and a substantial lithium storage capacity. Furthermore, in addition to their redox-active properties, the presence of conjugated $\pi$–$\pi$ interaction sites within the structure also contributed to the storage of lithium ions. In conclusion, the limitations of pristine COFs as anode materials for LIBs, various modifications, and synthetic strategies have been employed to enhance their electrochemical performance. One approach involves functionalizing COF structures with carboxyl and nitrile groups, which not only improve conductivity but also increase the number of active redox sites and hinder the dissolution of active materials in the electrolyte through pi-pi interactions. Another method focuses on incorporating redox-active groups such as triazole, phloroglucinol, benzene, and anthraquinone into the COF backbone to enable reversible binding of lithium ions.

*Exfoliated COF Composites as Anode Materials for Lithium Ion-Batteries*: COFs have the potential to serve as alternative anodes due to their composition of lightweight atoms. However, for COFs to effectively replace the commonly used graphite anodes, they need to provide a sufficient number of sites where lithium can reside within their unit cells. Exfoliating the COF material can facilitate the attachment electroactive surface groups, which, in turn, could lead to higher capacities and faster charging. Haldar et al. demonstrated how anthracene-based COFs can be chemically exfoliated into nanosheets, consisting of several layers, using maleic anhydride as a functionalizing, exfoliation and pillaring agent (**Figure 11**a–h).[250] The exfoliated COF provided abundant lithiophilic carbonyl functional groups, with a total Li-storage capacity of 120 atoms per unit-cell (vs one Li per C6 for the case of graphite) (Figure 11g). A full-cell device employing this COF as anode and $LiCoO_2$ as cathode delivered a specific capacity of 220 mAh $g^{-1}$ during a 200-cycle period. In another example of exfoliated COFs, a few-layered 2D-COF of (E-TFPB-COF) was exfoliated using a chemical stripping process and the restacking was prevented by introducing $MnO_2$ nanoparticles between the layers (Figure 11i–l).[204] The electron microscopy images of the exfoliated COF clearly showed the presence of thin films being exfoliated and decorated with $MnO_2$. Exfoliation enabled faster ion/electron kinetics than the bulk TFPB-COF, and displayed active Li-storage sites linked to the exposed by the exfoliation conjugated aromatic moieties. After 300 cycles, the E-TFPB-COF/$MnO_2$ and E-TFPB-COF electrodes displayed superior and reversible capacities of 1359 and 968 mAh $g^{-1}$, respectively (Figure 11m). In situ Raman and FTIR spectroscopies for the exfoliated and the bulk COF it was found that $Li^+$ was interacting with the C═C groups in the conjugated C6 rings, the C═N groups, and with the Mn-O groups (Figure 11n–q). It was also observed a reduced amount of $sp^2$ carbons in Raman, indicating the interaction of $Li^+$ with benzene rings. In the case of the bulk COF, the C═N groups were found to interact with $Li^+$ whereas C═C and benzene groups were found to be mainly inactive toward Li storage.

In a different approach, well-distributed $Co_3O_4$ nanoparticles on N-doped porous carbon were obtained from the carbonization of a MOF/COF composite.[251] In particular, the ZIF-67/COF hybrid was produced by growing ZIF-67 microcrystals in the presence of benzoic acid-modified COF units. The final $Co_3O_4$/NPC composite was synthesized after the calcination of ZIF-67/COF. The fine dispersion of $Co_3O_4$ nanoparticles was achieved due to the interactions developed with the benzoic acid groups which were present on the starting COF. Due to the COF's porosity, the produced $Co_3O_4$/NPC exhibited an SSA of 228.0 $m^2$ $g^{-1}$, and when tested as an anode for LIBs it delivered 785 mAh $g^{-1}$ of specific capacitance at 500 mA $g^{-1}$. DFT calculations showed that the exceptional morphology and electronic band structure of $Co_3O_4$/NPC, and improved the adsorption/desorption of electrolytes and ions and accelerated electron transport. **Table 1** shows the comparison of different COF materials as anode and cathode for Lithium batteries.

### 6.1.2. COFs for Na/K-Ion batteries

To meet the increasing need for sustainable and cost-effective EES technologies, concerted efforts are focused on investigating alternative energy storage chemistries beyond lithium-ion batteries, as a way to circumvent the limited lithium resources. Consequently, there is a growing interest for the adoption of new alkaline-ion batteries, involving elements like Na and K. Currently, organic electrode materials face several challenges when it comes to their use in Na/K-ion batteries.[252–255] Consequently, the design and development of new organic electrode materials to enhance their efficiency in the respective chemistries is of paramount importance. In this section, the latest developments in the application of structural frameworks related to COFs for Na/K-ion batteries (NIBs/PIBs) are discussed.

*COFs for Na-Ion Battery Applications*: NIBs are a promising chemistry for energy storage, due to their similar chemistry to LIBs (thus compatible with current production methodologies), abundance in nature, and economic benefits. The reaction potential of Na (−2.71V) is remarkably close to the reaction potential of Li (−3.04 V). However, SIBs have much lower energy densities and cycle stability than LIBs, due to the bigger radius than Li that causes significant volume changes in the electrode materials throughout the charge-discharge process. The continuous volume changes during charging/discharging create voids in the material and lead to the loss of conductive pathways. Commercial graphite anode is incompatible with SIBs due to the larger $Na^+$ ions which do not intercalate into the graphite layers. In the pursuit of developing COF-based electrodes for SIBs, Park et al. demonstrated that few-layered COF nanosheets could display large charge-carrier conductivity by securing the planarity of the polymer framework backbone and by increasing the SSA, eventually leading to high Na-ion storage capacities.[256] By using different monomer combination to build COF, the macromolecular ring diameter has been tuned from 2.8 to 4.2 nm. The sample prepared with solvothermal method and having 2.8 nm of ring diameter showed 250 mAh $g^{-1}$ of capacity for 30 cycles at 100 mA $g^{-1}$, when used as an anode for SIBs. Liu et al. produced crystalline, layered, millimeter-sized CTF COF through liquid sonication and mechanical exfoliation process for NIBs.[257] The obtained CTF displayed an AB stacking motif with 0.6 nm of pore size, which is unique compared to AA stacking found commonly in COFs. Computational studies demonstrated that the specific interaction of triflic acid molecules with CTFs contributed to the AB stacking. The nanosheets of CTF

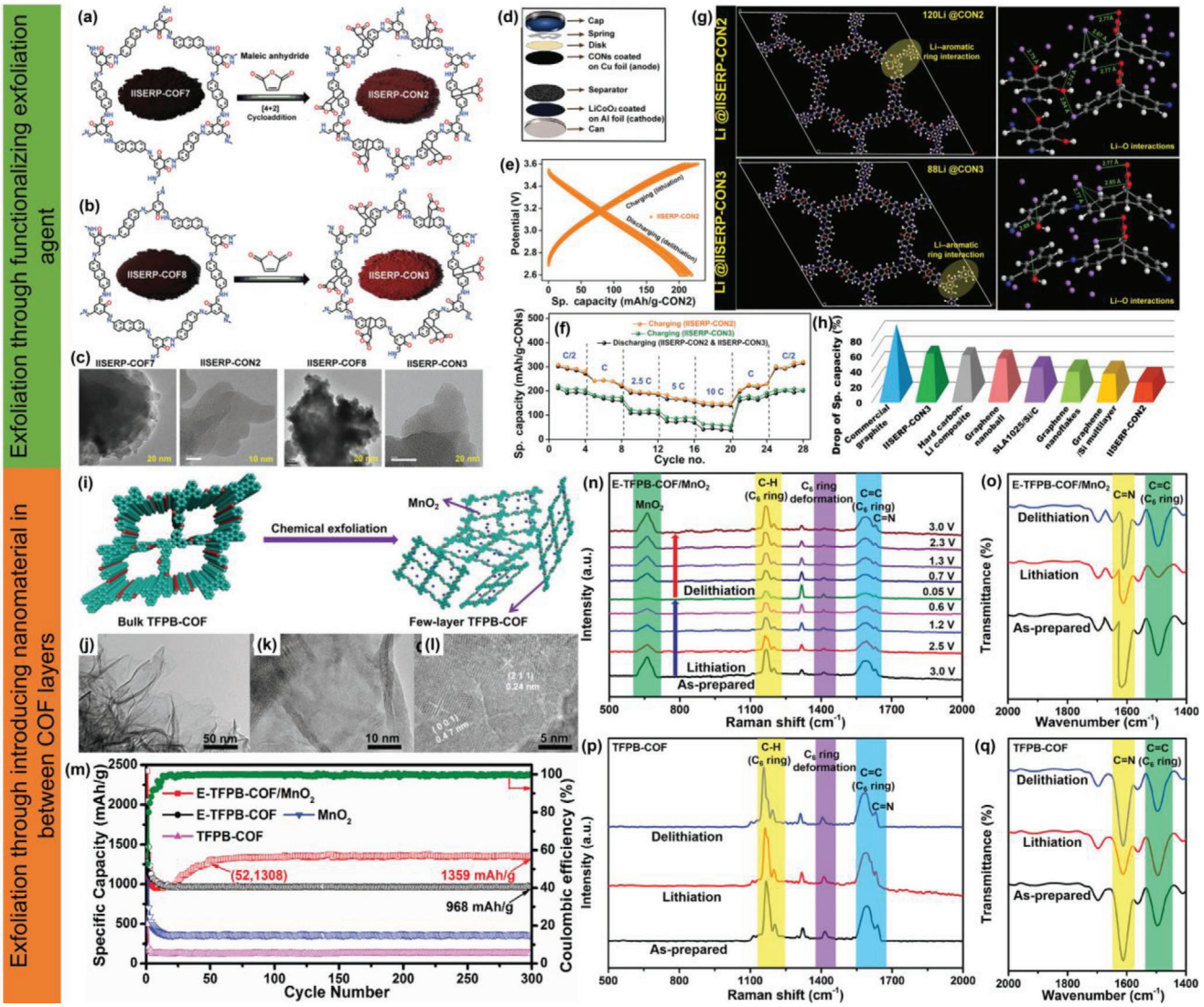


**Figure 11.** Exfoliation strategy for COFs: a,b) exfoliation of IISERP-COF-7 and IISERP-COF-8 COFs through their functionalization with maleic anhydride, c) TEM images of COFs before and after exfoliation, d) cell assembling utilizing the COFs as anodes, e) charge–discharge of IISERP-CON-2, f,g) rate performance and $Li^+$ interaction sites in the exfoliated COFs, h) capacity retention of the COFs and other materials (reproduced with permission,[250] Copyright 2019, John Wiley & Sons), i) exfoliation of TFPB-COF by inserting $MnO_2$ nanoparticles, j–l) TEM image of the exfoliated COF, m) cycling performance of different COFs, and n,o) in-situ Raman and FTIR for the exfoliated COFs and p,q) for bulk COF (reproduced with permission,[204] Copyright 2019, John Wiley & Sons).

experienced only a 5% capacity loss over 1200 cycles retaining 198 mAh $g^{-1}$ of the initial capacity. Apart from this, increasing the porosity of the material further enabled improved diffusion paths for $Na^+$ in the host material. In this direction, Patra et al. produced a novel micro-spherical COF structure (TFPB-TAPT COF) with an opened and ordered nanoporous framework. The COF showed extended cycle stability and initial reversible capacity (246 mAh $g^{-1}$) with a diffusion coefficient of $6.275 \times 10^{-15}$ $cm^2$ $s^{-1}$.[258] The interlayer distance of (002) plane is ≈3.4 Å, which is suitable for ion insertion in the TFPB-TAPT COF. During ion insertion/extraction, there is an increase in the interlayer distance (3.4–3.8 Å), which is observed in in-situ XRD where the peak position shifted from 25.8° to ≈22°. From the HRTEM analysis, the reversible structural changes have also been observed at different charging–discharging voltages. Jagt et al. synthesized four PI-based COFs by combining aromatic triamines with aromatic dianhydrides.[259] DFT calculations illustrated the preferred assembly of imide linkages in an eclipsed perpendicular stacking, thereby breaking the 2D symmetry and shrinking the channel diameter, while also expanding the pore wall thickness. At a working potential over 1.5 V vs $Na/Na^+$, these specific geometric shapes provided a framework for $Na^+$ intercalation and stable cycle life. The nitrogen on the amine linkages provided greater rotational flexibility which made torsion significantly more durable in COF structures with the TAPA connecting molecule. On the other hand, a study found that the integration of redox-active quinones in COFs through linkers significantly enhances their electrochemical performance when applied

**Table 1.** Electrochemical performance comparison of different COF structures and its composites for Lithium Batteries.

| Electrode | Material | Electrolyte | Potential vs $Li/Li^+$ [V] | CC/DC/R | Cyclic stability RC/R/CN | Refs. |
|---|---|---|---|---|---|---|
| Cathode | Tp-DANT/COF | 1 M $LiPF_6$ in DMC/EC/EMC | 1.5–4.0 | 78.9,93.4,200 | 92.3/200/200 | [196] |
| Cathode | Tb-DANT/COF | 1 M $LiPF_6$ in DMC/EC/EMC | 1.5–4.0 | 135.4/144.4/50 | 80.1/200/300 | |
| Cathode | DAAQ-ECOF | 1 M LiTFSI in TEGDME | 1.5–4.0 | -/145/20 | 104/500/1800 | [197] |
| Cathode | PCT-1 | 1 M $LiPF_6$ in EC/DEC | 1.75–3.0 | -/288/500 | – | [198] |
| Cathode | PIBN-G | 1 M LiTFSI in DOL and DME | 1.5–3.5 | -/271/0.1C | 271/0.1C/300 | [201] |
| Cathode | E CIN-1/CNT | 1 M $LiPF_6$ in EC/DEC | 0.001–3.0 | 520/1269/100 | 744/100/250 | [203] |
| Cathode | BQ1-COF | 1 M LiTFSI in DOL/DME | 1.2–3.5 | -/321/390 | 158/3870/1500 | [174] |
| Cathode | F-CQN-1-600 | 1.2 M LiPF6 in EC/EMC | 1.5–4.5 | -/250/100 | 120/2000/2000 | [205] |
| Cathode | 2D PAI@CNT | 1 M LiTFSI in DOL/DME | 1.5–3.5V | – | 104.4/100 | [168] |
| Cathode | CTF/rGO | 1 M LiPF6 in EC/DEC | 1.5–4.5 | -/235/100 | – | [209] |
| Cathode | PIX/rGO | 1 M LiTFSI in DOL/DME | 1.5–3.4 | -/172/500 | – | [215] |
| Cathode | IEP-11 | 1 M LiTFSI in DOL/DME | 1.5–3.5 | -/147/149 | – | [216] |
| Cathode | AQ-COF@CNT | 1 M LiTFSI in TEGDME | 1.5–3.5 | -/144/50 | 131/500/3000 | [218] |
| Cathode | Pyr-2D COF | 1 M $LiPF_6$ in EC/DEC | 2.8/4.5 | -/210.1/600 | – | [220] |
| Cathode | COF-TRO | 11 M $LiPF_6$ in EC/DEC | 0.5–4.5 | */268/0.1C | | [241] |
| Anode | PA-COF | 1 M $LiPF_6$ in EC/DEC/DMC | 0.01–3.5 | 267/321.9/1000 | 401.3/100/500 | [171] |
| Anode | TB-COF | 1 M $LiPF_6$ in EC/DEC/DMC | 0.01–3.5 | 262.4/311.4/1000 | 379.1/100/500 | |
| Anode | Cz-COF1 | 1 M $LiPF_6$ | 0.005–3.0 | -/628/100 | 236/200/400 | [243] |
| Anode | JUC-526 | 1 M $LiPF_6$ in EC/DEC | 0.01–3.0 | 509.6/750.6/50 | 503.3/100/500 | [245] |
| Anode | DBA-COF 3 | 1 M $LiPF_6$ in EC/DMC | 2.0–4.0 | -/522/50 | 207/50/90 | [246] |
| Anode | rCTF | 1 M $LiPF_6$ in EC/DEC | 0.005–3.0 | -/1750/300 | 1190/300/1000 | [248] |
| Anode | IISERP-CON1 | 1 M $LiPF_6$ in EC/DMC | 0.01–3.0 | -/2060/100 | 720/100/100 | [247] |
| Anode | IISERP-CON2 | 1 M $LiPF_6$ in EC/DMC | – | -/790/100 | – | [250] |
| Anode | E-TFPB-COF | 1 M $LiPF_6$ in EC/DEC | 0.005–3.0 | 1211/-/100 | 968/100/300 | [204] |
| Anode | E-TFPB-COF/$MnO_2$ | 1 M $LiPF_6$ in EC/DEC | 0.005–3.0 | 1274/2423/100 | 1359/100/300 | |

Abbreviations: LiTFSI- lithium bis(trifluoromethanesulfonyl)imide, DOL- 1,3-dioxolane DME- dimethoxyethane, DMC- dimethyl carbonate, EC- ethylene carbonate, DEC-diethyl carbonate, TEGDME- tetraethylene glycol dimethyl ether, EMC-ethyl methyl carbonate, CC-charge capacity (mAh $g^{-1}$), DC-discharge capacity (mAh $g^{-1}$), R-Rate (mA $g^{-1}$), RC- Reversible capacity (mAh $g^{-1}$), CN- Cycle number.

as electrodes. These COFs are stable preventing the dissolution of quinones in the organic electrolytes, while their ordered, porous structures facilitate ion diffusion. Enhancing these frameworks with linkers that contain additional replaceable sites further amplifies the redox-active components in COF electrodes, thereby boosting their specific capacities. A COF was synthesized by condensing 2,6-diaminoanthraquinone (DAAQ) with hexachlorocyclotriphosphazene (HCCP), a linker endowed with six replaceable chlorine sites, resulting in an ordered porous DAAQ-HCCP COF.[260] During the condensation process, all chlorine sites in the HCCP linker were substituted with the redox-active DAAQ molecules, markedly enriching the framework's content of electroactive groups. The resultant DAAQ-HCCP COF outperformed DAAQ in terms of cycling stability and exhibited superior rate performance as an anode in SIBs. The COF demonstrated specific capacities of 88 mAh $g^{-1}$ at 100 mA $g^{-1}$ after 100 cycles and maintained 72 mAh $g^{-1}$ at 2 A $g^{-1}$ after 1000 cycles.

The dissolution of active materials in NIBs is known to be a severe limitation that restricts stability. On this basis, Ha et al. reported the mitigation of active material dissolution in electrolytes and increased electron mobility of organic electrodes by esterifying 2,5-dihydroxyterephtalic acid (DHTPA) into carbon black (CB).[261] The sample DHTPA/CB showed outstanding rate capabilities and maintained 90% of its initial capacitance after 100 cycles. The coulombic efficiency during the initial cycle was approximately 74.2%, which was ascribed to the irreversible decomposition of the electrolyte leading to the formation of a SEI. Additionally, the detachment of the weakly-grafted DHTPA onto the CB surfaces contributed to this phenomenon. The storage of Na can also be enhanced by incorporating functional groups that can

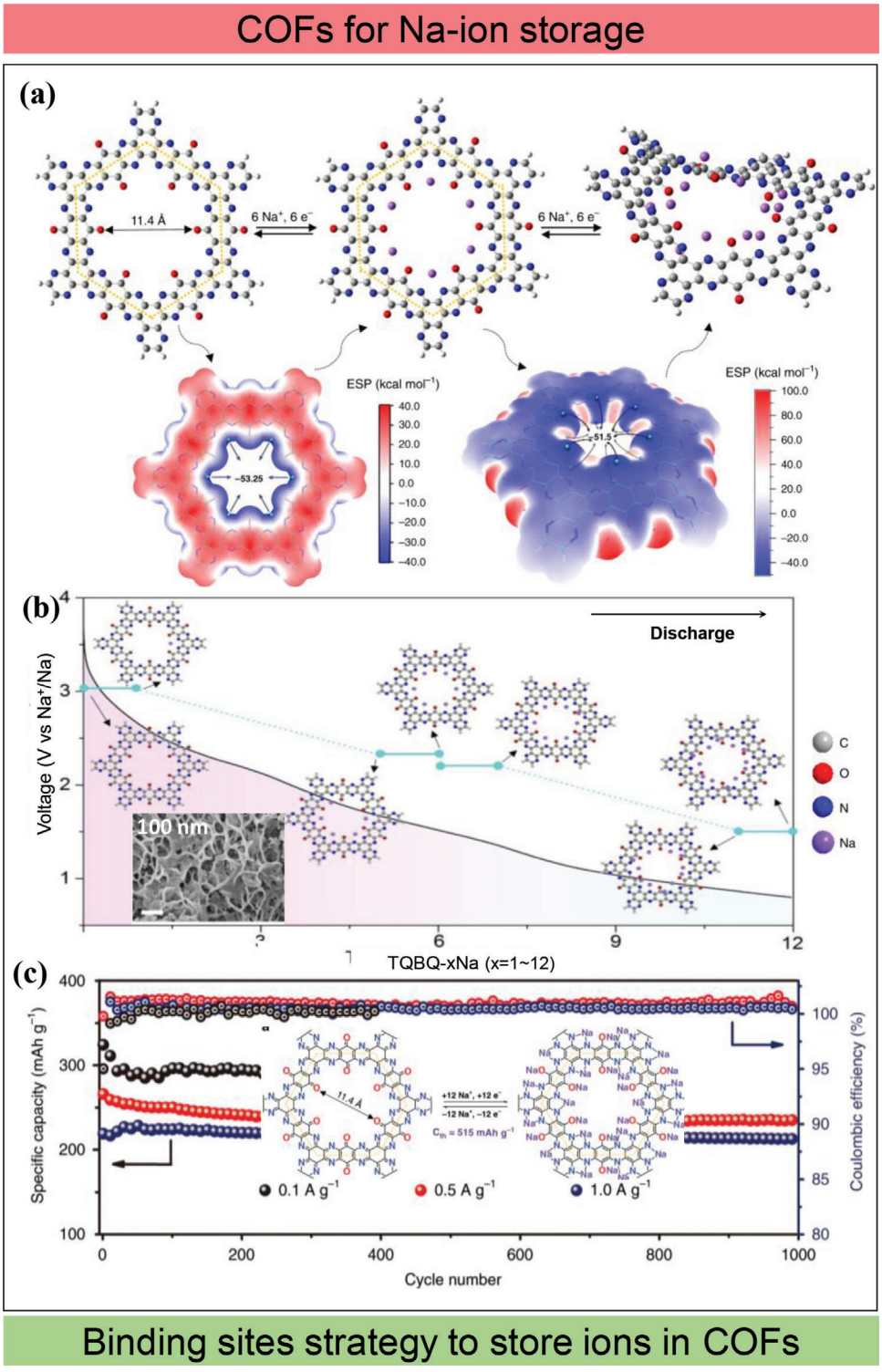


**Figure 12.** Binding sites strategy to store ions in COF structure: TQBQ for Na-ion batteries. a) DFT calculation on TQBQ COF to determine the Na binding sites, b) schematic of structural changes during discharging (inset: SEM image of TQBQ COF), c) cyclic stability of TQBQ at different charge–discharge rates (inset: attachment of $Na^+$ ions at the COF single unit). Reproduced with permission.[262] Copyright 2020, Springer Nature.

**Table 2.** Electrochemical performance comparison of different COF structures and its composites for NIB and PIBs.

| Anode Materials | Electrolyte | Potential (V) | CC/DC/R | RC/R/CN | Refs. |
|---|---|---|---|---|---|
| CON-16 | 1 M $NaClO_4$ in PC/FEC | 0.01-2.5 | -/850/100 | 250/100/30 | [256] |
| 2DP | 1 M $NaPF_6$ in EC/DMC | 0.01-2.5 | -/262/100 | – | [257] |
| TFTB-TAPT COF | 1 M $NaPF_6$ in EC/DMC | 0.05-1.6 | -/246/30 | 125/30/500 | [258] |
| PID | 1 M $NaClO_4$ in EC/DMC | 1.5-3.5 | -81/15 | – | [259] |
| DAAQ-HCCP COF | 1 M $NaPF_6$ in diglyme | 0.1-2.0 | -/209/100 | 88/100/100 | [260] |
| Na-DHTPA/CB | 1 M $NaPF_6$ EC/DMC | 0.01-2.0 | 96/25 | – | [261] |
| TQBQ-COF | $NaPF_6$/DEGDME | 1.0-3.5 | -/452/20 | 352.3/20/100 | [262] |
| COF derived carbon | 1 M $NaPF_6$ in EC/DMC | 0.01-2.0 | – | 330/100/1000 | [265] |
| DAAQ-COF | 1 M $NaClO_4$ in EC/DMC | 0.05-3.0 | -/500/50 | 198/500/1000 | [264] |
| F-COF | 0.8 M $KPF_6$ in EC/DEC | 0.01-3.0 | -/90/1000 | – | [266] |
| AHF@COF | 0.8 M $KPF_6$ in EC/DEC | 0.0-3.0 | -/404/100 | 179/1000/2000 | [267] |
| COF-10@CNT | 1 M KFSI in EC/DEC | 0.05-3.0 | 348/-/100 | 161/1000/4000 | [268] |

Abbreviations: PC-propylene carbonate, FEC-fluoroethylene carbonate, DMC- dimethyl carbonate, EC- ethylene carbonate, DEC-diethyl carbonate, DEGDME- diethylene glycol dimethyl ether, CC-charge capacity (mAh $g^{-1}$), DC-discharge capacity (mAh $g^{-1}$), R-Rate (mA $g^{-1}$), RC- Reversible capacity (mAh $g^{-1}$), CN- Cycle number.

interact with Na. For example, both pyrazines and carbonyls may store 12 $Na^+$ in each block unit, as evidenced by DFT simulations. Based on this, Chen et al. proposed triquinoxaline (TQ) and benzoquinone (BQ) units for the generation of new COF structure, which may reach the theoretical capacity of 515 mAh $g^{-1}$ when used as cathodes for NIBs.[262] The DFT calculations showed that 6 $Na^+$ can bind in the internal ring of the COF unit, whereas 6 $Na^+$ can bind in the outer ring of the COF unit (**Figure 12a**). The synthesized TQBQ COF showed a porous structure that exhibits multiple redox couples, which was manifested by the discharge curves (Figure 12b). The multi-electron redox activity was primarily responsible for the superior energy storage capability. TQBQ also showed high cycling stability with 96.4% of capacitance retention after 1000 cycles (Figure 12c). In another report, dual electroactive centers and trimodal (i.e., macro–meso–micro) pore structure were attained by using an eco-friendly oxidative polymerization strategy with conjugated poly(2,4,6-tri(thiophen-2-yl)-1,3,5-triazine).[263] The highly conjugated molecule, exposed electroactive sites, and displayed low solubility in the electrolyte delivering high-rate performance and cyclic stability as a NIB anode. In-situ TEM studies revealed 12-electron reaction with dual electroactive centers and 6–25% of volume expansion.

In the context of organic materials for EES, radicals play a crucial and inevitable role during the charging and discharging cycles. Enhancing the reactivity of these radicals can significantly boost both capacity and rate capability, yet it poses a challenge to the cycling stability of the electrodes and electrolytes. Balancing the redox reactivity and stability of these radicals is essential for optimizing electrochemical properties. Gu et al. reported the redox behavior and adjustable stability of radical intermediates within COFs, which showed promise as high-capacity and stable anodes in SIBs.[264] Experimental data and theoretical simulations, demonstrated that the redox activities of C—O and $\alpha$-C radical intermediates were crucial in the sodiation/desodiation cycles. Importantly, the stacking properties of these radicals within the 2D COFs could be fine-tuned through control of the COF thickness, directly influencing their redox reactivity and stability. For instance, a COF with a thickness of 4–12 nm demonstrated a specific capacity of 420 mAh $g^{-1}$ at 100 mA $g^{-1}$, maintaining 99% retention over 10 000 cycles at 5 A $g^{-1}$. The **Table 2** below shows the comparison of different COF structures as electrodes for sodium and potassium ion batteries.

*COFs for K-Ion Battery Applications*: Potassium ion batteries (PIBs) are another potential replacement for LIBs due to their similar chemistry with Li and Na. For instance, K metal exhibits almost equal potential for $K^+/K$ (−2.92 V) when compared to $Li^+/Li$ (−3.04 V). Additionally, $K^+$ is less acidic than $Li^+$ and $Na^+$ in terms of Lewis acidity, which increases its transfer number and mobility. However, the large size of potassium can produce strain in the electrode material which can lead to the degradation of the active material. Regarding this, due to the structural flexibility and open-pore channels, organic electrodes can provide more reactive sites and transmission pathways for K storage compared to inorganic ones. Creating a carbon material endowed with all these properties is challenging, however, PIBs can benefit from the versatile and diverse chemistry, structure, and properties of COFs. Lee et al. created a fluorine-rich COF (F-COF) as a cathode for PIBs.[266] F-COF improved the reversibility of bond transitions during charge/discharge cycles by stabilizing the intercalation kinetics of $K^+$ ions and strengthening their electron affinity and conductivity. Hence, F-COF outperformed the pure COF-based electrodes lacking F atoms by offering a high specific capacity of 95 mAh $g^{-1}$ at 5 C with exceptional cycling stability achieving ≈ 99.7% capacity retention after 5000 cycles. In another report, a COF was used as a precursor to produce a carbon material with homogeneous co-doping of nitrogen and phosphorus.[267] The evolving gaseous side-product during the pyrolysis of COF enlarged the interlayer spacing of the carbon layers to ≈0.4 nm. The resulting N and P doping served as active sites for $K^+$ adsorption with improved binding strength. When used as an anode, the material retained exceptionally long-term stability with high reversible K-ion capacity (179 mAh $g^{-1}$ over 2000 cycles). Often CNTs are used to create conductive pathways for fast electron transfer. Inspired by this, Chen et al. produced a COF/CNT composite (COF-10/CNT) as anode for PIBs.[268] During the synthesis process, the used linker produced

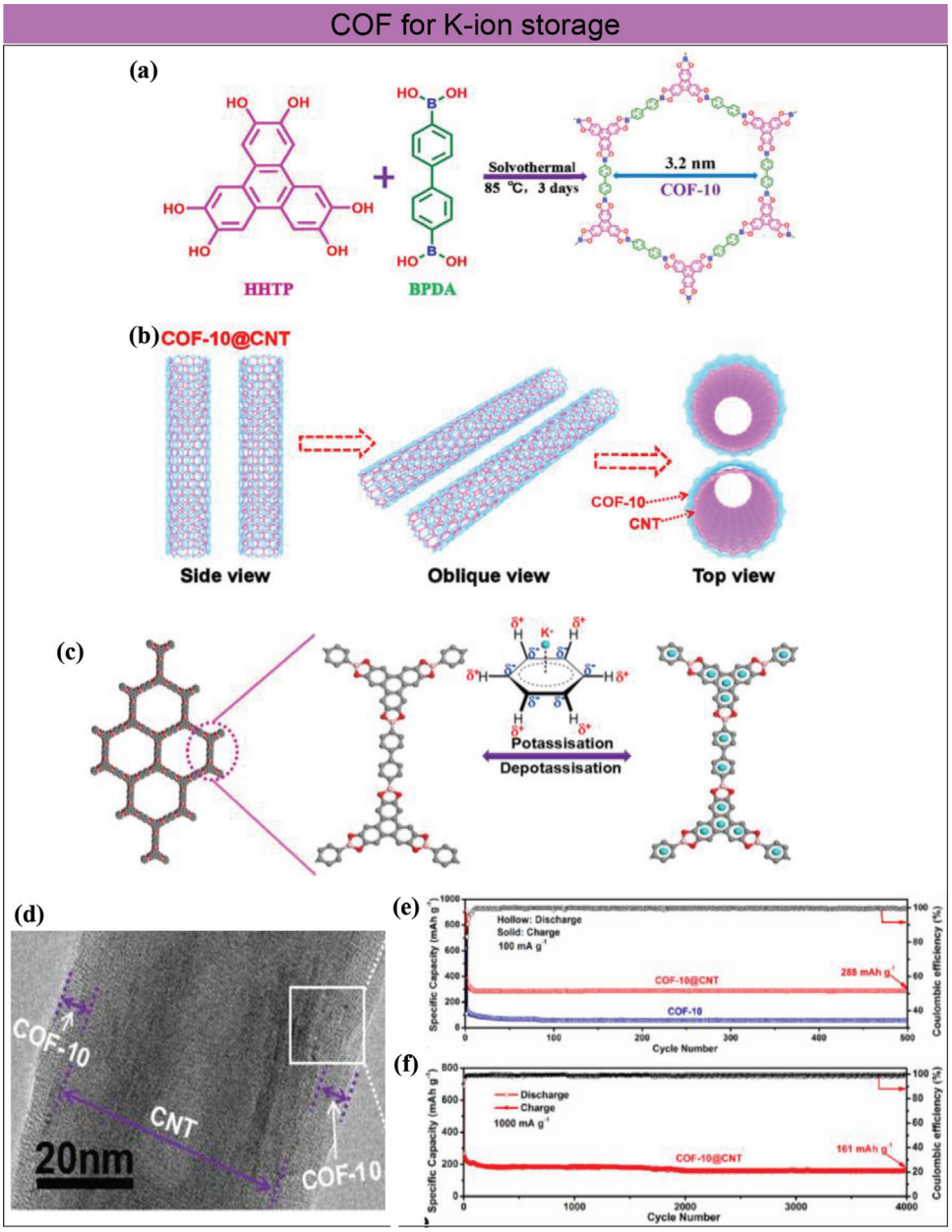


**Figure 13.** COF-10@CNT for K-ion batteries. a) Synthesis scheme of COF-10, b) schematic of COF-10@CNTs structure, c) interaction sites of $K^+$ in COF-10 structure, d) TEM image of COF-10@CNTs, e) cyclic stability comparison of COF-10@CNTs and CNTs at 0.1 A $g^{-1}$, and f) Cyclic stability of COF-10@CNTs at 1 A $g^{-1}$. Reproduced with permission.[268] Copyright 2019, American Chemical Society.

interfacial interactions between the COF and CNTs composite (**Figure** 13a–d). The layered structure of COF with CNTs as an exfoliant and conductivity promoter induced a large number of active sites. Further, the pi–pi conjugated motives in the COF structure provided the binding site for $K^+$ (Figure 13c). The sample delivered 288 mAh $g^{-1}$ of reversible capacity when used as an anode. In the absence of COF, the larger size of potassium tends to create more dendrites than lithium. However, the homogeneous and well-organized pore structure of COF prevented the uncontrolled accumulation and deposition of K metal, delivering a substantially more stable life-cycle (Figure 13e, f).

### *6.1.3. COF for Lithium–Sulfur Batteries Applications*

Lithium–sulfur batteries (LSB), are environmentally friendly EES technologies, with low cost, and have a significantly higher capacity value (1672 mAh $g^{-1}$) and energy density (2600 Wh $kg^{-1}$) than LIBs. However, LiS batteries are limited by several challenges, including the short cycle life due to the shuttle effect of polysulfides and large volume changes in the cathode. Recent research on LSBs has primarily centered around the advancement of sulfur carrier materials to alleviate some of the challenges associated with these battery chemistries. COFs, known

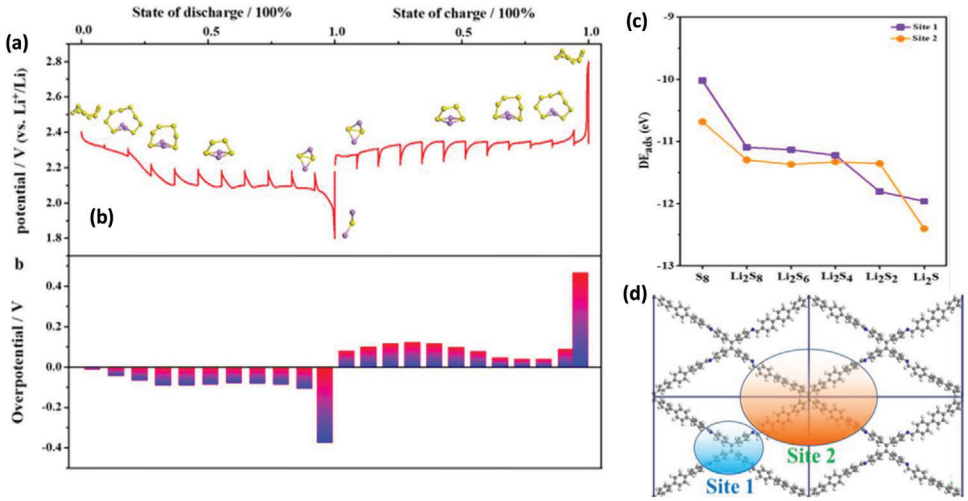


**Figure 14.** Reduction of LiPSs by introducing binding sites in the COF structures. a) Galvanostatic Intermittent Titration Technique (GITT) curve of the COF-ETTA-ETTCA-S cathode showing different LiPSs products at different states of charge, b) overpotential values from experimental data at different steps, c,d) binding energy of different LiPSs species with site 1 (imine) and site 2 (12 phenyl rings) in the COF structure. Reproduced with permission.[274] Copyright 2020, American Chemical Society.

for their outstanding crystallinity and adjustable pore size distribution, have emerged as a promising solution to tackle the shuttling effect. Further, COFs have also been investigated as efficient frameworks for incorporating elemental sulfur into Li–S batteries, yielding significant advances.

*COFs as Inhibitors for Polysulphide Shuttling in Li–S Batteries*: LSBs are constrained by an irreversible shuttling mechanism, involving lithium polysulfides[269] and for this reason, it is extremely challenging to create cathodes that can sufficiently mitigate the lithium polysulfide (LiPSs) shuttling.[270] It is currently accepted that lithium polysulfides can be accommodated in N-doped porous carbons due to the interaction of N with·Li-polysulfides via the electron-rich $\pi-\pi$ conjugated moieties, which also promote high electrical conductivity.[271–273] Based on this knowledge, Lu et al. created a 2D COF (COF@ETTA@ETTCA) architecture with a large interlayer space and uniform micropore network, containing several conjugated units which could store 88.4 wt.% of sulfur.[274] The galvanostatic intermittent titration technique showed the presence of multiphase Li-polysulfide products during the charging–discharging processes (**Figure 14a**), with a maximum polarization near 0.5 V (Figure 14b) which was dependent on the scan rate indicating the involvement of interfacial processes (solid–solid/solid–liquid). The imine units in the COF structure acted as strong linkers of the building blocks, and coordination sites for $Li^+$ cations through their N atoms. The material demonstrated exceptional electrochemical performance, including a high theoretical capacity of 1617 mA h $g^{-1}$ at 0.1 C, satisfactory rate capability, and a low-capacity decay (0.077% per cycle after 528 cycles at 0.5 C). DFT calculations revealed the structural factors contributing to the high performance of the battery, emphasizing the role of high degrees of conjugation and high interlayer space of 4.8 Å. Particularly, the adsorption energy of smaller-sized LiPS species (such as $Li_2S$, $Li_2S_2$, and $Li_2S_4$), into the COF's interlayer space was more negative (i.e., stronger adsorption) for the smaller Li-polysulfide species (which are also more prone to shuttling effects), indicating their effectively stabilization within the COF layers. DFT calculations also revealed the strong binding of Li-polysulfides with the two types of conjugated regions present in the COF structure (the 12 phenyl rings -site 2) and the tetraphenylethene units with imines (site 1) (Figure 14c,d). Notably, the adsorption of Li-polysulfides at site 2 was more robust than at site 1, attributed to the higher degree of conjugation in the former. The findings overall suggest that the COF-ETTA-ETTCA exhibits a strong interaction with Li-polysulfides due to the combination of abundant electron-rich conjugated regions, nitrogen atoms, and the well-suited interlayer space. This synergy was considered a key factor behind the exceptional electrochemical performance of the COF-ETTA-ETTCA-S cathode.

In another report, sulfur-mediated polymerization of dinitrile monomers was used to generate a novel class of highly permeable phthalazinone-based COFs (P-COFs) with rGO.[275] The sample delivered an initial specific capacity of 1130 mAh $g^{-1}$ at 5 C and a remarkable capacity retention of 81.4% after 500 cycles. The organized nanoporous structure of COF facilitated effectively the suppression of LiPSs shuttling, promoted by the strong interaction of sulfur with the polar groups of phthalazinone and triazine in COF structure (**Figure 15a–c**). Polar materials with strong anchoring units have been proven effective for avoiding the shuttle effect even for high-order $Li_2S_x$ intermediates. Consequently, COFs with polar sites acting as chelators can also mitigate polysulfide shuttling. In this direction, COFs based on eight types of linkages in COFs, including triazine (Tr), borazine (Bz), secondary amine (SA), boronate ester (BE), imide (Im), amide (Am), and hydrazone (Hy) were investigated theoretically. These linkages were joined by benzene groups to form hexagonal COF structures. and studied as a cathode for Li–S batteries.[276] The nucleophilic groups at the branches enhanced the anchoring capacity of polysulfides inside the nanoporous COFs. Particularly, the synergistic effect of oxygen atoms in the secondary amine linkages and the sequence of the N1–N2–C–O1 atoms acted as "clamp" for LiPS, improving their immobilization. The COFs

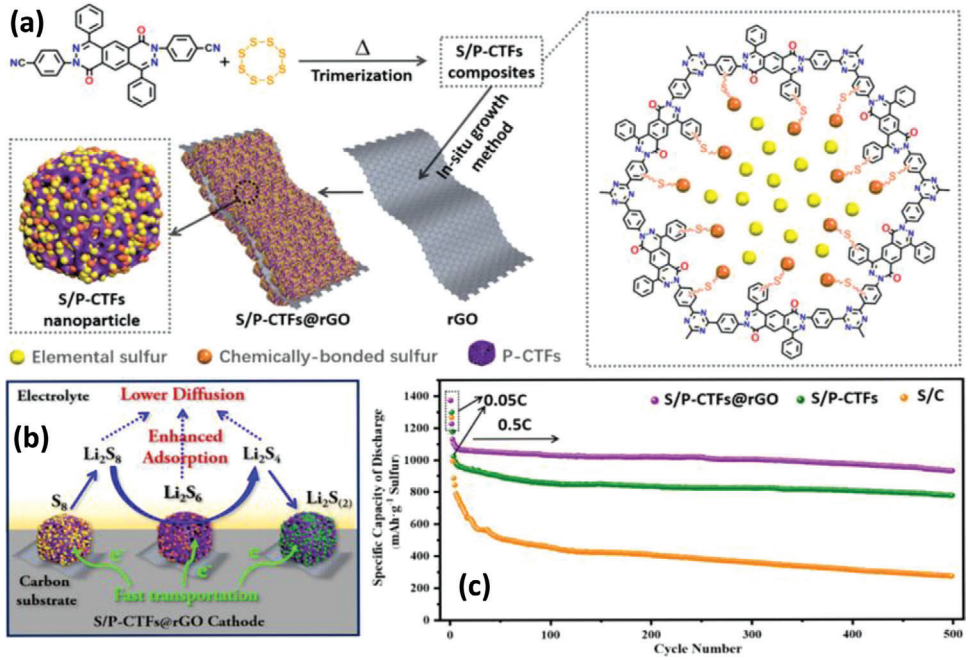


**Figure 15.** a) Synthesis of S/P-CTF@rGO composites, b) the discharge process in S/P-CTF@rGO cathode, c) the cyclic performance of different cathode materials. Reproduced with permission.[275] Copyright 2020, American Chemical Society.

based on the secondary amines, on hydrazone, and on functionalized (with a nucleophilic group branch of $-OCH_2CH_3$) hydrazone structures showed a strong ability to anchor $Li_2S_x$ and impeded the shuttling of high-order polysulfides.

In addition to the shuttle effect, accelerating the breakdown of $Li_2S$ into LiS and $Li^+$ ions is essential for achieving high coulombic efficiency. Interestingly, lithium-polysulfides ($Li_2S_x$) showed remarkable interaction with single metal atoms which can be used as single-atom accelerators. The use of metal phthalocyanine COFs (MPc@COFs, where M = Ti, V, Mn) as scaffolds within COFs architecture can produce an environmentally benign and effective cathode.[277] DFT studies performed on MPc-COFs cathode for $Li_2S_x$ adsorption and catalytic activity showed that axial coordination compounds are produced by the coordination of LiPS on TiPc-COF and VPc-COF with extraordinarily strong adsorption strength. In another report, a fluorinated covalent organic polymer (F-COP), as a novel approach to enhance the efficiency and durability of Li–S batteries. The fluorination of the polymeric COD backbone played a pivotal role allowing for the covalent attachment of sulfur to the porous polymer framework via nucleophilic aromatic substitution reactions. This chemical bonding leads to high (over 70 wt%) sulfur content in the cathode material.[278] When operated as cathode, the sample delivered an impressive capacity of 1287.7 mAh $g^{-1}$ at 0.05 C.

Moreover, there is a growing interest in enhancing rate performance through the strategy of the homogeneous distribution of heteroatoms. In this context, Zhang et al. conducted an analysis to explore how heteroatoms affect the charge-discharge mechanism in CTFs, with the goal of improving the current electrode materials.[279] Wide surface areas and adequate pore volumes in N, O-containing CTFs cathodes allowed the formation of rapid electron/$Li^+$ transport channels and high sulfur content (70%). The presence of N and O heteroatoms, which possess extra pairs of electrons, was crucial for interacting with the strong Lewis acid of terminal Li atoms in LiPS. This interaction facilitated the redox conversion reactions of polysulfides, which is a key factor in enhancing the performance of Li–S batteries. This approach resulted in an improved capacity 1250 mA h $g^{-1}$ at 0.1 C, a remarkable cycling stability with a capacity retention of 92% at 0.5 C over 300 cycles, and an excellent rate performance of up to 678 mA h $g^{-1}$ at 2 C. Another study by Royuela et al. reported the development of a novel porphyrin-based 2D-COF, named $H_2P$-COF-BATA, incorporating allyl moieties. This design allowed for the loading of sulfur into the COF via diffusion, followed by robust carbon-sulfur binding through inverse vulcanization process involving the copolymerization of sulfur with allyl groups in the COF's channels at high temperatures. The combined effect of covalent bonding and physical encapsulation of sulfur in the COF's pores improved cycling performance and facilitated faster ion diffusion, while alleviating the redox shuttling process in Li-S batteries.[280] In another report, COF-300 & COF-301, having layered porous frameworks and large pore volumes were synthesized.[281] COF-301 was functionalized with abundant hydroxyl groups in the pore walls. These hydroxyl groups enabled COF-301 not only to trap LiPSs via physical adsorption inside the pores but also to capture PSs through chemical interactions, thereby alleviating the shuttle effect. The cycling stabilities of the Li/COF@S cells revealed that COF-301@S had better long-term performance compared to COF-300@S. After 500 cycles at 0.5 C, COF-301@S maintained a capacity of 411.6 mAh $g^{-1}$ with only a 0.081% decay per cycle. This contrasted with COF-300@S, which showed a significantly lower capacity after the same number of cycles. These results highlight the advantage of hydroxyl groups

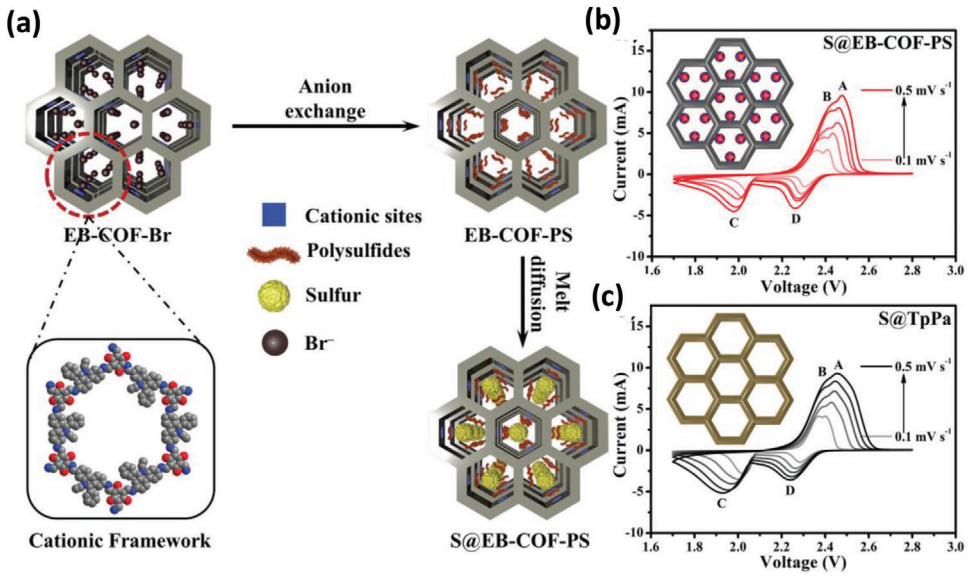


**Figure 16.** a) Synthesis of ethidium bromide-COF-polysulfide (EB-COF-PS), b) CV curve of cationic S@COF (EB-COF-PS) at different scan rates, and c) CV curve of cationic S@COF (TpPa) at different scan rate. Reproduced with permission.[282] Copyright 2020, John Wiley & Sons.

in the pore walls of COF-301 in enhancing the battery performance.

COFs containing cationic sites can improve the shuttling by limiting the LiPSs dissolution.[282] During discharge, cationic active sites accept electrons from the anode and facilitate the rapid breakdown of polysulfides. Conversely, during the charging process, cationic sites can accept electrons from polysulfides and transfer them to the anode, thereby promoting the oxidation of polysulfides. In this direction, ethidium bromide-COF-polysulfide (EB-COF-PS) has been employed as a cathode for LiS batteries. Even at high current densities, cationic COF-based batteries have longer cyclic lifetimes than electrically neutral COFs. The specific capacity was 468 mAh $g^{-1}$ after 300 cycles at 4.0 °C when S@ethidium bromide-COF-PS was used as cathode material for Li-S batteries (**Figure 16**a–c). The analysis of the CV curve of cationic COF and neutral COF showed that the cationic COF expressed a higher slope in the $I$–$v^{1/2}$ curve, indicating a more efficient $Li^+$ transfer. In another report, investigations into the function of N, O, and other heteroatoms to achieve $Li_2S$ nucleation sites reported the utilization of electron donor groups in imine linkages to produce COF-TPT(OH) COF,[283] where the presence of electron donating group (—OH) improved the overall crystallinity as well as rigidity of the framework through hydrogen bonding. Moreover, the large content of N, O, centers and $\pi$-conjugated rings granted large numbers of active sites for LiPSs adsorption. When used as a cathode for Li–S batteries, the sample retained the capacity of 1203 mAh $g^{-1}$ after 80 cycles at 0.1 C charge/discharge rate with 0.045% of capacity decay for each cycle.

*COF as Host Materials for Li–S Batteries*: COFs can serve as porous frameworks for accommodating foreign materials with conductive channels through conjugated linkers. Unlike carbon materials typically used as hosts for sulfur, COFs offer both physical support and chemical interaction. Thanks to their structured pores and functional groups they are capable of housing sulfur. For example, CTF-1 COF stored 34% of sulfur, and it was used as a host material for sulfur.[284] Such high loading capability of the sulfur delivered 1197 mAh $g^{-1}$ of capacity in the first cycle, which was reduced to 762 mAh $g^{-1}$ after 50 cycles. In another report, a porphyrin-based COF demonstrated 55% of sulfur storage.[285] When used as cathode, it delivered 923 mAh $g^{-1}$ of capacity. The SSA of the COFs also plays an important role in storing the high amount of sulfur. In this direction, Py-COF (pyrene-based 2D COF) was produced with SSA of 2000 $m^2$ $g^{-1}$, which resulted in a 74 wt.% of sulfur loading.[286] However, it is also crucial to reduce the shuttle effect in addition to the high sulfur loading by incorporating functionalities with a high binding affinity for sulfur. Wang et al. created fluoro-COF which adsorbed 60 wt.% of sulfur. The presence of fluoro groups could interact with the LiPSs and reduce the shuttle effect even at such high sulfur loadings.[287] When used as a cathode, the material delivered 1120 mAh $g^{-1}$ of specific capacity. After 1000 charging-discharging cycles, the device still retained 22% of its original capacity. Kim et al. proposed an innovative technique for incorporating 1D charged polypyrrole chains into a 2D CTF (cPpy-S-CTF) to improve the conductive pathways along with high loading of sulfur.[288] The strong sulfur interaction of the cPpy-S-CTF leads to 83 wt% sulfur loading. The cPpy-S-CTF containing charged polypyrrole (cPpy) chains formed 3D nanochannels expressing outstanding ionic and electrical kinetics. The cPpy-S-CTF showed 94.1% coulombic efficiency, a specific capacitance of 1203.4 mAh $g^{-1}$ at 0.05 C, and 86.8% capacity retention after 500 cycles. These results indicate that the electrochemical behavior of organosulfur COFs in LiS batteries may be improved through the use of charged polymeric components. Boron/oxygen co-doped carbons (BOC) originating from COF precursors can also enhance the electronic conductivity. Moreover, BOC can interact with polysulfides.[289] Due to the complexity of the molecular structure of such doped surfaces, their potential as useful LiPSs binding sites has not yet been adequately investigated. The BOC

network on the surface of CNTs can be constructed using an appropriate organic condensation polymerization architecture. The COF precursor's homogeneous distribution of boron and oxygen heteroatoms was crucial for enabling uniform doping of carbon-based materials. The BOC@CNT with 68.5 wt.% sulfur exhibited superior LiPS absorptivity and electrochemical characteristics as a cathode for Li-S batteries, resulting into enhanced reversible capacitance (1077 mAh $g^{-1}$) and outstanding cycle life (794 mAh $g^{-1}$). To improve the cycling stability in Li-S batteries, Wang et al. produced an imine-linked material, TAPB-PD@COF (where TAPD stands for 1, 3, 5-tris (4-aminophenyl) benzene and PDA for terephthaldehyde) and utilized it for sulfur loading.[290] The host material could retain 60 wt.% sulphur. The COF structure possessed a beehive-like architecture with high thermal stability (up to 500 °C). Conductivity enhancers of acetylene black (A-B) and super-P (S-P) were employed to improve the electron transport in the material. TAPB-PDA-COF/S@A-B and TAPB-PDA-COF/S@S-P had initial discharge capacities of 991 mAh $g^{-1}$ and 1357 mAh $g^{-1}$, respectively, due to the higher conductivity of S-P in comparison to the A-B additive. When the current density was increased to 2 A $g^{-1}$, the S-P reinforced cathode materials delivered an initial discharge capacity of 630 mAh and 274 mAh $g^{-1}$ after 940 cycles.

To engineer efficient Li–S batteries, it is also necessary to explore alternative ways to boost the performance through the seamless integration of conductive additives due to the insulating nature of sulfur and mitigate the trade-off between high capacity (i.e., high sulfur loading) and reduction in conductivity. For example, Li-S batteries can exploit MXenes, a class of electroactive and conducting materials, as conducting additives in the cathode's host matrix. However, MXenes exhibit poor wettability in organic solvents and interaction with lithium ions. 2D COFs, on the other hand, display considerable surface area promoting sulfur immobilization. Therefore, the combination of MXenes with COFs can bring exciting synergistic effects. In line with this strategy, a stacked covalent triazine scaffold was grown on top of $Ti_3C_2$ MXene nanosheets (CTF/TNS) and tested for LiS batteries.[291] The composite material showed improved kinetics while retaining substantial sulfur and exhibiting fast electron/ion transport. Due to the lithiophilic N sites in CTF and sulfurophilic Ti sites in the MXene structure, polysulfides could bind strongly. The S@CTF/TNS cathode showed a high reversible capacity of 1441 mAh $g^{-1}$ at 0.2 C in addition to outstanding rate and exceptional cycling durability (up to 1000 cycles at 1 C with 0.014% capacity loss per cycle). After 100 cycles, even with a large sulfur loading of 5.6 mg $cm^{-2}$, 94% of the initial capacity was retained. The triazine ring with abundant N atoms and imine linkages was critical for the overall stability of the COF hybrid structure. The presence of C═N bonds also exerted electrostatic repulsion forces increasing the interlayer spacing, which was crucial for creating fast S-transport channels.

In summary, the presence of conjugated moieties and electronegative groups in the material's framework are beneficial for the adsorption of $LiPS_x$, whereas the crystallinity and porous structure of COFs provide fast $Li^+$ and S-transport channels. Although conductivity issues are currently tackled through the use of conductive additives, their, usually, low Li-ion storage capacity remains an issue. For this reason, the development of porous, rigid, and intrinsically conductive COFs which can host large amounts of sulfur keeping ultrafast electron transport is highly required.

### 6.2. COFs for Other Batteries

Previously, we reviewed COFs which are widely explored in LIBs and LSBs. There are also several reports exploring the use of COFs as electrodes for Na/K-ion batteries (NIBs/PIBs). Besides, researchers are also shifting their interest in other battery chemistries like metal-oxygen batteries, and multivalent ion batteries, such as Zn-ion batteries (ZIBs). In this sub-section, we review these categories of batteries where COFs have been less intensively explored, but have the potential to attract widespread attention in near future.

Banerjee et al. created a $\beta$-ketoenamine COF (HqTp-COF) for ZIBs cathodes for the first time.[292] The primary constituents for $Zn^{2+}$ storage are the C2 symmetric C═O group produced by the electrochemical oxidation of the hydroquinone linkage unit and the C3 symmetric C═O group produced by the conversion of enol to keto tautomerism. Excellent discharge capacity for HqTp-COF is provided by the reversible interlayer interaction of $Zn^{2+}$ with the C═O groups of the neighboring layers. At 125 mA $g^{-1}$, it demonstrated a specific capacity of 276 mAh $g^{-1}$, and it retained the initial capacity of 95% after 1000 cycles. Following that, Liu et al. designed Tp-PTO-COF employing 2,7-diaminopyrene-4,5,9,10-tetrone (PTO) and 1,3,5-triformylphloroalucinol (Tp) in order to further improve electrochemical performance of the ZIB cathode.[293] $Zn^{2+}$ is stored in the double-active sites of the $\beta$-keto carbonyl and neighboring carbonyl acting as nucleophilic centers. Tp-PTO-COF employs an ionic coordination mechanism to store charges. To be more precise, during the electrochemical reduction of carbonyl groups, each $Zn^{2+}$ is coordinated to two negatively charged oxygen atoms in the interlayers and reversibly delocalized during the charging process. Consequently, the Tp-PTO-COF achieved a reversible capacity of 301 mAh $g^{-1}$ at 0.2 A $g^{-1}$. In another report, Li et al. designed a TA-PTO-COF generated by covalently bonding tris(4-formylbiphenyl)amine (TA) and PTO-$NH_2$ for ZIB cathode application.[294] The electron delocalization and intermolecular interaction were amplified with the highly conjugated skeleton, resulting in high electronic conductivity. TA-PTO-COF cathode delivered a capacity of 255 mAh $g^{-1}$ at 0.1 A $g^{-1}$ along with a promising rate capability of 186 mAh $g^{-1}$ at 10 A $g^{-1}$. The reactive sites such as C═O, C═N, and charge transport pathways (i.e., the open channels present within the TA-PTO-COF) were deemed responsible for the exceptional performance.

Several intrinsic limitations in conventional zinc metal anodes like dendrites development, parasitic reactions, research also focuses on developing smart solutions for improving the plating of the metal on the anode. Thus, the development of zinc anode protective layers and the pursuit of novel anode materials are essential components in promoting the performance and safety of ZIBs. Yu et al. synthesized a two-dimensional polyarylimide covalent organic framework (PI-COF) by mixing with CNTs, TAPA and NTCDA, which was used as an anode for $Zn^{2+}$ storage.[295] The ordered pore network of PI-COF allowed the effective diffusion and interaction of the zinc ions with the built-in redox-active carbonyl groups. Experimental and theoretical data indicated a

two-step $Zn^{2+}$-storage mechanism, in which the carbonyl groups reversibly formed negatively charged enolates. Thus, the PI-COF anode exhibited a specific capacity of 92 mAh $g^{-1}$ at 0.7 A $g^{-1}$, a high rate capability (79.8% at 7 A $g^{-1}$), and a long cycle life (85% over 4000 cycles).

By increasing the exposed Zn anode surface, the development of zinc dendrites amplifies the side reactions, such as hydrogen evolution reactions and corrosion. In addition, the device impedance increases deteriorating further ZIB capacity.[296–298] The dendritic nucleation sites hamper the smooth plating and striping of zinc metal that eventually result in a short circuit and battery failure.[299] As a result, scientists have developed a number of strategies, such as constructing scaffolds or nucleation layers, improving electrolytes SEI formation with additives, or developing surface-protective layers.[300–302] COFs have thus been utilized for the modification of the interfacial interactions between the electrolyte and the electrode materials and inhibition of dendrite formation by promoting the uniform deposition of metal ions during stripping/electroplating.[298] Owing to their high surface area, COFs can efficiently manage the spatial electric field and distribution of $Zn^{2+}$ flow, slowing down $H_2$ production and decreasing the energy barriers of zinc deposition.[303] The synthesis of a large-area COF film by condensation of 1,3,5-tri-formylphloroglucinol (TFP) and different aromatic amines was demonstrated by Grzybowski et al. using a dip-coating technique.[304] This efficiently prevented dendritic development and surface-side reactions after the self-assembly of the COF on the anode current collector. Such COF-protective thin films resulted in stable ZIB cycling for 420 h at 1 mA $cm^{-2}$ without compromising Coulombic efficiency and showed a significant improvement compared to the ≈40 h of stable cycling for the bare Zn anode. To develop a zinc anode devoid of dendrite formation, Wang et al. studied a porous CTF as a zinc protective layer.[305] By cooperatively coordinating with $Zn^{2+}$, the nitrogen-rich sites in CTF efficiently reduced the $Zn^{2+}$ concentration gradient and nucleation overpotential while promoting Zn nucleation. Furthermore, while controlling the $Zn^{2+}$ diffusion process, the CTF coating secured the uniform Zn deposition, prevented side reactions by isolating the Zn anode from the electrolyte. Thus, a Zn//Zn symmetric cell using the CTF-protected anode achieved stable operation for 7000 h. Guo et al. used a hydrothermal method to directly metalize COFs with $Zn(CH_3COO)_2$ in order to better explain the effect of various components on inhibiting HER and dendrite growth.[306] They synthesized Zn-AAn-COF, Zn-DAA-COF, and Zn-DAAQ-COF as model platforms to control $Zn^{2+}$ flux and $H_2$ evolution in zinc-air batteries (ZABs). Zn-AAn-COF was used as an effective model platform for ZABs study because of its high porosity, many Zn nucleation sites, and zincophilic groups (such as C═O and C═N). The inhibition of HER on the electrode based on the Zn-AAn-COF was established both theoretically and empirically. By pouring a COF-based polyvinyl chloride (PVC) suspension over the zinc plate (PVC-Zn-AAn-COF@Zn), the electrodes were protected by the COF layer. A control experiment with an unprotected zinc anode showed that after 10 cycles protrusions and nucleations on the zinc foil were visible, and as the number of cycles increased they progressively transformed into zinc dendrites. Significant corrosion, large $H_2$ bubbles, and highly disordered Zn deposition were observed after 100 cycles on the bare Zn foil surface. On the PVC-Zn-AAn-COF@Zn protected foil, however, homogeneous thick Zn deposits were observed after 100 cycles under identical conditions, without any indications of $H_2$ bubbles or development of dendrites.

The unique chemical groups in COFs can develop specific interactions with oxygen from the air during the operation of metal-oxygen batteries. Recently, functionalized COFs have also explored for zinc–air batteries with promising results. For instance, Cao et al. demonstrated the use of fluorinated COF.[307] To improve the affinity of $O_2$ in the cathode electrode, the authors used fluorinated alkyl chains decorating the COF structure with hydrophilic NiFe layered-double-hydroxide as an electrocatalyst. With the help of the COF porous structure, it was possible to segregate the water and $O_2$ at the nanoscale which greatly enhanced the migration of $O_2$ within the cathode. Furthermore, Zhang et al. employed a composite made of porphyrin COF and CNT (POF@CNT) as the cathode in liquid as well as flexible all-solid-state zinc-air batteries.[308] The all-solid-state battery had a high energy efficiency (61.6% at 1.0 mA $cm^{-2}$), while the liquid Zn-air battery showed good stability (200 cycles) and a narrow voltage gap (0.71 V). Considering the intricate chemistry in metal–air batteries rendering stable cycling very challenging, the Zn–air battery's outstanding performance was ascribed to the complementary actions of CNT and porphyrin COF (POF). The hydrophilic surface and well-defined cobalt-coordinated porphyrin active sites supplied by POF were complemented by the various electron routes and enhanced electron transport that were provided by interwoven CNTs. COF materials are gaining recognition for their potential to curb the migration of active materials in various other battery types. For instance, very recently, Zhang et al. used exfoliated COF structure as a cathode to hold bromine (Br) for Zn–Br batteries.[309] The abundant functional groups in COF provided the adsorption sites for polybromide whereas the same COF layer over the Zn anode regulated the Zn flux to reduce the production of dendrites. The full cell delivered the 183 mAh $g^{-1}$ of capacity after 1000 cycles with capacity retention of 83% at 2 A $g^{-1}$. In another study, Khayum M et al. used $\beta$-ketonamine COF coupled to hydroquinone for the first time, functioning as a $Zn^{2+}$ anchor in an aqueous rechargeable zinc ion battery (ZIB).[292] Efficient reversible interlayer interaction between $Zn^{2+}$ ions and the functional moieties in the neighboring COF layers accounts for the charge storage mechanism. Notably, a built-in complete cell exhibits a discharge capacity as high as 276 mAh $g^{-1}$ at a current rate of 125 mA $g^{-1}$ because of the well-defined nanopores and structural structure.

Beyond ZIBs, magnesium ion batteries (MIBs) and calcium ion batteries (CIBs) show great promise for large-scale energy storage due to their low cost, abundance, and exceptional safety in ambient environments. COFs are promising cathode materials for these batteries owing to its intriguing properties. However, research in this field is still nascent stage and only few reports are published till now. For instance, Sun et al. reported COF as cathode for the rechargeable MIB.[310] It shows a high-power density of 2.8 kW $kg^{-1}$, and a high specific energy density of 146 Wh $kg^{-1}$ along with extraordinary cycle life. This demonstrates that the ultrafast reaction kinetics are mostly explained by pseudocapacitive behavior, and the triazine ring sites in the COF are redox centers for reversible interaction with magnesium ions. Zhang et al. proposed TB-COF based on triquinoxalinylene and

benzoquinone units as anode for high-performance aqueous CIB.[311] In TB-COF, ion and electron transport are facilitated by the abundance of active sites and the $\pi$-conjugated structure. It therefore provides excellent rate performance (104 mAh $g^{-1}$ at 70 A $g^{-1}$) and a large reversible capacity (253 mAh $g^{-1}$ at 1.0 A $g^{-1}$). Thanks to its insoluble nature and stable structure, TB-COF has a long cycle life, with capacity loss of 0.01% per cycle at 5 A $g^{-1}$ after 3000 cycles. Following three intercalation stages, which include three different types of $Ca^{2+}$ ion storage sites, a maximum of nine $Ca^{2+}$ ions may be stored per TB-COF repeating unit.

Besides, divalent metal ion batteries, trivalent ion ($Al^{3+}$) based batteries also attracted researchers' attention in recent times. COFs can show promising performance when utilized as an electrode for Al ion batteries (AIB). For instance, Lu et al. reported a 2,2'-bipyridine moieties-based COF as cathode material in AIB.[312] Because of their strong frameworks and hierarchical pores with a large specific surface area, the COFs allow rapid anion diffusion and intercalation without structural collapse, which is verified by both theoretical and experimental studies. After 13 000 cycles at 2 A $g^{-1}$, the resulting AIB shows exceptional long-term stability, with a reversible discharge capacity of 150 mAh $g^{-1}$. Additionally, it has a remarkable rate capability of 113 mAh $g^{-1}$ at 5 A $g^{-1}$. Similarly, Liu et al. reported two PIs based 2D COFs cathodes with redox-bipolar capacity in rechargeable AIB.[313] The porous polymer skeleton of 2D-COFs incorporated the active centers of n-type imide and p-type triazine which is responsible for effective charge transfer. The ideal 2D-COF electrode reached a high specific capacity of 132 mAh $g^{-1}$. Nonetheless, the available literature on COF applications in dual-ion batteries remains scarce, leaving ample room for further exploration and research in this domain.

### 6.3. COFs as Separators and Coatings in Batteries

The application of COFs is not only limited to the cathodic and anodic materials but it is also extended to the generation of protective layers for electrode materials and separation membranes. This is due to their high porosity, flexible nature, and most importantly electrically insulating but ionically permeable nature that COFs can provide through appropriate synthetic design. Xu et al. proposed a redox-active COF as a separator for Li–S batteries,[314] whereby the 1D pore channels of COF assisted for $Li^+$ transport and the pyridine subunits of the framework facilitates sulfate adsorption. The material delivered a specific capacity of 977 mAh $g^{-1}$ at 0.2 C after 100 cycles, a value that was 5.2 times higher than the respective values observed using the same electrode materials but with glass or cellulose as separators. Wang et al. developed a straightforward technology based on a coated functional separator forming a network by combining COFs with CNTs, which was not permeable to the dissolved polysulfides (COF-CNT-separator).[315] With an 80% sulfur concentration in the cathode, the cell retained a considerably high capacity of 1068 mAh $g^{-1}$ at 1 A $g^{-1}$ after 500 cycles. Straightforward methods based on the integration and network formation for developing separators is a promising strategy for the assembly of highly efficient Li-S batteries. In such an example, ionic covalent organic nanosheets (iCON) based on guanidinium were deposited over $Ti_3C_2$ MXenes to form a coating layer on the polypropylene separator.[316] This modification suppressed the shuttle effect of polysulfides by efficiently intercepting their diffusion, accelerated the redox kinetics of sulfur species, and promoted efficient conversion of intercepted polysulfides owing to the synergistic effects from $Ti_3C_2$ and iCON. Particularly, this was attributed to the dynamic adsorption of polysulfides at the $Ti_3C_2$@iCON-PP separator and their subsequent catalytic conversion. The electrochemical efficiency of carbon nanotube/sulfur cathodes was significantly enhanced through the use of such functionalized separators, leading to an average capacity decay per cycle over 2000 cycles at 2 C only by 0.006%, keeping 706 mAh $g^{-1}$ of the initial specific capacity of 810 mAh $g^{-1}$. At 0.05 C, the battery achieved an initial discharge capacity of 1417 mAh $g^{-1}$, corresponding to 85% of the theoretical capacity of sulfur. Even at a 5C rate the discharging capacity was 687 mAh $g^{-1}$, while at a commercially relevant electrode mass loading of 7.6 mg $cm^{-2}$, the cell still delivered a high initial capacity of 1186 mAh $g^{-1}$.

Another common issue encountered during battery operation is the rise of internal resistance with working cycles. This is often due to the dissolution of metal oxides in the electrolyte and the subsequent deposition of oxides at the anode. The inadequacy of the traditional separators to control the metal oxides' diffusion from the cathode to the anode is typically the reason behind this phenomenon. To decrease the impact of such processes, a high-grade separator can be used, because it has very small pores that can only let $Li^+$ to pass through. However, using such separators is very costly, drastically decreasing the advantages that they aim to bring. Therefore, modern LIBs using transition metal oxide cathodes require separators that are extremely permeable for $Li^+$ and cheap, but also non-conductive for transition metal ions. In this context, Wen et al. proposed a new polymer separator that can control both $Li^+$ and transition metal ion mobility.[317] It was produced by laminating a COF based on 2,5-dimethoxybenzene-1,4-dialdehyde and 1,3,5-tris(4-aminophenyl) benzene on an industrial polymer separator. Electrochemical measurements and physical characterization demonstrate that the lithium-ion transference number of this separator was two times that of the uncoated one, and successfully intercepted the soluble transition metal ions from the cathode before reaching the anode half-cell. Therefore, the performance stability during cycling and rate capability. were significantly improved.

Lightweight membranes of under 10 microns are of particular interest in batteries architecture because their deployment may increase the energy density. It is extremely challenging to produce such fine membranes using traditional nanofabrication methods. In one report, a 7.1 µm thin hetero-layered Kevlar/COF composite membrane was developed using a bottom-up layer-by-layer method (**Figure 17**a–e)[318] that allowed for precise control over the structure and thickness of the membrane. The weak $\pi$-$\pi$ stacking of the guanidinium-based cationic COF was confirmed from XRD which then was ultrasonically exfoliated to obtain single-layer COF sheets (Figure 17b–d). The 2D COF sheets are tightly interlocked with the Kevlar units via electrostatic coupling, enabling quick $Li^+$ transfer (Figure 17e). The developed membrane showed high $Li^+$ conductivity ($1.6 \times 10^4$ S $cm^{-1}$ at 30 °C) which allowed the operation of an all-solid-state lithium battery with an improved energy density, that could prevent short-circuiting even after 500 hours of cycling. When used in a full cell of LIBs, the battery exhibited excellent rate performance with

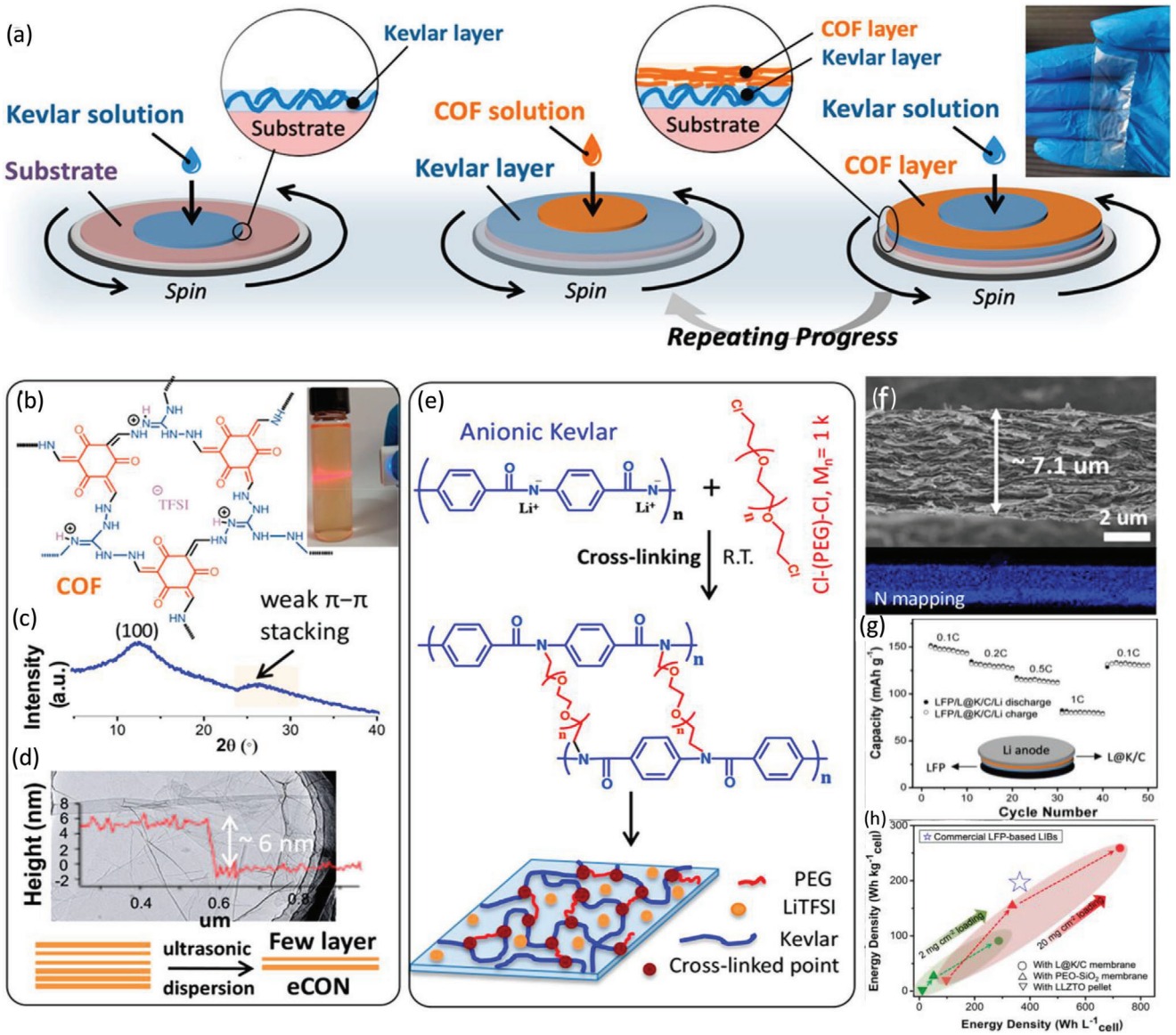


**Figure 17.** a) Schematic of assembling a 7.1 µm thick heterolayered Kevlar/COF composite membrane (inset: 500-bilayer L@K/C membrane), b) COF structure, c) XRD of COF, d) TEM and AFM profile of COF film, e) cross-linking Kevlar with PEG polymer, f) SEM of L@K/C membrane, g) electrochemical performance of assembled cell (LFP/L@K/C/Li), and h) Gravimetric and volumetric energy densities of cell with different membrane. Reproduced with permission.[318] Copyright 2020, American Chemical Society.

high energy density of almost 250 Wh $kg^{-1}$ (Figure 17g,h). Similarly, Zhang et al. demonstrated that a fluorine COF (F-COF) based nanofluidic and negatively charged membrane was capable to improve the shuttling effect in Li-S batteries.[319] The highly ordered and negatively charged membrane (−46.7 mV) acted as a permselective barrier that allowed the $Li^+$ diffusion but limited the migration of LiPSs. With the use of 4F-COF membrane only 0.018% capacity fading per cycle was achieved. Under the same conditions, a COF membrane with less negative charge (−28.9 mV) failed after 520 h of operation. It was observed that already after 10 h, the electrolyte color changed, indicating the migration of LiPSs to the electrolyte.

The control of the porosity of the cathode and the catalytic properties for the sulfur reactions can provide a significant improvement of the overall performance of the Li–S batteries. For instance, Wang et al. demonstrated the use of TpPa-1 COF cobalt-decorated titanium oxynitride ($TiO_xNy$) as a cathode material for LiS batteries.[320] The presence of the COF layer reduced the migration of LiPSs, whereas the cobalt atoms acted as a catalytic site for sulfur reactions. Furthermore, the oxygen deficiency and macropores present in the oxide framework retained the flow of electrons as well as the high loading of sulfur. The cathode underwent a 0.031% of capacity fade per cycle for 500 cycles at 1C rate, while the pouch cell retained 554.5 mAh $g^{-1}$ of capacity at 0.1 C after 50 cycles.

COF-based solutions have been also developed to tackle the unfavorable dendrite growth and inefficient Li consumption in lithium metal batteries which has so far limited the widespread

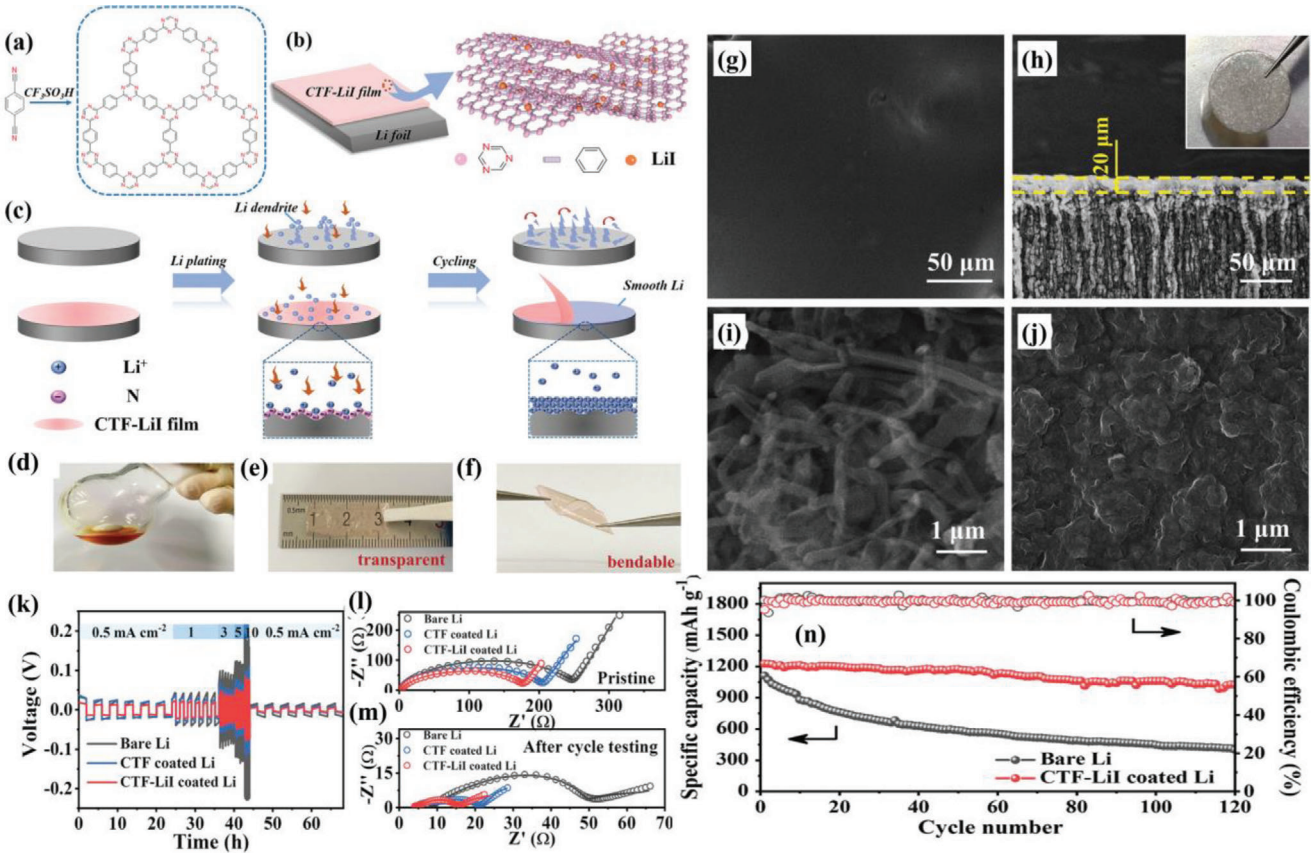


**Figure 18.** a) Schematic of CTF synthesis starting from the precursor dicyanobenzene, b) coating of CTF-LiI over lithium foil, c) schematic of the effect of CTF coating over the Li anode for smooth lithium deposition, d) CTF-LiI solution, e) prepared CTF-LiI film, f) bending test of film, g,h) SEM of CTF-LiI over lithium foil, i) lithium anode SEM after 20 cycles, and j) CTF-LiI coated lithium anode SEM after 20 cycles, k) rate performance of different anode, l) Nyquist plot for anode before cycling, m) Nyquist plot for anode after cycling, n) cycling performance of different anode. Reproduced with permission.[235] Copyright 2020, John Wiley & Sons.

Li–metal batteries.[321] To address this, Xu et al. developed COF-LZU1 as a protective layer between the Li-anode and the separator.[322] The COF was synthesized by the reaction between 1,3,5-triformylbenzene and 1,4-diaminobenzene. TFSI anions (bis(trifluoromethanesulonyl)imide anions) were immobilized on COF-LZU1 by interactions with the aldehyde functional groups, reducing the impact of space charge (typically achieved by reducing the anion mobility) and hence limiting dendrite growth. The imine-linked COF-LZU1 was also lithophilic, which enabled a homogenous distribution and transport of lithium ions. This homogeneity in ion flux distribution further contributed in reducing space charge effects and resulted in lower voltage hysteresis during battery operation, and hence further limiting dendritic proliferation. With the assistance of the COF-LZU1 protective layer, Li metal was smoothly and densely deposited onto the anode, while dendritic Li deposition occurred on a bare Cu electrode. The anode surface of COF-LZU1-modified cells remained dense and smooth even after several cycles, which contributed to improved lithium utilization and cyclability, leading to high coulombic efficiency and reversible rate capacity. The dendrite-free anode demonstrated 99% Li utilization and a cycle life of up to 2000 h. Furthermore, Li–S batteries containing COF-LZU1 layers also showed better rate performance and cyclic stability. In contrast, bare lithium symmetric cells operated effectively for <750 h. In another report, a flexible and conformal CTF-LiI coating was coated on metallic Li anode (**Figure 18**a,b).[235] The bendable and foldable CTF-LiI coating minimized parasitic reactions between metallic Li and the electrolyte while rendering the Li electrodeposition uniform, and dendrite-free (Figure 18c–f). Upon charging–discharging, the assembled cells with bare Li and CTF-LiI-coated anodes, significant Li dendrites were grown only in the case of the uncoated anode (Figure 18g,h). Furthermore, EIS analysis after cycling, showed that the CTF-LiI coated Li anode retained a very low charge transfer resistance. The observed behavior and the reduction of dendrite growth were assigned particularly to the high lithiophillicity brought by LiI and the protective layer of CTF (Figure 18 l,m). The Li symmetric batteries exhibited an impressively low voltage fluctuation with stable operation for 2500 cycles at 10 mA $cm^{-2}$. The capacity of the cell with bare Li dropped to almost 450 mAh $g^{-1}$ from 1150 mAh $g^{-1}$ after 120 cycles, whereas the cell with CTF-LiI coating retained more than 1000 mAh $g^{-1}$ of capacity (Figure 18k). The production of ultrathin and rigid COF films remains a significant challenge due to the powdered nature of COFs. To resolve this issue, Bian et al. produced stable ultrathin COF films by using a side-chain engineering strategy to weaken the

interlayer interactions in the COF structure.[323] The produced COF–C16/PE composite membrane (≈9 µm thick) retained high chemical and mechanical stability. The membrane was tested in Li–$LiFePO_4$, Li-S, and quasi-solid batteries. In the case of Li–$LiFePO_4$ batteries, the device remained stable up to 850 cycles with 128 mAh $g^{-1}$ of capacity.

## 7. COFs as Supercapacitors

Supercapacitors possess distinctive characteristics, including a high-power density, extended cycle lifespan, excellent cost-efficiency, and a broad operational voltage range. Thus far, two distinct approaches have been recognized for the energy storage mechanism of supercapacitors. Energy storage through faradaic processes[324,325] pertains to the reversible redox reactions of electrode materials (pseudocapacitance), in contrast to non-Faradaic processes[326] where ion adsorption occurs on the electrochemical double layer (double layer capacitance). Effective ion adsorption requires a large surface area and readily accessible pores.[327,328] Therefore, it is considered that among the best materials for developing supercapacitor electrodes are those with high surface areas, accessible pore networks, conductivity, and reversible redox-activity.[329,330] COFs fulfill such criteria very efficiently.[331] Furthermore, 2D COF architectures facilitate bidirectional electrochemical processes and can include functional linker moieties ascribing redox activity. For instance, An et al. fabricated an anthraquinone-based 2D COFs/graphene composite aerogel (DAAQ-COFs/GA) electrode which delivered a superior and long-term cycling stability with a capacitance of 380 F $g^{-1}$ in 1 M electrolyte and high retention of 87.8% after 20 000 cycles.[332] Li et al. developed a 2D conductive Ni-COF with square-planar Ni(II) coordination centers[333] by reacting 1,2,4,5-benzenetetraamine and 2,5-dihydroxy-1,4-benzenedicarboxaldehyde with Ni(OAc) $\cdot 4H_2O$. The Ni centers did not form nodes (as in metal covalent frameworks) but were immobilized on the side functional groups of the COF building blocks. The electrical conductivity of the Ni-COF thin film registered a value, of 1.2 S/cm. These remarkable electrical properties were attributed to the highly conjugated framework, well-structured pores, and the presence of numerous redox centers. Consequently, the material exhibited an impressive specific capacitance of 1257 F $g^{-1}$ (in 3 M KOH, 1 A $g^{-1}$, 3 electrode system) and it maintained 94% of its capacitance after 10 000 cycles. Moreover, when utilized in an asymmetric supercapacitor configuration (with activated carbon as the other electrode), the Ni-COF featured a high capacitance of 417 F $g^{-1}$ at a current density of 1 A $g^{-1}$. Notably, it achieved an exceptional energy density of 130 Wh $kg^{-1}$ at a power density of 839 W $kg^{-1}$, surpassing the performance of previously reported COF electrode materials. The electrochemical behavior of COF nanofibers was studied and compared with those of COF particles and hollow spheres by Dong et al. COF nanofibers exhibited higher overall pore volumes, more regular built-in vertically oriented channels, and larger BET-specific surface area compared to COF particles and hollow spheres.[334] With over 80% of the original capacitance retained after 10 000 cycles, the as-prepared COF nanofibers exhibited extraordinary cycling endurance with a maximum specific capacitance of up to 235 F $g^{-1}$ at 0.5 A $g^{-1}$. These favorable performance features were also promoted by the 1D shape of the COF, boosting the charge transport. Zhang et al. synthesized imine-based COF by using the Schiff base reaction between TAPB and BPY (2,2′-bipyridyl-5,5′-dialdehyde).[335] The solvothermal and gas–liquid interface synthesis methods were used to create the bulk COF and self-supporting COF films, respectively. These bulk COF showed specific capacitance values of 633.4 F $g^{-1}$ at 1 A $g^{-1}$ and the thin-film COF 0.26 mF $cm^{-2}$ at 0.001 mA $cm^{-2}$ for an ≈10 nm nanofilm. Moreover, COF nanofilms were modified by introducing $Ni^{2+}$ ions by the reversible redox reaction of $Ni^{2+}/Ni^{3+}$, where it was verified that $Ni^{2+}$ cations were coordinated on the N sites of the BPY molecules. The incorporation of single $Ni^{2+}$ cations resulted in the increase of the specific capacitance to 0.38 mF $cm^{-2}$ at 0.001 mA $cm^{-2}$. In another report, using solvothermal Schiff base condensation between 1,3,5-triformylphloroglucinol (Tp) and 3,3'- diaminobenzidine, a new benzimidazole-based covalent organic polymer (TpDAB) was produced.[336] TpDAB showed outstanding rate capability, maintaining 93% of its original specific capacitance after 1000 cycles, and a specific capacitance of 335 F $g^{-1}$ at 2 mV $s^{-1}$. The nitrogen functionalities of the TpDAB polymer with its microporosity were found to be responsible for the high electrochemical activity.

A major advantage of some COF structures is their crystalline 2D architecture with highly unsaturated carbon-carbon bonds. Regarding this, a 2D conjugated COF with an olefin link (g-$C_{34}N_6$-COF) was recently reported.[337] An extended $sp^2$-bonded carbon skeleton with side cyanide ligands, a sheet structure, and crystalline layered architecture was formed using a variant of Knoevenagel condensation. The COF integrated 3,5-dicyano-2,4,6-trimethylpyridine and 1,3,5-triazine units, resulting in improved $\pi$-electron communication and electrochemical activity. Its uniform nanofibrous morphology, when combined with carbon nanotubes, formed a flexible thin-film electrode. This electrode showed high performance in a micro-supercapacitor, with an areal capacitance of 15.2 mF $cm^{-2}$, high energy density (7.3 mWh $cm^{-3}$), and remarkable rate capability. In another report, the first successful synthesis of a 2D COF with a fully $sp^2$-bonded carbon skeleton was achieved, by using 2D poly(phenylenevinylene) (2DPPV). This COF was synthesized using a Knoevenagel polycondensation reaction involving 1,4-phenylene diacetonitrile and three-armed aromatic aldehyde.[338] The subsequent annealing of the 2D PPV at high temperature delivered extremely porous nanosheets with a high SSA. These nanosheets exhibited enhanced electrochemical performance, especially in supercapacitor applications and ORR. As supercapacitor electrodes, they exhibited a capacitance of 0.5 A $g^{-1}$ in a 6 M KOH aqueous solution, and exceptional cycling stability with almost no capacitance loss even after 10 000 cycles. The energy density and power density of the 2DPPV material were 30 Wh $kg^{-1}$ and 6654 W $kg^{-1}$, respectively. Also, a 2D PDC–MA–COF with redox-active triazine segments was produced using 1,4-piperazinedicarboxaldehyde (PDC) and melamine (MA) as functional groups.[339] It exhibited large SSA (748.2 $m^2$ $g^{-1}$), constricted pore thickness (1.9 nm), and a large pore volume (1.21 $cm^3$ $g^{-1}$). The PDCMACOF delivered 335 F $g^{-1}$ of capacitance at the power density of 750 W $kg^{-1}$ with an energy density of 29.2 Wh $kg^{-1}$. Using 2,5-dibromothiophene (DBT) and melamine (MA) organic linkers a new 2D COF structure (DBT-MA-COF) was synthesized with intralayer hydrogen bonding leading to a

flat and rigid structure.[340] The material's quasi-reversible redox function, involving the reversible transformation of quinone in the triazine units, provided the basis for the generation of DBT-MA-COF pseudocapacitance. DBT-MA-COF had a significant heteroatom concentration in the triazine & thiophene moieties, which improved the transfer of electroactive species over the interface and promoted solution conductance. The assembled asymmetrical device with nitrogen-doped graphitized chitosan as the cathode material exhibited an energy density of 32.1 Wh $kg^{-1}$ at the power density of 800 W $kg^{-1}$ with 83% capacitance retention after 30000 charging/discharging cycles. In general, pseudo capacitors require the assembly of porous electrode compositions containing extended conductive pathways, large surface coverage, and high ionic conductivity as a way to accelerate the further development of EES platforms. In this context, Phos-COF-1, a novel phosphine-based COF, was reported for SCs,[75] with a BET SSA of 818 $m^2$ $g^{-1}$ and a pore dimension of 1.56 nm and a microporous composition. The phosphine moieties in the Phos-COF-1 electrode demonstrated excellent reversible redox characteristics, resulting in a high energy density of 32 Wh $kg^{-1}$.

The electrochemical performance can also be improved by the existence of donor-acceptor conjugation and ion transport within the electrode material. For instance, the produced COF TPDA-1 with 1,3,5-tris(4-aminophenyl)triazine and 2,4,6-trihydroxyisophthalaldehyde linkers exhibited such a donor-acceptor conjugation responsible for the intense redox activity.[341] The TPDA-1 material delivered a significant capacitive performance of 469.4 F $g^{-1}$ at 2 mV $s^{-1}$. Additionally, the material retained 95% of capacitance after 1000 cycles, validating the reversibility of redox reactions. Similarly, 1,3,5-tris(4-aminophenyl) triazine with 2,6-diformyl-4-methylphenol was used to produce TDFP-1 COF. The material with 651 $m^2$ $g^{-1}$ of SSA also demonstrated improved donor–acceptor features. The sample showed 354 F $g^{-1}$ of specific capacitance at 2 mV $s^{-1}$. The presence of the conjugated polymeric scaffolding in the TDFP-1 COF facilitated the charge transport within the micropores. In another report, 1,3,5-triformylphloroglucinol (TFP) and 1,5-diaminonaphthalene were combined via solvothermal Schiff base condensation to form a porous and extended network in the TFP-NDA-COF (NDA) material.[342] When tested as a supercapacitor electrode, it delivered 379 F $g^{-1}$ of specific capacitance at the scan rate of 2 mV $s^{-1}$ with 75% capacitance retention after 8000 charging/discharging cycles. The permanent porosity and extended conjugated aromatic network were crucial for the fast ion and electron propagation within the electrode and the constant permeability of the framework boosted the electrocatalytic activity. The production of porous structures with variable diameter can further improve the ion transport capabilities of the materials. For instance, C3-symmetric benzotrithiophene tricarbaldehyde (BTT)-based COFs exhibited such an extended set of properties.[343] The rigid and planar conjugated structure of BTTs, the extended aromatic core due to the thiophene fused rings and the intermolecular $\pi$-stacking endows them with high charge transport properties. Moreover, the three-dimensional functionalization of BTTs with side groups is an effective strategy for improving their redox activity and system integration.

The presence of conductive pathways in the electrode materials is a decisive factor that must be taken into consideration during the material's engineering, because facilitates the fast electron transport from the electrodes to the current collectors and minimizes the device resistance. Therefore, growing COFs over conductive substrates is one of the simple but effective methods to produce efficient materials for supercapacitor applications. Han et al., for the first time, engineered nanocoatings composed of COFs grown on nickel nanowires (NiNWs), that gave significantly improved electrochemical performance for supercapacitors.[344] The electrode material constructed using COFs nanocoating delivered 314 F $g^{-1}$ of specific capacitance when discharged at 50 A $g^{-1}$ of current density. The presence of electrical and electrochemical features of NiNWs and the microporosity of COF were responsible for delivering high specific capacitance. Furthermore, Shanavaz et al. developed triazine-based COF via Schiff base formation using polycondensation reaction of melamine and terephthalaldehyde.[345] The COF was decorated with niobium cations to create a Nb@COF and studied as a supercapacitor electrode in a three-electrode setup. At a scan rate of 2 mV/s, Nb@COF showed enhanced specific capacitance (367 F $g^{-1}$) in comparison to pure COF (244 F $g^{-1}$). The porosity and interlayer spacing, as well as the pseudocapacitance in Nb@COF due to the $Nb^{2+}$ cations ascribed the system with better electrochemical performance. Even after 5000 cycles, Nb@COF demonstrated strong stability during charging–discharging, holding 89% of the initial specific capacitance. In another report, a novel benzimidazole-arylamide COF was synthesized through the condensation polymerization pathway exhibiting an SSA of 177 $m^2$ $g^{-1}$ and a pore diameter of 30–32 Å.[346] The sample showed fast ion transport and delivered 88.4 F $g^{-1}$ of specific capacitance at 0.5 A $g^{-1}$ and 93.61% capacitance retention after 5000 discharging cycles in 1 M $H_3PO_4$ electrolyte. SWCNTs coated with COFs were produced by in situ polymerization of TpPa-COF.[347] The supercapacitors tested based on this composite, combining the high conductivity of SWCNTs with the porosity and high redox potential of TpPa-high COF, delivered substantially higher capacitance than the pure COF, of 153 F $g^{-1}$ at the current density of 0.5 A $g^{-1}$. COFs may also improve their conductivity by introducing polymeric materials via post-synthesis modification. PANI-customized triazine-based COFs were recently prepared by Dutta et al. upon in situ polymerization of aniline inside the permeable COF scaffolds.[348] The sample showed high conductivity 1.4–1.9 × $10^{-2}$ S $cm^{-1}$ at ambient temperature and a 20-fold improvement in specific capacitance over the pristine frameworks. The fabricated supercapacitor showed a high energy density of 24.4 Wh $kg^{-1}$ at the power density of 200 W $kg^{-1}$. Similarly, a 3D porphyrin-based COF supported on CNTs was synthesized by one-pot polymerization.[349] After annealing, the CNT N-doped carbon nanospheres (N-C@CNTs) were obtained that showed a specific capacitance of 250 F $g^{-1}$. The distinctive architecture of these COF precursors, containing the flexible triangular pyramid-shaped tris(4-formylphenyl) amine and the rigid porphyrin units, allowed the creation of CNT twined N-doped carbon nanocomposites, in addition to exposing active N entities onto the carbon surfaces. In another report, the electrical characteristics of COF thin layers were enhanced by in situ solid-state infiltration of carbon nanofibers (CNF) within the COF substrate.[350] The COF and CNF in the COF-CNF composites exhibited strong intermolecular interactions. Therefore, these COF-CNF blends (DqTp-CNF and DqDaTp-CNF) encoded high electrical conductance (103 S $cm^{-1}$) and good electrochemical

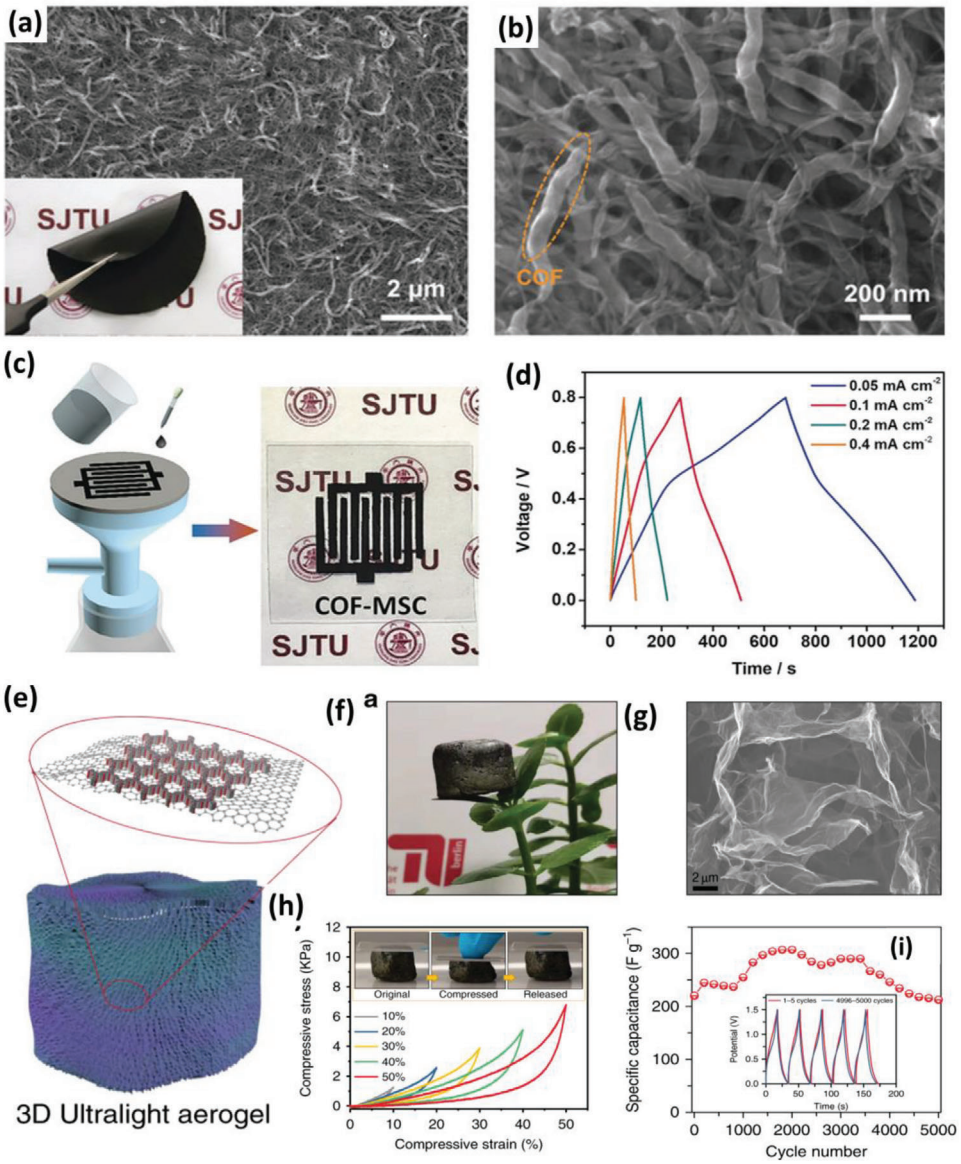


**Figure 19.** Flexible Supercapacitor based on COF. a) SEM image of g-$C_{34}N_6$-COF (inset: optical photo of the electrode). b) SEM image of the COF layer. c) Schematic description of the method used for electrode preparation for g-$C_{34}N_6$-COF. d) GCD of g-$C_{34}N_6$-COF. Reproduced with permission.[337] Copyright Wiley, 2019. e) Schematic of COF/rGO aerogel, f) optical image of COF/rGO aerogel, g) SEM image of COF/rGO aerogel, h) Stress–strain behavior of COF/rGO aerogel, and i) cycling stability and (inset) cyclic charge–discharge performance of COF/rGO aerogel. Reproduced with permission.[185] Copyright 2020, Springer Nature.

properties (464 mF $cm^{-2}$ at 0.25 mA $cm^{-2}$). Further, integrating DqDaTp-CNF SC with a perovskite solar cell resulted into a unified self-charging power pack. After photo charging for 300 s, the developed self-charging power unit showed excellent device-level performance (42 mF $cm^{-2}$). In another report, COF/rGO aerogels prepared by a hydrothermal method were successfully synthesized (**Figure 19**).[185] Upon freeze-drying, the COFs grown over the interface of the graphene layers, which were ordered in a 3D manner, culminated in a lightweight aerogel. The material featured a multilayer porous structure that could both compress and extend repeatedly without collapsing. In particular, the produced aerogel showed excellent stability against compression. When tested as a supercapacitor electrode, the aerogel delivered a high capacitance of 269 F $g^{-1}$ at 0.5 A $g^{-1}$. The device retained almost 100% of its capacitance even after 5000 charging–discharging cycles. Furthermore, the COF/rGO composite was used to produce micro-supercapacitors which with 15.2 mF $cm^{-2}$ of aerial capacitance and 7.3 mWh $cm^{-3}$ of energy density. In an interesting report, Dong et al. developed COF crystallites by in situ growth along carbon skeleton surfaces, producing a carbon/rGO-supported COF composite foam utilizing a graphene-wrapped carbon foam.[351] When studied as self-supported electrodes for supercapacitors, the resultant composite foam provided a high capacitance of 129 F $g^{-1}$ at 0.5 A $g^{-1}$. Moreover, after 20 000 cycles

at 10 A $g^{-1}$, there was no discernible decrease in capacitance, suggesting outstanding long-cycling stability. Because the composite foam has a robust carbon backbone, it exhibits impressive compressibility and fatigue tolerance. This further permits the use of pre-fabricated composite foams that may be put together to create flexible supercapacitors. In another study, An et al. developed COF/MXenes thin films via cation-driven-self-assembly process for supercapacitor applications.[352] The superior intrinsic conductivity of MXenes and the ordered pore structure of COFs significantly boosted the electron transfer and ion migration rates. The integrated film electrode provided exceptional mechanical strength, good kinetic energy storage characteristics, and a capacitance of 390 F $g^{-1}$ at 0.5 A $g^{-1}$ with a capacitive contribution of 96.7% at 50 mV $s^{-1}$.

Supercapacitor electrodes benefit largely from using porous nanocarbons, graphene, and conducting polymeric materials that are rich in nitrogen.[353] However, for the electrode materials to be able to act efficiently requires high N doping concentration and large SSAs. For these reasons, the linkers with high N content can enrich the COF backbones and then, after pyrolysis, nanostructures can be obtained by combining the high concentration of N-center sites with the high porosity of the carbon structure. For instance, Suzuki coupling was used to create a porous aromatic framework (PAF) material (LNU-18) comprising two nitrogen atoms of different nature (N-triazine and N-amine).[354] The porous aromatic framework, encompassing robust covalent bonds, expressed an N atom-rich chemical composition. The porous carbon structure with tailored nitrogen atoms (N-triazine and N-amine) improved the overall capacitance. The LNU-18 framework displayed a capacitance of 269 F $g^{-1}$, which was 3–4 times better than the capacitance on a similar COF without N-doping. The role of N-doping was also verified in the case of a microporous N-doped carbon material which was produced by carbonizing ACOF1, which encoded an azine group connected to two structural lattices.[355] The produced microporous carbon exhibited 1596 $m^2$ $g^{-1}$ of surface area with 1 nm average pore size distribution. The micro-porous patterns were formed in the material as a result of the evolution of nitrogen gas during the thermal decomposition of the azine bond. Moreover, the N-doped centers were created in the structure in such a way that gave rise to redox activity. In another report, a covalent triazine-based framework (TCNQ-CTFs) was produced with a significant nitrogen concentration (> 8%) and a very large SSA (>3600 $m^2$ $g^{-1}$).[356] The material delivered an excellent power density (42.8 Wh $kg^{-1}$), a high specific capacitance (380 F $g^{-1}$), and excellent cycling reliability, with no capacity decrease after 10 000 cycles. In another report, an ultrafast microwave-driven method was used to produce polytriazine COF with extremely high N concentration (approximately 50.5 wt%) using melamine and cyanuric chloride as reactants.[357] The sample delivered 1256 F $g^{-1}$ of specific capacitance at 1 mV/s and 656 F $g^{-1}$ at 1 A $g^{-1}$. After 5000 cycles the sample retained 87.4% of its initial capacitance. Lavillunière et al. optimized the structure of COF-5 using a solvothermal technique aided by microwave radiation.[358] The practicality of microwave irradiation as an alternative method for COF synthesis was demonstrated, effectively synthesizing covalent organic framework-based compounds, including COFs with hexagonal structure. The obtained COFs displayed high crystallinity and electrical conductivity up to $2.35 \times 10^{-2}$ S $cm^{-1}$. However the specific capacitance of the microwave-synthesized COF-5 as an active electrode material in supercapacitor applications was mediocre, and even with conducting additives a specific capacitance of 85 F $g^{-1}$ at 2 mV $s^{-1}$ was achieved. It was found that only ≈15% of the active material was utilized in the electrochemical process, ascribed, probably, to poor ion transport at the interface between the COF-5 grains. This observation underscores the role of the continuous 1D structure of COF nanofibers, previously discussed, in improving the charge transport in the bulk of the electrode.

Apart from the nitrogen content, other heteroatoms such as oxygen, sulfur, and boron also contribute to the redox activity and charge transfer properties. For instance, by using N and O-rich triazine-driven PI (TPI-P/TPI-N) structures, N-doped porous carbon-based materials were synthesized through pyrolysis.[359] The material treated at 700 °C (TPI-P-700) gave a high specific capacity of 423 F $g^{-1}$ in 1 M $H_2SO_4$. Additionally, after 10 000 charge/discharge cycles, the material retained 100% of initial capacitance. In another report, a salt-assisted thermal decomposition procedure was used to decompose COFs structure. Using this strategy, O and N co-doped carbon (ONC-T1s) treated in presence of potassium carbonate ($K_2CO_3$) was successfully obtained.[360] The porous layered structure of ONC-T1s had a significant SSA (3451 $m^2$ $g^{-1}$) and delivered an exceptional 1711 F $g^{-1}$ of specific capacitance at 1 A $g^{-1}$, and delivered an ultra-fast charge–discharge rate, with a specific capacitance of 856 F $g^{-1}$ at 500 A $g^{-1}$.

Besides O, COFs rich in N and boron (B) were also produced by reacting melamine and 4-formylphenylboronic acid in a single pot procedure to create B, N-codoped carbons (B-N-C).[361] In contrast to other microporous carbon plates obtained from COFs, the B-N-C material exhibited distinctive hollow capsule shapes and, notably, showed a dominant mesoporous nature. The formation of these hollow B-N-C capsules was attributed to the facile decomposition of melamine-boroxine organic building blocks and the templating role played by copper species such as $Cu(NO_3)_2$, $Cu_2(NO_3)(OH)_3$, and Cu. The B-N-C capsules were very efficient in oxygen reduction reaction (ORR) in wide pH electrolytes, especially in alkaline solution. When tested in supercapacitors applications, the material acted as a sophisticated counter electrode with a capacitance of 230 F $g^{-1}$. Upon mixing an activating agent with a COF during the pyrolysis step the SSA can be improved. In this context, a COF prepared from 2,5-dihydroxy-1,4-benzoquinone and p-phenylenediamine was carbonized in the presence of KOH.[362] The derived DQPAC-700 displayed microporous characteristics with high SSA (16 607 $m^2$ $g^{-1}$) and significant N/O concentrations (4.09 wt.% and 10.84 wt.%, respectively). In 6 M KOH solution, DQPAC-700 delivered the specific capacitance of 292 F $g^{-1}$ with 96% capacitance retention after 20 000 charging/discharging cycles. Activating agents can also be implanted in the material as functional units, specifically as halogen-based functionalities for the generation of novel electrodes. The halogen-functionalization approach has been reported to engineer rGO, carbon nanosheets, (CNS), CNTs, CTFs, and others.[363] Moreover, the electronic and geometric properties of pristine materials (including charge transfer, energy band gap, Gibbs free energy, electron spin density, localized electronic state, and topological defect) compared to those emerging from halogen inclusions are completely changed. Besides this, the

**Table 3.** Electrochemical performance comparison of different COF structures and its composites for supercapacitors.

| Materials | Electrolyte | $C_s/C_D$ | $E_D$ | $P_D$ | $C_R/C_N$ | Refs. |
|---|---|---|---|---|---|---|
| DAAQ-COF/GA | 1 M $H_2SO_4$ | 378/1 | 30.5 | 700 | 88.9/20000 | [332] |
| Ni-COF | 3 M KOH | 1257/1 | 130 | 839 | 94/10000 | [333] |
| TpDAB | 1 M $Na_2SO_4$ | 432/0.5 | – | – | – | [336] |
| 2DPPV-800 | 6 M KOH | 334/0.5 | – | – | – | [338] |
| PDC-MA-COF | 6 M KOH | 335/1 | 29.2 | 750 | 88/200000 | [339] |
| DBT-MA-COF | 6 M KOH | 407/1 | 32.1 | 800 | 83/30000 | [340] |
| TPDA-1 | 1 M $H_2SO_4$ | 348/0.5 | – | – | – | [341] |
| TFP-NDA-COF | 1 M $H_2SO_4$ | 348/0.5 | – | – | – | [342] |
| NiNWs@TpPa-COFs | 1 M LiCl | 426/2 | – | – | – | [344] |
| BIBDZ | 1 M $H_3PO_4$ | 88.4/0.5 | – | – | – | [346] |
| DqDaTp-CNF | | 364mF $cm^{-2}$/0.25 mA $cm^{-2}$ | 5.8 μWh $cm^{-2}$ | 125 μW $cm^{-2}$ | 76 (4500) | [350] |
| CMF | 6 M KOH | 390/0.5 | 27.5 | 350 | 88.9(20000) | [352] |
| LNU-18-800 | 6 M KOH | 269/0.5 | | | | [354] |
| TCNQ-CTF | 1 M KOH | 380/0.2 | – | – | – | [356] |
| NENP-1 | 0.1 M $H_2SO_4$ | 656/1 | 102 | 1600 | – | [357] |
| TPI-P-700 | 1 M $H_2SO_4$ | 423/1 | 10.5 | – | 100(6000) | [359] |
| ONC-T1-850 | 1 M $H_2SO_4$ | 1711/0.5 | – | – | – | [360] |
| DQPAC-700 | 6 M KOH | 292/0.5 | 11.3 | 103 | 96 (20000) | [362] |
| COF/rGO | 0.5 M $H_2SO_4$ | 269/0.5 | – | – | – | [185] |
| SWCNTs-TpPa-COFs | 1 M $H_2SO_4$ | 153/0.5 | – | – | – | [347] |
| PANI/TCOF-2 | 1 M $H_2SO_4$ | 275/0.5 | 24.4 | 200 | – | [348] |

Abbreviations: $E_D$-Energy Density (Wh $kg^{-1}$), $P_D$-Power Density (W $kg^{-1}$), $C_s$- Specific Capacitance (F $g^{-1}$), $C_D$-current density (A $g^{-1}$), $C_R$-Capacitance Retention (%), $C_N$-Cycle Number Note: ED, PD and $C_R$ are reported for 2-electrode setup for supercapacitor device.

introduction of functional groups and metals through doping further equips COFs to function as pseudocapacitive materials. The availability of a wide range of linkers, can introduce to the COF n- and p-type functionalities, which can serve two purposes at the same time. Very recently, Gu et al. produced COF with n-type imide and p-type quaternary nitrogen centers to support the adsorption of $Li^+$ as well as $PF_6^-$.[364] The material showed 91% capacity retention after 4000 cycles with 165 mAh $g^{-1}$ of capacity at 30 mA $g^{-1}$ of discharge rate. From all these studies, it is evident that the field of COFs is emerging rapidly for supercapacitor applications. However, the research on supercapacitors is explored majorly on the laboratory scale, and before it is applied on an industrial scale, a number of obstacles pertaining to cost and availability of materials must be resolved. **Table 3** presents the performance characteristics of different COFs and COFs composite materials as electrodes for supercapacitors.

## 8. Critical Assessment of Application of COFs in Batteries and Supercapacitors

Considerable efforts are dedicated to the discovery of innovative materials and chemical compositions that can enhance energy storage performance. Among the various materials being explored, COFs have been employed in the research for both supercapacitors and batteries.[319,365–369] The structural customizability of COFs, achieved through the use of different linker combinations, enables the creation of diverse pore networks and size distributions, functional groups, reactivity profiles, and stabilities in these EES devices. The field of COF materials has not yet witnessed an explosive growth, but over the past decade, there have been substantial advances and interest in synthetic methods and COF designs. In terms of COFs' ability to address various challenges in the realm of energy storage, they stand as emerging candidates with other innovative materials like MOFs and MXenes. However, despite a decade of research, the COF field in energy storage cannot be considered mature enough for commercialization. Numerous critical issues and challenges must be addressed before their practical application becomes feasible. The primary prerequisites for a material that will be used in an energy storage device are the conductivity and redox activity. One of the main problems preventing COFs from performing at a high electrochemical level is the witnessed low redox activity and electrical conductivity. To increase the overall activity and conductivity, post-modification techniques can be used to overcome this issue, such as addition of metal ions or conductive agents. Among different conductive agents, conducting polymers have been frequently employed in the past few decades to increase the conductivity and redox activity of different materials.[370] By combining COF with compounds like PEDOT, PPy, polyaniline, the conductive channels and electrochemical activity can be enhanced.[371,372] Electrochemical techniques can be used to infiltrate conducting polymers inside the COF structure.[373] The strong redox activity of the conducting polymers is an advantage over the use of activated carbons, CNTs, or graphene. While the conducting polymers may provide efficient conductive pathways

and redox reversible processes to generate high charge storage capabilities, the composite incorporating COFs can give a high surface area for the adsorption and the active sites required for the electrochemical reactions.

Another approach to enhance the activity and conductivity of COFs is by developing products that retain the parent structure while introducing additional new physical properties. For instance, COFs have been used as templates to derive carbon structures with highly nano-porous networks.[374] Template pyrolysis can further be combined with metal salt precursor as additives to produce metal sites entrapped into the carbon structures with high redox activity. It is also possible to increase the electrochemical activity of COFs by exploitation and exploration of their beneficial tailored superstructures, such as 2D sheets, containing precisely positioned active centers and functional groups.[25] To develop a novel COF structure tailored for specific applications, the current stage of COF research on energy storage materials requires the integration of theoretical and experimental methods to comprehend the mechanisms of charge storage and transfer.[7,375] Modifying the COF structure is an alternative means to enhance electrical conductivity. By introducing dopant materials such as TCNQ, HQ, BQ, and similar substances, it becomes feasible to generate nonbonded electrons capable of unrestricted movement within the crystal lattice.[375,376]

Apart from this, the concentration of host ions within COF nanochannels is very low compared to inorganic compounds. To address this issue, a promising approach involves the deliberate design of nanochannels with a heightened affinity for ions, after a thorough investigation of the impact of nanochannel pore structure, particularly their pore size, on ionic conduction dynamics. From previous studies it is understood that as the pore size decreases to the nano-/molecular-scale, the resulting high "surface to volume ratios" create a confined effect within COF nanochannels, enhancing ion-conduction efficiency. Consequently, surface properties of nanochannels play a pivotal role in optimizing ion-conduction ability. Inadequate ion-conducting groups within COF nanochannels further impede efficient ionic transport, as typically only half of the COF building blocks offer ion-conducting capabilities. Maximizing the incorporation of Li+-affinity building blocks into COF structures through tailored monomer design or post-synthetic strategies is therefore essential for augmenting the concentration of mobile ions and accelerating ion conduction rates. Anionic groups with expanded conjugated structures represent another avenue for enhancing ionic conductivity by minimizing binding energy with mobile cations, thereby facilitating ion transport. Moreover, enriching perpendicular channels through crystallographic orientation control of COFs can bolster ionic conduction. However, achieving anisotropic orientation of ion-conducting COFs remains challenging, with only limited success in demonstrating this approach to date.

As an alternative, the COF can be used as a separator in Li–S batteries, serving both as a membrane and reservoir for electrolytes, while mitigating the shuttle effect via exclusion.[377] A very limited number of COFs have also been reported to act as ion and mass transfer reservoirs. The development of COFs as electrolyte reservoirs relies critically on maintaining the ionic conductivity inside the bulk of the porous structure and improving the accessibility of electrolytes. However, the intricate interaction between COFs and electrolytes remains a complex and underexplored area. Understanding the charge transfer mechanisms, interfacial stability, and potential side reactions at this interface is crucial for optimizing battery performance and ensuring long-term stability. Advanced characterization techniques and computational modeling can provide valuable insights into these complex processes, paving the way for the development of strategies to mitigate interfacial challenges. Strategic incorporation of functional groups within COFs offers a powerful tool for manipulating ion transport behavior. Exploring novel functional groups and their impact on ionic conductivity, selectivity, and interfacial compatibility. This may involve tailoring the electronic structure, introducing redox-active groups, or incorporating Lewis acid/base functionalities to enhance specific interactions with desired ions. In the context of safe batteries development, the primary concern is the need to inhibit dendrite formation, particularly for the case of metal-ion batteries.

Further, the advantages and disadvantages of COFs with different dimensionality in energy applications are intricately linked to their structural features, which dictate their performance in various energy storage and conversion devices. 2D COFs, characterized by their layered structures with extensive $\pi$-conjugated systems, offer notable advantages in energy storage due to their high and freely accessible surface area. The planar arrangement of atoms in 2D COFs facilitates efficient ion transport and provides abundant active sites for ion storage reactions, such as ion accumulation on redox-active sites. However, their 2D crystalline structure requires efficient pathways for ion and solvent molecule insertion/intercalation. In the absence of such pathways, the 2D layered structure might become inaccessible and electrochemically inactive if it is not stabilized via interlayer pillars. Furthermore, porosity mismatch upon layering may block diffusion pathways in all three dimensions, which is critical for electrodes with high mass loading and, consequently, for the device's energy density. 3D hierarchical COFs, which combine features of both 2D and 3D architectures, offer promising synergistic effects, such as enhanced surface area, charge transport pathways, and ion diffusion kinetics. These structures typically consist of few-layer assemblies with mixed-stacked charge-transfer (CT) complexes, offering additional active sites and pathways for electron transfer. However, fabricating hierarchical COF structures with well-defined morphology and controlled porosity remains a challenge, requiring further optimization and understanding of the structure-properties relationship. In summary, the choice of COF dimensionality in energy applications involves a delicate interplay of surface area, charge transport properties, synthesis complexity, and structural stability. Advancements in the understanding of COF structure-property relationships, particularly regarding $\pi$-conjugation, layering, and electron transfer mechanisms, are essential for unlocking the full potential of COFs in next-generation EES devices.

Last but not least, meeting industrial demands for large-scale, sustainable manufacturing of COFs while ensuring economic viability, ecological responsibility, and safety is a paramount challenge in advancing their practical applications. The scalability and efficiency of COF synthesis methods are crucial factors in achieving this goal. However, one major difficulty lies in the complexity of current synthetic methodologies, which often involve multiple steps and intricate reaction conditions.

These methods may not be easily adaptable to large-scale manufacturing processes, requiring optimization for efficiency and reproducibility. Developing manufacturing techniques that are both cost-effective and environmentally friendly is essential for widespread adoption. Traditional COF synthesis methods typically involve the use of toxic solvents, harsh reaction conditions, and lengthy purification steps, which can significantly increase production costs and environmental impact. Further, the majority of synthetic procedures employed for assembling diverse COF-composites with enhanced conductivity currently lack precise control over the final structure and morphology, particularly when scaled-up. However, the precise engineering of the electrode material is imperative for preserving the inherent benefits of such structures, thereby significantly enhancing their performance in energy storage and facilitating their rapid commercialization. Another barrier to the widespread adoption of COFs is the often-prohibitive cost associated with synthesizing specific multifunctional organic building units. This challenge can be mitigated by utilizing sustainable raw materials derived from the conversion of chemical and biomass waste, coupled with strategies for commercialization and upscaling, resulting in reduced raw materials costs and optimization of production processes and supply chain logistics. Another challenge is the scalability of COF production, as the yield and quality of the materials may vary when synthesized in bulk quantities. Achieving uniformity and consistency in COF properties across large batches is essential for industrial applications but remains a significant hurdle. Addressing these challenges requires innovative approaches to streamline industrial synthesis methods, optimize reaction conditions, and minimize energy requirements and waste generation. Efforts aimed at simplifying and standardizing COF synthesis protocols will further improve their applicability across various industries.

## 9. Conclusions and Outlook

The demand for EES devices has led to a rise in the development of advanced electrochemically active materials. However, existing energy storage materials like graphite, conducting polymers, and metal oxides exhibit notable limitations, such as low energy density and insufficient recyclability in view of the future escalating needs of energy storage from renewable resources and for the electrification of the transportation sector. Emerging and promising materials tailored for EES applications embrace porous nanoassemblies, such as MOFs and COFs. COFs are distinguished from MOFs due to their stability under both acidic and alkaline environments. This approach promises the realization of crystalline yet supple frameworks, substantially broadening the structural possibilities. Importantly, their metal-free composition renders them sustainable materials. One of the major challenges in the field of EES with COFs is their low conductivity, which can be tackled by the development of COFs with extended interacting areas of fused $\pi$-systems combined with macroscopic order. In this scenario, the majority of studies of COFs have been concentrated primarily on LIBs, LSBs, SIB/PIBs, and supercapacitors. In addition, to these applications, COFs are also recently gaining interest on other battery chemistries, such as multivalent ion batteries, metal-oxygen batteries, or metal-halogen batteries. Though studies in these areas remain limited, they are rapidly expanding owing to their promising features. Research on COF-based EES is still emerging and the systematic study of their properties in relation to their molecular/chemical structure and composition, their crystal motives, pore network architecture, and their mesoscale engineering will contribute to the development of the next generation of EES technologies. Integrating diverse functional units into a unified structure will also enhance the functionality of COFs, offering pathways to intricate molecular architectures. Such advancements could include structures with interpenetrating pore networks and COFs that are adaptable, altering their structure, volume, and function in reaction to external forces, such as guest molecules from the electrolytes and metal atoms from the anodes. The pursuit of further developments on COFs also broadens the horizon in porous and coordination materials for energy storage. Further, the significance of crystalline order in COF for energy storage applications remains poorly understood, underscoring the need for a deeper comprehension of the factors influencing the structural arrangement of COFs with tailored functionalities. Such insights are crucial for unlocking the potential of developing more intricate structures at the molecular level.

COFs have also great potential in membrane energy storage technologies, as it has been demonstrated by several reports utilizing them as coating materials for commercial separators or for developing novel stand-alone membranes. Their application as coatings has also shown considerable promise for the modulation of SEI formation and restriction of unwanted side reactions, as well as for promoting the homogenous and reversible metal ion deposition and stripping in pure metal anodes. Their flexibility and stability required in EES devices are also being valorized by using COFs as separators, because they can express high porosity and low electron conductivity while exhibiting fast ionic transport. These properties are also particularly attractive for the development of thin solid-state devices, for application in wearable electronics. To improve their performance, COFs can be doped or functionalized with redox-active groups and metal ions, which can then function as redox-active electrodes, separators, electrolyte reservoir, and catalysts in sulfur chemistries and metal-air batteries. Operando experimental and computational studies, in silico screening, and machine learning methods also offer wide room for further optimization in miscellaneous areas like the tuning of structure-property relationships, interface optimization between the electrode and the electrolyte, the fine-tuning of electrical and ionic conductivity, and enhancing the performance of redox-active groups. To fully utilize all the pores in COF electrodes during charging and discharging cycles, it is essential to explore innovative approaches to electrode material deposition or for on-surface growing on current collectors, keeping their crystallinity and ascribing mesoscale order for large areas and thicknesses. A possible cost-effective method for creating ordered films is by utilizing printing technologies and COF inks. The optimal choice of a linker is another prospective ground in COFs research for improving the electrochemical activity. The selected linkers have a significant impact on the properties of the COF electrodes. Appropriate linkers may afford extended conjugated networks that improve the conductivity of COFs and their long-range crystallinity, avoiding the insulating interfaces created when nano-sized COF crystals are deposited or grown on the current collector surfaces.

Moreover, flexible energy storage devices offer versatility for a wide range of applications, including wearable electronics, flexible displays, and medical devices. In this context, COFs emerge as highly suitable materials due to their organic-based structure and inherent flexibility. Thin film COFs, endowed with high structural modularity and mechanical robustness hold particular promise for flexible battery applications. The possibility to be precisely engineered at the molecular level allows for the customization of pore size, surface chemistry, and electrochemical properties, making them ideal candidates for thin, flexible electrode materials. Moreover, the composite nature of COFs, when combined with conductive polymers such as PEDOT, PPy, or polyaniline, enhances their conductivity and mechanical stability, which are crucial factors for efficient flexible EES devices. In particular, when covalent bonds are developed between the polymers and COFs utilizing side functionalities purposefully installed in the latter, flexibility properties can be drastically improved. Such polymers create conductive and interconnected networks within the COF matrix, facilitating charge transport and improved mechanical strength. The ability to tailor COFs for specific applications allows for the design of flexible batteries with optimized performance metrics, including capacity, cycle life, and mechanical durability. As research in this field evolves, the utilization of COFs in flexible batteries holds great promise for powering the next generation of wearable and flexible electronics. Developments in COFs for EES are expected to substantially contribute in EES technologies and thus to the requirements for clean energy and sustainability, resonating with the United Nations Sustainable Development Goals, which emphasize on the necessity for universal access to affordable, reliable, and sustainable energy.

## Acknowledgements

P.D. and V.S. contributed equally to this work. S.S. acknowledges the support from Horizon Europe under the Marie Skłodowska-Curie project ZION (grant agreement No 101065296). V.S. acknowledges the support from Horizon Europe under the Marie Skłodowska-Curie grant agreement No 847639. R.Z. acknowledges support from ERDF/ESF project TECHSCALE (No. CZ.02.01.01/00/22_008/0004587). G.Z. acknowledges support from the Ministry of the Environment of the Czech Republic under the REFRESH – Research Excellence for Region Sustainability and High-tech Industries project number CZ.10.03.01/00/22_003/0000048 via the Operational Programme Just Transition. A.B. acknowledges support from the Czech Science Foundation (grant no. 22–27973K).

Open access publishing facilitated by Univerzita Palackeho v Olomouci, as part of the Wiley - CzechELib agreement.

## Conflict of Interest

The authors declare no conflict of interest.

## Keywords

batteries, organic, porous networks, supercapacitors

Received: January 31, 2024
Revised: March 19, 2024
Published online:

[1] H. Wang, H. Wang, Z. Wang, L. Tang, G. Zeng, P. Xu, M. Chen, T. Xiong, C. Zhou, X. Li, *Chem. Soc. Rev.* **2020**, *49*, 4135.
[2] P. J. Waller, F. Gándara, O. M. Yaghi, *Acc. Chem. Res.* **2015**, *48*, 3053.
[3] S.-Y. Ding, W. Wang, *Chem. Soc. Rev.* **2013**, *42*, 548.
[4] A. P. Cote, A. I. Benin, N. W. Ockwig, M. O'Keeffe, A. J. Matzger, O. M. Yaghi, *Science* **2005**, *310*, 1166.
[5] K. Geng, T. He, R. Liu, S. Dalapati, K. T. Tan, Z. Li, S. Tao, Y. Gong, Q. Jiang, D. Jiang, *Chem. Rev.* **2020**, *120*, 8814.
[6] E. Ploetz, H. Engelke, U. Lächelt, S. Wuttke, *Adv. Funct. Mater.* **2020**, *30*, 1909062.
[7] A. K. Mandal, J. Mahmood, J.-B. Baek, *ChemNanoMat* **2017**, *3*, 373.
[8] N. Li, J. Du, D. Wu, J. Liu, N. Li, Z. Sun, G. Li, Y. Wu, *Trends Analyt Chem* **2018**, *108*, 154.
[9] M. Liu, Y.-J. Chen, X. Huang, L.-Z. Dong, M. Lu, C. Guo, D. Yuan, Y. Chen, G. Xu, S.-L. Li, Y.-Q. Lan, *Angew. Chem., Int. Ed.* **2022**, *61*, 202115308.
[10] X. Liu, D. Huang, C. Lai, G. Zeng, L. Qin, H. Wang, H. Yi, B. Li, S. Liu, M. Zhang, R. Deng, Y. Fu, L. Li, W. Xue, S. Chen, *Chem. Soc. Rev.* **2019**, *48*, 5266.
[11] I. Ahmed, S. H. Jhung, *Coord. Chem. Rev.* **2021**, *441*, 213989.
[12] S. Pourebrahimi, M. Pirooz, *Clean. Chem. Eng.* **2022**, *2*, 100012.
[13] X. Xu, X. Wu, K. Xu, H. Xu, H. Chen, N. Huang, *Nat. Commun.* **2023**, *14*, 3360.
[14] M. Zhou, M. Liu, J. Wang, T. Gu, B. Huang, W. Wang, K. Wang, S. Cheng, K. Jiang, *Chem. Commun.* **2019**, *55*, 6054.
[15] S. Jin, O. Allam, S. S. Jang, S. W. Lee, *InfoMat* **2022**, 4.
[16] K. Zhang, K. O. Kirlikovali, R. S. Varma, Z. Jin, H. W. Jang, O. K. Farha, M. Shokouhimehr, *ACS Appl. Mater. Interfaces* **2020**, *12*, 27821.
[17] B. Ball, C. Chakravarty, P. Sarkar, *J. Phys. Chem. Lett.* **2020**, *11*, 1542.
[18] X. Guo, H. Mu, T. Hu, Q. Li, Z. F. Wang, *Phys. Rev. B* **2022**, *105*, 155415.
[19] Y.-J. Li, W.-R. Cui, Q.-Q. Jiang, Q. Wu, R.-P. Liang, Q.-X. Luo, J.-D. Qiu, *Nat. Commun.* **2021**, *12*, 4735.
[20] A. Esrafili, A. Wagner, S. Inamdar, A. P. Acharya, *Adv. Healthcare Mater.* **2021**, *10*, 2002090.
[21] S. B. Alahakoon, C. M. Thompson, G. Occhialini, R. A. Smaldone, *ChemSusChem* **2017**, *10*, 2116.
[22] B. Ball, P. Sarkar, *Phys. Chem. Chem. Phys.* **2021**, *23*, 12644.
[23] B. Ball, P. Sarkar, *J. Phys. Chem. C* **2020**, *124*, 15870.
[24] B. Ball, C. Chakravarty, P. Sarkar, *J. Phys. Chem. C* **2019**, *123*, 30155.
[25] M. Li, J. Liu, T. Zhang, X. Song, W. Chen, L. Chen, *Small* **2021**, *17*, 2005073.
[26] P. Simon, Y. Gogotsi, *Nat. Mater.* **2008**, *7*, 845.
[27] V. Shrivastav, S. Sundriyal, P. Goel, H. Kaur, S. K. Tuteja, K. Vikrant, K.-H. Kim, U. K. Tiwari, A. Deep, *Coord. Chem. Rev.* **2019**, *393*, 48.
[28] M. Chafiq, A. Chaouiki, Y. G. Ko, *Energy Storage Mater.* **2023**, *63*, 103014.
[29] P. Xiong, S. Zhang, R. Wang, L. Zhang, Q. Ma, X. Ren, Y. Gao, Z. Wang, Z. Guo, C. Zhang, *Energy Environ. Sci.* **2023**, *16*, 3181.
[30] H. M. El-Kaderi, J. R. Hunt, J. L. Mendoza-Cortés, A. P. Côté, R. E. Taylor, M. O'Keeffe, O. M. Yaghi, *Science* **2007**, *316*, 268.
[31] H. Furukawa, O. M. Yaghi, *J. Am. Chem. Soc.* **2009**, *131*, 8875.
[32] A. Nagai, Z. Guo, X. Feng, S. Jin, X. Chen, X. Ding, D. Jiang, *Nat. Commun.* **2011**, *2*, 536.
[33] Y. Yang, H. Niu, L. Xu, H. Zhang, Y. Cai, *Appl Catal B* **2020**, *269*, 118799.
[34] H. Wang, C. Yang, F. Chen, G. Zheng, Q. Han, *Angew. Chem., Int. Ed.* **2022**, *61*, 202202328.
[35] C. Dai, T. He, L. Zhong, X. Liu, W. Zhen, C. Xue, S. Li, D. Jiang, B. Liu, *Adv. Mater. Interfaces* **2021**, *8*, 2002191.
[36] F. Zhang, H. Hao, X. Dong, X. Li, X. Lang, *Appl Catal B* **2022**, *305*, 121027.

[37] Y.-B. Zhang, J. Su, H. Furukawa, Y. Yun, F. Gándara, A. Duong, X. Zou, O. M. Yaghi, *J. Am. Chem. Soc.* **2013**, *135*, 16336.
[38] Q. Zhu, X. Wang, R. Clowes, P. Cui, L. Chen, M. A. Little, A. I. Cooper, *J. Am. Chem. Soc.* **2020**, *142*, 16842.
[39] J. Hu, S. K. Gupta, J. Ozdemir, H. Beyzavi, *ACS Appl. Nano Mater.* **2020**, *3*, 6239.
[40] W. Cao, W. D. Wang, H.-S. Xu, I. V. Sergeyev, J. Struppe, X. Wang, F. Mentink-Vigier, Z. Gan, M.-X. Xiao, L.-Y. Wang, G.-P. Chen, S.-Y. Ding, S. Bai, W. Wang, *J. Am. Chem. Soc.* **2018**, *140*, 6969.
[41] T. Ma, E. A. Kapustin, S. X. Yin, L. Liang, Z. Zhou, J. Niu, L.-H. Li, Y. Wang, J. Su, J. Li, X. Wang, W. D. Wang, W. Wang, J. Sun, O. M. Yaghi, *Science* **2018**, *361*, 48.
[42] A. M. Evans, L. R. Parent, N. C. Flanders, R. P. Bisbey, E. Vitaku, M. S. Kirschner, R. D. Schaller, L. X. Chen, N. C. Gianneschi, W. R. Dichtel, *Science* **2018**, *361*, 52.
[43] Q. Gao, X. Li, G.-H. Ning, H.-S. Xu, C. Liu, B. Tian, W. Tang, K. P. Loh, *Chem. Mater.* **2018**, *30*, 1762.
[44] S. Vijayakumar, A. Ajayaghosh, S. Shankar, *J. Mater. Chem. A* **2023**, *11*, 26340.
[45] T. Banerjee, F. Haase, S. Trenker, B. P. Biswal, G. Savasci, V. Duppel, I. Moudrakovski, C. Ochsenfeld, B. V. Lotsch, *Nat. Commun.* **2019**, *10*, 2689.
[46] M. Liu, S. Liu, C.-X. Cui, Q. Miao, Y. He, X. Li, Q. Xu, G. Zeng, *Angew. Chem., Int. Ed.* **2022**, *61*, 202213522.
[47] Y. Li, X. Guo, X. Li, M. Zhang, Z. Jia, Y. Deng, Y. Tian, S. Li, L. Ma, *Angew. Chem.* **2020**, *132*, 4197.
[48] X. Yang, L. Gong, X. Liu, P. Zhang, B. Li, D. Qi, K. Wang, F. He, J. Jiang, *Angew. Chem., Int. Ed.* **2022**, *61*, 202207043.
[49] C. Gropp, T. Ma, N. Hanikel, O. M. Yaghi, *Science* **2020**, *370*, eabd6406.
[50] S. Wan, J. Guo, J. Kim, H. Ihee, D. Jiang, *Angew. Chem., Int. Ed.* **2009**, *48*, 5439.
[51] C.-Z. Guan, D. Wang, L.-J. Wan, *Chem. Commun.* **2012**, *48*, 2943.
[52] M. Dogru, M. Handloser, F. Auras, T. Kunz, D. Medina, A. Hartschuh, P. Knochel, T. Bein, *Angew. Chem.* **2013**, *125*, 2992.
[53] L. Zhai, N. Huang, H. Xu, Q. Chen, D. Jiang, *Chem. Commun.* **2017**, *53*, 4242.
[54] N. Huang, L. Zhai, H. Xu, D. Jiang, *J. Am. Chem. Soc.* **2017**, *139*, 2428.
[55] P. Wang, Q. Xu, Z. Li, W. Jiang, Q. Jiang, D. Jiang, *Adv. Mater.* **2018**, *30*, 1801991.
[56] R. L. Li, N. C. Flanders, A. M. Evans, W. Ji, I. Castano, L. X. Chen, N. C. Gianneschi, W. R. Dichtel, *Chem. Sci.* **2019**, *10*, 3796.
[57] G. Chen, H.-H. Lan, S.-L. Cai, B. Sun, X.-L. Li, Z.-H. He, S.-R. Zheng, J. Fan, Y. Liu, W.-G. Zhang, *ACS Appl. Mater. Interfaces* **2019**, *11*, 12830.
[58] Y. Su, Y. Liu, P. Liu, D. Wu, X. Zhuang, F. Zhang, X. Feng, *Angew. Chem., Int. Ed.* **2015**, *54*, 1812.
[59] M.-X. Wu, Y.-W. Yang, *Chin. Chem. Lett.* **2017**, *28*, 1135.
[60] M. Alharbi, R. Aljohani, R. Alzahrani, Y. Alsufyani, N. Alsmani, *Comput. Chem.* **2023**, *11*, 53.
[61] M. Lu, M. Zhang, J. Liu, Y. Chen, J.-P. Liao, M.-Y. Yang, Y.-P. Cai, S.-L. Li, Y.-Q. Lan, *Angew. Chem.* **2022**, *134*, 202200003.
[62] Z. Li, Y. Zhi, X. Feng, X. Ding, Y. Zou, X. Liu, Y. Mu, *Chemistry* **2015**, *21*, 12079.
[63] G. Zhang, X. Li, Q. Liao, Y. Liu, K. Xi, W. Huang, X. Jia, *Nat. Commun.* **2018**, *9*, 2785.
[64] D. Kaleeswaran, P. Vishnoi, R. Murugavel, *J. Mater. Chem. C* **2015**, *3*, 7159.
[65] J. F. Dienstmaier, D. D. Medina, M. Dogru, P. Knochel, T. Bein, W. M. Heckl, M. Lackinger, *ACS Nano* **2012**, *6*, 7234.
[66] S. Bi, C. Yang, W. Zhang, J. Xu, L. Liu, D. Wu, X. Wang, Y. Han, Q. Liang, F. Zhang, *Nat. Commun.* **2019**, *10*, 2467.
[67] Y. Wang, H. Liu, Q. Pan, C. Wu, W. Hao, J. Xu, R. Chen, J. Liu, Z. Li, Y. Zhao, *J. Am. Chem. Soc.* **2020**, *142*, 5958.
[68] X.-T. Li, J. Zou, T.-H. Wang, H.-C. Ma, G.-J. Chen, Y.-B. Dong, *J. Am. Chem. Soc.* **2020**, *142*, 6521.
[69] W. K. Haug, E. R. Wolfson, B. T. Morman, C. M. Thomas, P. L. McGrier, *J. Am. Chem. Soc.* **2020**, *142*, 5521.
[70] X. Li, J. Qiao, S. W. Chee, H.-S. Xu, X. Zhao, H. S. Choi, W. Yu, S. Y. Quek, U. Mirsaidov, K. P. Loh, *J. Am. Chem. Soc.* **2020**, *142*, 4932.
[71] S. Jhulki, A. M. Evans, X.-L. Hao, M. W. Cooper, C. H. Feriante, J. Leisen, H. Li, D. Lam, M. C. Hersam, S. Barlow, J.-L. Brédas, W. R. Dichtel, S. R. Marder, *J. Am. Chem. Soc.* **2020**, *142*, 783.
[72] P.-L. Wang, S.-Y. Ding, Z.-C. Zhang, Z.-P. Wang, W. Wang, *J. Am. Chem. Soc.* **2019**, *141*, 18004.
[73] M. Zhang, J. Chen, S. Zhang, X. Zhou, L. He, M. V. Sheridan, M. Yuan, M. Zhang, L. Chen, X. Dai, F. Ma, J. Wang, J. Hu, G. Wu, X. Kong, R. Zhou, T. E. Albrecht-Schmitt, Z. Chai, S. Wang, *J. Am. Chem. Soc.* **2020**, *142*, 9169.
[74] S. Mondal, B. Mohanty, M. Nurhuda, S. Dalapati, R. Jana, M. Addicoat, A. Datta, B. K. Jena, A. Bhaumik, *ACS Catal.* **2020**, *10*, 5623.
[75] R. Tao, X. Shen, Y. Hu, K. Kang, Y. Zheng, S. Luo, S. Yang, W. Li, S. Lu, Y. Jin, L. Qiu, W. Zhang, *Small* **2020**, *16*, 1906005.
[76] Z. Mi, P. Yang, R. Wang, J. Unruangsri, W. Yang, C. Wang, J. Guo, *J. Am. Chem. Soc.* **2019**, *141*, 14433.
[77] F. Auras, L. Ascherl, A. H. Hakimioun, J. T. Margraf, F. C. Hanusch, S. Reuter, D. Bessinger, M. Döblinger, C. Hettstedt, K. Karaghiosoff, S. Herbert, P. Knochel, T. Clark, T. Bein, *J. Am. Chem. Soc.* **2016**, *138*, 16703.
[78] X. Feng, X. Ding, L. Chen, Y. Wu, L. Liu, M. Addicoat, S. Irle, Y. Dong, D. Jiang, *Sci. Rep.* **2016**, *6*, 32944.
[79] S. Dalapati, M. Addicoat, S. Jin, T. Sakurai, J. Gao, H. Xu, S. Irle, S. Seki, D. Jiang, *Nat. Commun.* **2015**, *6*, 7786.
[80] Z. Li, N. Huang, K. H. Lee, Y. Feng, S. Tao, Q. Jiang, Y. Nagao, S. Irle, D. Jiang, *J. Am. Chem. Soc.* **2018**, *140*, 12374.
[81] J. Shi, R. Chen, H. Hao, C. Wang, X. Lang, *Angew. Chem., Int. Ed.* **2020**, *59*, 9088.
[82] B. Zhang, H. Mao, R. Matheu, J. A. Reimer, S. A. Alshmimri, S. Alshihri, O. M. Yaghi, *J. Am. Chem. Soc.* **2019**, *141*, 11420.
[83] X. Feng, Y. Dong, D. Jiang, *CrystEngComm* **2013**, *15*, 1508.
[84] S. Dalapati, E. Jin, M. Addicoat, T. Heine, D. Jiang, *J. Am. Chem. Soc.* **2016**, *138*, 5797.
[85] X. Chen, M. Addicoat, E. Jin, H. Xu, T. Hayashi, F. Xu, N. Huang, S. Irle, D. Jiang, *Sci. Rep.* **2015**, *5*, 14650.
[86] L. Guo, S. Jia, C. S. Diercks, X. Yang, S. A. Alshmimri, O. M. Yaghi, *Angew. Chem. Int. Ed.* **2020**, *59*, 2023.
[87] N. Huang, P. Wang, D. Jiang, *Nat. Rev. Mater.* **2016**, *1*, 16068.
[88] C. Qian, L. Feng, W. L. Teo, J. Liu, W. Zhou, D. Wang, Y. Zhao, *Nat. Rev. Chem.* **2022**, *6*, 881.
[89] P. Leidinger, M. Panighel, V. P. Dieste, I. J. Villar-Garcia, P. Vezzoni, F. Haag, J. V. Barth, F. Allegretti, S. Günther, L. L. Patera, *Nanoscale* **2023**, *15*, 1068.
[90] W. Zheng, C.-S. Tsang, L. Y. S. Lee, K.-Y. Wong, *Mater Today Chem* **2019**, *12*, 34.
[91] S. Wan, J. Guo, J. Kim, H. Ihee, D. Jiang, *Angew. Chem., Int. Ed.* **2008**, *47*, 8826.
[92] J. M. Rotter, S. Weinberger, J. Kampmann, T. Sick, M. Shalom, T. Bein, D. D. Medina, *Chem. Mater.* **2019**, *31*, 10008.
[93] S. Cao, B. Li, R. Zhu, H. Pang, *Chem. Eng. J.* **2019**, *355*, 602.
[94] X. Liang, Z. Ni, L. Zhao, B. Ge, H. Zhao, W. Li, *Mater. Chem. Phys.* **2021**, *270*, 124725.
[95] S. Xiong, J. Liu, Y. Wang, X. Wang, J. Chu, R. Zhang, M. Gong, B. Wu, *J. Appl. Polym. Sci.* **2022**, *139*, 51510.
[96] S. Ren, M. J. Bojdys, R. Dawson, A. Laybourn, Y. Z. Khimyak, D. J. Adams, A. I. Cooper, *Adv. Mater.* **2012**, *24*, 2357.

[97] S. L. James, C. J. Adams, C. Bolm, D. Braga, P. Collier, T. Friščić, F. Grepioni, K. D. M. Harris, G. Hyett, W. Jones, A. Krebs, J. Mack, L. Maini, A. G. Orpen, I. P. Parkin, W. C. Shearouse, J. W. Steed, D. C. Waddell, *Chem. Soc. Rev.* **2011**, *41*, 413.
[98] D. Tan, T. Friščić, *Eur. J. Org. Chem.* **2018**, *2018*, 18.
[99] J. Hu, Z. Huang, Y. Liu, *Angew. Chem., Int. Ed.* **2023**, *62*, 202306999.
[100] G. Das, D. B. Shinde, S. Kandambeth, B. P. Biswal, R. Banerjee, *Chem. Commun.* **2014**, *50*, 12615.
[101] S. Chandra, S. Kandambeth, B. P. Biswal, B. Lukose, S. M. Kunjir, M. Chaudhary, R. Babarao, T. Heine, R. Banerjee, *J. Am. Chem. Soc.* **2013**, *135*, 17853.
[102] Y. Cao, M. Wang, H. Wang, C. Han, F. Pan, J. Sun, *Adv. Energy Mater.* **2022**, *12*, 2200057.
[103] X. Li, C. Yang, B. Sun, S. Cai, Z. Chen, Y. Lv, J. Zhang, Y. Liu, *J. Mater. Chem. A* **2020**, *8*, 16045.
[104] R. I. Walton, *Chem. Soc. Rev.* **2002**, *31*, 230.
[105] K. M. Ø. Jensen, C. Tyrsted, M. Bremholm, B. B. Iversen, *ChemSusChem* **2014**, *7*, 1594.
[106] X. Feng, X. Ding, D. Jiang, *Chem. Soc. Rev.* **2012**, *41*, 6010.
[107] Y. Xia, P. Yang, Y. Sun, Y. Wu, B. Mayers, B. Gates, Y. Yin, F. Kim, H. Yan, *Adv. Mater.* **2003**, *15*, 353.
[108] S. Khalil, M. D. Meyer, A. Alazmi, M. H. K. Samani, P.-C. Huang, M. Barnes, A. B. Marciel, R. Verduzco, *ACS Nano* **2022**, *16*, 20964.
[109] L. K. Ritchie, A. Trewin, A. Reguera-Galan, T. Hasell, A. I. Cooper, *Microporous Mesoporous Mater.* **2010**, *132*, 132.
[110] X. Han, J. Huang, C. Yuan, Y. Liu, Y. Cui, *J. Am. Chem. Soc.* **2018**, *140*, 892.
[111] Y. Zhao, L. Guo, F. Gándara, Y. Ma, Z. Liu, C. Zhu, H. Lyu, C. A. Trickett, E. A. Kapustin, O. Terasaki, O. M. Yaghi, *J. Am. Chem. Soc.* **2017**, *139*, 13166.
[112] R. Wang, Z. Chen, *Microchim. Acta* **2017**, *184*, 3867.
[113] Y.-F. Ma, F. Yuan, X.-H. Zhang, Y.-L. Zhou, X.-X. Zhang, *Analyst* **2017**, *142*, 3212.
[114] T. Bao, P. Tang, D. Kong, Z. Mao, Z. Chen, *J. Chromatogr. A* **2016**, *1445*, 140.
[115] M. Taddei, P. V. Dau, S. M. Cohen, M. Ranocchiari, J. A. van Bokhoven, F. Costantino, S. Sabatini, R. Vivani, *Dalton Trans.* **2015**, *44*, 14019.
[116] R. Sakamoto, K. Hoshiko, Q. Liu, T. Yagi, T. Nagayama, S. Kusaka, M. Tsuchiya, Y. Kitagawa, W.-Y. Wong, H. Nishihara, *Nat. Commun.* **2015**, *6*, 6713.
[117] Y. Li, C.-X. Yang, X.-P. Yan, *Chem. Commun.* **2017**, *53*, 2511.
[118] B. Gutmann, D. Cantillo, C. O. Kappe, *Angew. Chem., Int. Ed.* **2015**, *54*, 6688.
[119] J. W. Colson, A. R. Woll, A. Mukherjee, M. P. Levendorf, E. L. Spitler, V. B. Shields, M. G. Spencer, J. Park, W. R. Dichtel, *Science* **2011**, *332*, 228.
[120] J. W. Colson, J. A. Mann, C. R. DeBlase, W. R. Dichtel, *J. Polym. Sci. Part Polym. Chem.* **2015**, *53*, 378.
[121] D. D. Medina, J. M. Rotter, Y. Hu, M. Dogru, V. Werner, F. Auras, J. T. Markiewicz, P. Knochel, T. Bein, *J. Am. Chem. Soc.* **2015**, *137*, 1016.
[122] H. Ding, Y. Li, H. Hu, Y. Sun, J. Wang, C. Wang, C. Wang, G. Zhang, B. Wang, W. Xu, D. Zhang, *Chemistry* **2014**, *20*, 14614.
[123] J. Liu, G. Han, D. Zhao, K. Lu, J. Gao, T.-S. Chung, *Sci. Adv.* **2020**, *6*, eabb1110.
[124] C. R. DeBlase, K. E. Silberstein, T.-T. Truong, H. D. Abruña, W. R. Dichtel, *J. Am. Chem. Soc.* **2013**, *135*, 16821.
[125] X. Gou, Q. Zhang, Y. Wu, Y. Zhao, X. Shi, X. Fan, L. Huang, G. Lu, *RSC Adv.* **2016**, *6*, 39198.
[126] P. Nilsson, K. Olofsson, M. Larhed, In *Microwave Methods in Organic Synthesis* (Eds: M. Larhed, K. Olofssonq), Springer, Berlin, Heidelberg, **2006**, pp. 103–144.
[127] K. De Keukeleere, J. Feys, M. Meire, J. De Roo, K. De Buysser, P. Lommens, I. Van Driessche, *J. Nanoparticle Res.* **2013**, *15*, 2074.
[128] N. L. Campbell, R. Clowes, L. K. Ritchie, A. I. Cooper, *Chem. Mater.* **2009**, *21*, 204.
[129] H. Wei, S. Chai, N. Hu, Z. Yang, L. Wei, L. Wang, *Chem. Commun.* **2015**, *51*, 12178.
[130] A. R. Bagheri, N. Aramesh, *J. Mater. Sci.* **2021**, *56*, 1116.
[131] C.-X. Yang, C. Liu, Y.-M. Cao, X.-P. Yan, *Chem. Commun.* **2015**, *51*, 12254.
[132] G. Lin, C. Gao, Q. Zheng, Z. Lei, H. Geng, Z. Lin, H. Yang, Z. Cai, *Chem. Commun.* **2017**, *53*, 3649.
[133] C. Gao, G. Lin, Z. Lei, Q. Zheng, J. Lin, Z. Lin, *J. Mater. Chem. B* **2017**, *5*, 7496.
[134] Y. Peng, W. K. Wong, Z. Hu, Y. Cheng, D. Yuan, S. A. Khan, D. Zhao, *Chem. Mater.* **2016**, *28*, 5095.
[135] R. P. Bisbey, C. R. DeBlase, B. J. Smith, W. R. Dichtel, *J. Am. Chem. Soc.* **2016**, *138*, 11433.
[136] J. Britton, C. L. Raston, *Chem. Soc. Rev.* **2017**, *46*, 1250.
[137] H. Wang, Z. Zeng, P. Xu, L. Li, G. Zeng, R. Xiao, Z. Tang, D. Huang, L. Tang, C. Lai, D. Jiang, Y. Liu, H. Yi, L. Qin, S. Ye, X. Ren, W. Tang, *Chem. Soc. Rev.* **2019**, *48*, 488.
[138] P. Zhang, Y. Huang, X. Lu, S. Zhang, J. Li, G. Wei, Z. Su, *Langmuir* **2014**, *30*, 8980.
[139] W. Dai, F. Shao, J. Szczerbiński, R. McCaffrey, R. Zenobi, Y. Jin, A. D. Schlüter, W. Zhang, *Angew. Chem.* **2016**, *128*, 221.
[140] C. Stubenrauch, P.-A. Albouy, R. v. Klitzing, D. Langevin, *Langmuir* **2000**, *16*, 3206.
[141] F. Ravera, E. Santini, G. Loglio, M. Ferrari, L. Liggieri, *J. Phys. Chem. B* **2006**, *110*, 19543.
[142] J. I. Feldblyum, C. H. McCreery, S. C. Andrews, T. Kurosawa, E. J. G. Santos, V. Duong, L. Fang, A. L. Ayzner, Z. Bao, *Chem. Commun.* **2015**, *51*, 13894.
[143] D. Zhou, X. Tan, H. Wu, L. Tian, M. Li, *Angew. Chem.* **2019**, *131*, 1390.
[144] K. Dey, M. Pal, K. C. Rout, S. Kunjattu H, A. Das, R. Mukherjee, U. K. Kharul, R. Banerjee, *J. Am. Chem. Soc.* **2017**, *139*, 13083.
[145] M. Matsumoto, L. Valentino, G. M. Stiehl, H. B. Balch, A. R. Corcos, F. Wang, D. C. Ralph, B. J. Mariñas, W. R. Dichtel, *Chem* **2018**, *4*, 308.
[146] P. Zhang, F. Zhang, C. Zhao, S. Wang, M. Liu, L. Jiang, *Angew. Chem., Int. Ed.* **2016**, *55*, 3615.
[147] B. Bai, D. Wang, L.-J. Wan, *Bull. Chem. Soc. Jpn.* **2021**, *94*, 1090.
[148] Y. Li, M. Zhang, X. Guo, R. Wen, X. Li, X. Li, S. Li, L. Ma, *Nanoscale Horiz.* **2018**, *3*, 205.
[149] Q. Hao, C. Zhao, B. Sun, C. Lu, J. Liu, M. Liu, L.-J. Wan, D. Wang, *J. Am. Chem. Soc.* **2018**, *140*, 12152.
[150] R. Gutzler, H. Walch, G. Eder, S. Kloft, W. M. Heckl, M. Lackinger, *Chem. Commun.* **2009**, *0*, 4456.
[151] N. Chiang, X. Chen, G. Goubert, D. V. Chulhai, X. Chen, E. A. Pozzi, N. Jiang, M. C. Hersam, T. Seideman, L. Jensen, R. P. Van Duyne, *Nano Lett.* **2016**, *16*, 7774.
[152] K. Suenaga, H. G. Ji, Y.-C. Lin, T. Vincent, M. Maruyama, A. S. Aji, Y. Shiratsuchi, D. Ding, K. Kawahara, S. Okada, V. Panchal, O. Kazakova, H. Hibino, K. Suenaga, H. Ago, *ACS Nano* **2018**, *12*, 10032.
[153] X.-H. Liu, C.-Z. Guan, D. Wang, L.-J. Wan, *Adv. Mater.* **2014**, *26*, 6912.
[154] N. A. A. Zwaneveld, R. Pawlak, M. Abel, D. Catalin, D. Gigmes, D. Bertin, L. Porte, *J. Am. Chem. Soc.* **2008**, *130*, 6678.
[155] C. Chen, T. Joshi, H. Li, A. D. Chavez, Z. Pedramrazi, P.-N. Liu, H. Li, W. R. Dichtel, J.-L. Bredas, M. F. Crommie, *ACS Nano* **2018**, *12*, 385.
[156] S. Schlögl, T. Sirtl, J. Eichhorn, W. M. Heckl, M. Lackinger, *Chem. Commun.* **2011**, *47*, 12355.
[157] D. Rodríguez-San-Miguel, C. Montoro, F. Zamora, *Chem. Soc. Rev.* **2020**, *49*, 2291.
[158] L. Xu, X. Zhou, Y. Yu, W. Q. Tian, J. Ma, S. Lei, *ACS Nano* **2013**, *7*, 8066.

[159] X.-H. Liu, C.-Z. Guan, S.-Y. Ding, W. Wang, H.-J. Yan, D. Wang, L.-J. Wan, *J. Am. Chem. Soc.* **2013**, *135*, 10470.
[160] W. Liu, X. Luo, Y. Bao, Y. P. Liu, G.-H. Ning, I. Abdelwahab, L. Li, C. T. Nai, Z. G. Hu, D. Zhao, B. Liu, S. Y. Quek, K. P. Loh, *Nat. Chem.* **2017**, *9*, 563.
[161] Z. Song, H. Zhou, *Energy Environ. Sci.* **2013**, *6*, 2280.
[162] J. Wang, L. Liu, F. Wu, Z. Liu, Z. Fan, L. Chen, Y. Chen, *ChemSusChem* **2022**, *15*, 202102420.
[163] H. Lyu, X.-G. Sun, S. Dai, *Adv. Energy Sustain. Res.* **2021**, *2*, 2000044.
[164] X. Yin, S. Sarkar, S. Shi, Q.-A. Huang, H. Zhao, L. Yan, Y. Zhao, J. Zhang, *Adv. Funct. Mater.* **2020**, *30*, 1908445.
[165] Q. Zhao, Y. Lu, J. Chen, *Adv. Energy Mater.* **2017**, *7*, 1601792.
[166] L. Chen, K. Chen, S. Zhu, *Chem* **2018**, *4*, 1208.
[167] T. Sun, Z.-J. Li, Y.-F. Zhi, Y.-J. Huang, H. J. Fan, Q. Zhang, *Adv. Funct. Mater.* **2021**, *31*, 2010049.
[168] G. Wang, N. Chandrasekhar, B. P. Biswal, D. Becker, S. Paasch, E. Brunner, M. Addicoat, M. Yu, R. Berger, X. Feng, *Adv. Mater.* **2019**, *31*, 1901478.
[169] Z. Lei, Q. Yang, Y. Xu, S. Guo, W. Sun, H. Liu, L.-P. Lv, Y. Zhang, Y. Wang, *Nat. Commun.* **2018**, *9*, 576.
[170] J. Zhao, M. Zhou, J. Chen, L. Tao, Q. Zhang, Z. Li, S. Zhong, H. Fu, H. Wang, L. Wu, *Chem. Eng. J.* **2021**, *425*, 131630.
[171] H. Chen, Y. Zhang, C. Xu, M. Cao, H. Dou, X. Zhang, *Chemistry* **2019**, *25*, 15472.
[172] E. Vitaku, C. N. Gannett, K. L. Carpenter, L. Shen, H. D. Abruña, W. R. Dichtel, *J. Am. Chem. Soc.* **2020**, *142*, 16.
[173] L. Kong, M. Liu, H. Huang, Y. Xu, X.-H. Bu, *Adv. Energy Mater.* **2022**, *12*, 2100172.
[174] M. Wu, Y. Zhao, B. Sun, Z. Sun, C. Li, Y. Han, L. Xu, Z. Ge, Y. Ren, M. Zhang, Q. Zhang, Y. Lu, W. Wang, Y. Ma, Y. Chen, *Nano Energy* **2020**, *70*, 104498.
[175] C.-J. Yao, Z. Wu, J. Xie, F. Yu, W. Guo, Z. J. Xu, D.-S. Li, S. Zhang, Q. Zhang, *ChemSusChem* **2020**, *13*, 2457.
[176] Y. Lu, Y. Cai, Q. Zhang, J. Chen, *J. Phys. Chem. Lett.* **2021**, *12*, 8061.
[177] S.-Y. Li, W.-H. Li, X.-L. Wu, Y. Tian, J. Yue, G. Zhu, *Chem. Sci.* **2019**, *10*, 7695.
[178] Q. An, L. Wang, G. Zhao, L. Duan, Y. Sun, Q. Liu, Z. Mei, Y. Yang, C. Zhang, H. Guo, *Adv. Mater.* **2024**, *36*, 2305818.
[179] X. Liu, M. Xia, Y. Zhao, T. Xia, Y. Li, J. Xiao, Z. Sui, Q. Chen, *Mater Today Chem* **2022**, *23*, 100664.
[180] D. Zhu, G. Xu, M. Barnes, Y. Li, C.-P. Tseng, Z. Zhang, J.-J. Zhang, Y. Zhu, S. Khalil, M. M. Rahman, R. Verduzco, P. M. Ajayan, *Adv. Funct. Mater.* **2021**, *31*, 2100505.
[181] Z. Li, H. Li, X. Guan, J. Tang, Y. Yusran, Z. Li, M. Xue, Q. Fang, Y. Yan, V. Valtchev, S. Qiu, *J. Am. Chem. Soc.* **2017**, *139*, 17771.
[182] M. Wang, H. Guo, R. Xue, Q. Li, H. Liu, N. Wu, W. Yao, W. Yang, *ChemElectroChem* **2019**, *6*, 2984.
[183] D. Larcher, J.-M. Tarascon, *Nat. Chem.* **2015**, *7*, 19.
[184] R. Schmuch, R. Wagner, G. Hörpel, T. Placke, M. Winter, *Nat. Energy* **2018**, *3*, 267.
[185] C. Li, J. Yang, P. Pachfule, S. Li, M.-Y. Ye, J. Schmidt, A. Thomas, *Nat. Commun.* **2020**, *11*, 4712.
[186] K. T. Tan, S. Ghosh, Z. Wang, F. Wen, D. Rodríguez-San-Miguel, J. Feng, N. Huang, W. Wang, F. Zamora, X. Feng, A. Thomas, D. Jiang, *Nat. Rev. Methods Primers* **2023**, *3*, 1.
[187] T. Banerjee, F. Podjaski, J. Kröger, B. P. Biswal, B. V. Lotsch, *Nat. Rev. Mater.* **2021**, *6*, 168.
[188] A. Knebel, J. Caro, *Nat. Nanotechnol.* **2022**, *17*, 911.
[189] J. Yang, Y. Shi, P. Sun, P. Xiong, Y. Xu, *ACS Appl. Mater. Interfaces* **2019**, *11*, 42305.
[190] K. Borzutzki, J. Thienenkamp, M. Diehl, M. Winter, G. Brunklaus, *J. Mater. Chem. A* **2019**, *7*, 188.
[191] M. R. Kaiser, Z. Han, J. Liang, S.-X. Dou, J. Wang, *Energy Storage Mater.* **2019**, *19*, 1.
[192] M. Idrees, S. Batool, J. Kong, Q. Zhuang, H. Liu, Q. Shao, N. Lu, Y. Feng, E. K. Wujcik, Q. Gao, T. Ding, R. Wei, Z. Guo, *Electrochim. Acta* **2019**, *296*, 925.
[193] H. Liu, Y. Wang, H. Liu, Y. Sun, S. Guan, *J. Electroanal. Chem.* **2019**, *848*, 113289.
[194] Y. Song, Y. Hu, Y. Sha, H. Rong, H. Wen, H.-J. Liu, Q. Liu, *Ionics* **2019**, *25*, 2987.
[195] Y. Lu, X. Hou, L. Miao, L. Li, R. Shi, L. Liu, J. Chen, *Angew. Chem.* **2019**, *131*, 7094.
[196] D.-H. Yang, Z.-Q. Yao, D. Wu, Y.-H. Zhang, Z. Zhou, X.-H. Bu, *J. Mater. Chem. A* **2016**, *4*, 18621.
[197] S. Wang, Q. Wang, P. Shao, Y. Han, X. Gao, L. Ma, S. Yuan, X. Ma, J. Zhou, X. Feng, B. Wang, *J. Am. Chem. Soc.* **2017**, *139*, 4258.
[198] K. Nakashima, T. Shimizu, Y. Kamakura, A. Hinokimoto, Y. Kitagawa, H. Yoshikawa, D. Tanaka, *Chem. Sci.* **2020**, *11*, 37.
[199] C.-X. WANG, F. YU, J. MA, *Acta Phys.-Chim. Sin.* **2016**, *32*, 2411.
[200] J.-L. JIANG, X. ZHANG, J.-F. DU, Q. WANG, J.-F. DAI, Z.-Q. WEI, *Acta Phys.-Chim. Sin.* **2016**, *32*, 1839.
[201] Z. Luo, L. Liu, J. Ning, K. Lei, Y. Lu, F. Li, J. Chen, *Angew. Chem., Int. Ed.* **2018**, *57*, 9443.
[202] C. R. DeBlase, W. R. Dichtel, *Macromolecules* **2016**, *49*, 5297.
[203] Z. Lei, X. Chen, W. Sun, Y. Zhang, Y. Wang, *Adv. Energy Mater.* **2019**, *9*, 1801010.
[204] X. Chen, Y. Li, L. Wang, Y. Xu, A. Nie, Q. Li, F. Wu, W. Sun, X. Zhang, R. Vajtai, P. M. Ajayan, L. Chen, Y. Wang, *Adv. Mater.* **2019**, *31*, 1901640.
[205] Z. Yang, T. Wang, H. Chen, X. Suo, P. Halstenberg, H. Lyu, W. Jiang, S. M. Mahurin, I. Popovs, S. Dai, *ACS Energy Lett.* **2021**, *6*, 41.
[206] K. A. See, S. Hug, K. Schwinghammer, M. A. Lumley, Y. Zheng, J. M. Nolt, G. D. Stucky, F. Wudl, B. V. Lotsch, R. Seshadri, *Chem. Mater.* **2015**, *27*, 3821.
[207] K. Sakaushi, G. Nickerl, F. M. Wisser, D. Nishio-Hamane, E. Hosono, H. Zhou, S. Kaskel, J. Eckert, *Angew. Chem., Int. Ed.* **2012**, *51*, 7850.
[208] K. Sakaushi, E. Hosono, G. Nickerl, H. Zhou, S. Kaskel, J. Eckert, *J. Power Sources* **2014**, *245*, 553.
[209] R. Yuan, W. Kang, C. Zhang, *Materials* **2018**, *11*, 937.
[210] A. Jaffe, A. Saldivar Valdes, H. I. Karunadasa, *Chem. Mater.* **2015**, *27*, 3568.
[211] H. Chen, M. Armand, M. Courty, M. Jiang, C. P. Grey, F. Dolhem, J.-M. Tarascon, P. Poizot, *J. Am. Chem. Soc.* **2009**, *131*, 8984.
[212] B. Tian, G.-H. Ning, W. Tang, C. Peng, D. Yu, Z. Chen, Y. Xiao, C. Su, K. P Loh, *Mater. Horiz.* **2016**, *3*, 429.
[213] S. Muench, A. Wild, C. Friebe, B. Häupler, T. Janoschka, U. S. Schubert, *Chem. Rev.* **2016**, *116*, 9438.
[214] Z. Wang, Y. Li, P. Liu, Q. Qi, F. Zhang, G. Lu, X. Zhao, X. Huang, *Nanoscale* **2019**, *11*, 5330.
[215] H. Gao, B. Tian, H. Yang, A. R. Neale, M. A. Little, R. S. Sprick, L. J. Hardwick, A. I. Cooper, *ChemSusChem* **2020**, *13*, 5571.
[216] A. Molina, N. Patil, E. Ventosa, M. Liras, J. Palma, R. Marcilla, *ACS Energy Lett.* **2020**, *5*, 2945.
[217] A. Molina, N. Patil, E. Ventosa, M. Liras, J. Palma, R. Marcilla, *Adv. Funct. Mater.* **2020**, *30*, 1908074.
[218] K. Amin, J. Zhang, H.-Y. Zhou, R. Lu, M. Zhang, N. Ashraf, C. YueLi, L. Mao, C. F. J. Faul, Z. Wei, *Sustain. Energy Fuels* **2020**, *4*, 4179.
[219] W. Liu, P. Oh, X. Liu, M.-J. Lee, W. Cho, S. Chae, Y. Kim, J. Cho, *Angew. Chem., Int. Ed.* **2015**, *54*, 4440.
[220] S. E. Jerng, B. Chang, H. Shin, H. Kim, T. Lee, K. Char, J. W. Choi, *ACS Appl. Mater. Interfaces* **2020**, *12*, 10597.
[221] A. Manthiram, X. Yu, S. Wang, *Nat. Rev. Mater.* **2017**, *2*, 16103.
[222] J. Janek, W. G. Zeier, *Nat. Energy* **2016**, *1*, 16141.
[223] K. Jeong, S. Park, S.-Y. Lee, *J. Mater. Chem. A* **2019**, *7*, 1917.
[224] J. C. Bachman, S. Muy, A. Grimaud, H.-H. Chang, N. Pour, S. F. Lux, O. Paschos, F. Maglia, S. Lupart, P. Lamp, L. Giordano, Y. Shao-Horn, *Chem. Rev.* **2016**, *116*, 140.

[225] K. (Kelvin) Fu, Y. Gong, G. T. Hitz, D. W. McOwen, Y. Li, S. Xu, Y. Wen, L. Zhang, C. Wang, G. Pastel, J. Dai, B. Liu, H. Xie, Y. Yao, E. D. Wachsman, L. Hu, *Energy Environ. Sci.* **2017**, *10*, 1568.
[226] Y. Kato, S. Hori, T. Saito, K. Suzuki, M. Hirayama, A. Mitsui, M. Yonemura, H. Iba, R. Kanno, *Nat. Energy* **2016**, *1*, 16030.
[227] H. Chen, H. Tu, C. Hu, Y. Liu, D. Dong, Y. Sun, Y. Dai, S. Wang, H. Qian, Z. Lin, L. Chen, *J. Am. Chem. Soc.* **2018**, *140*, 896.
[228] Y. Zhang, J. Duan, D. Ma, P. Li, S. Li, H. Li, J. Zhou, X. Ma, X. Feng, B. Wang, *Angew. Chem., Int. Ed.* **2017**, *56*, 16313.
[229] S. S. Park, Y. Tulchinsky, M. Dincă, *J. Am. Chem. Soc.* **2017**, *139*, 13260.
[230] Z. Wang, R. Tan, H. Wang, L. Yang, J. Hu, H. Chen, F. Pan, *Adv. Mater.* **2018**, *30*, 1704436.
[231] P. Knauth, *Solid State Ion.* **2009**, *180*, 911.
[232] H. Adenusi, G. A. Chass, S. Passerini, K. V. Tian, G. Chen, *Adv. Energy Mater.* **2023**, *13*, 2203307.
[233] H. Wu, H. Jia, C. Wang, J.-G. Zhang, W. Xu, *Adv. Energy Mater.* **2021**, *11*, 2003092.
[234] K. Jeong, S. Park, G. Y. Jung, S. H. Kim, Y.-H. Lee, S. K. Kwak, S.-Y. Lee, *J. Am. Chem. Soc.* **2019**, *141*, 5880.
[235] Y. Zheng, S. Xia, F. Dong, H. Sun, Y. Pang, J. Yang, Y. Huang, S. Zheng, *Adv. Funct. Mater.* **2021**, *31*, 2006159.
[236] X. Li, K. P. Loh, *ACS Mater. Lett.* **2019**, *1*, 327.
[237] X. Liang, Y. Tian, Y. Yuan, Y. Kim, *Adv. Mater.* **2021**, *33*, 2105647.
[238] Z. Gadjourova, Y. G. Andreev, D. P. Tunstall, P. G. Bruce, *Nature* **2001**, *412*, 520.
[239] X. Li, Q. Hou, W. Huang, H.-S. Xu, X. Wang, W. Yu, R. Li, K. Zhang, L. Wang, Z. Chen, K. Xie, K. P. Loh, *ACS Energy Lett.* **2020**, *5*, 3498.
[240] M. D. Tikekar, S. Choudhury, Z. Tu, L. A. Archer, *Nat. Energy* **2016**, *1*, 16114.
[241] X. Yang, Y. Hu, N. Dunlap, X. Wang, S. Huang, Z. Su, S. Sharma, Y. Jin, F. Huang, X. Wang, S. Lee, W. Zhang, *Angew. Chem., Int. Ed.* **2020**, *59*, 20385.
[242] L. Bai, Q. Gao, Y. Zhao, *J. Mater. Chem. A* **2016**, *4*, 14106.
[243] S. Feng, H. Xu, C. Zhang, Y. Chen, J. Zeng, D. Jiang, J.-X. Jiang, *Chem. Commun.* **2017**, *53*, 11334.
[244] G. Zhao, Y. Zhang, Z. Gao, H. Li, S. Liu, S. Cai, X. Yang, H. Guo, X. Sun, *ACS Energy Lett.* **2020**, *5*, 1022.
[245] X. Yu, C. Li, Y. Ma, D. Li, H. Li, X. Guan, Y. Yan, V. Valtchev, S. Qiu, Q. Fang, *Microporous Mesoporous Mater.* **2020**, *299*, 110105.
[246] E. R. Wolfson, N. Xiao, L. Schkeryantz, W. Karl Haug, Y. Wu, P. L. McGrier, *Mol Syst Des Eng* **2020**, *5*, 97.
[247] S. Haldar, K. Roy, S. Nandi, D. Chakraborty, D. Puthusseri, Y. Gawli, S. Ogale, R. Vaidhyanathan, *Adv. Energy Mater.* **2018**, *8*, 1702170.
[248] O. Buyukcakir, J. Ryu, S. H. Joo, J. Kang, R. Yuksel, J. Lee, Y. Jiang, S. Choi, S. H. Lee, S. K. Kwak, S. Park, R. S. Ruoff, *Adv. Funct. Mater.* **2020**, *30*, 2003761.
[249] T. Zhou, Y. Zhao, J. W. Choi, A. Coskun, *Angew. Chem.* **2019**, *131*, 16951.
[250] S. Haldar, K. Roy, R. Kushwaha, S. Ogale, R. Vaidhyanathan, *Adv. Energy Mater.* **2019**, *9*, 1902428.
[251] G. Zhuang, Y. Gao, X. Zhou, X. Tao, J. Luo, Y. Gao, Y. Yan, P. Gao, X. Zhong, J. Wang, *Chem. Eng. J.* **2017**, *330*, 1255.
[252] Y.-J. Lei, H.-W. Liu, Z. Yang, L.-F. Zhao, W.-H. Lai, M. Chen, H. Liu, S. Dou, Y.-X. Wang, *Adv. Funct. Mater.* **2023**, *33*, 2212600.
[253] E. Goikolea, V. Palomares, S. Wang, I. R. de Larramendi, X. Guo, G. Wang, T. Rojo, *Adv. Energy Mater.* **2020**, *10*, 2002055.
[254] R. Rajagopalan, Y. Tang, X. Ji, C. Jia, H. Wang, *Adv. Funct. Mater.* **2020**, *30*, 1909486.
[255] J. Hu, Y. Hong, M. Guo, Y. Hu, W. Tang, S. Xu, S. Jia, B. Wei, S. Liu, C. Fan, Q. Zhang, *Energy Storage Mater.* **2023**, *56*, 267.
[256] M.-S. Kim, W.-J. Lee, S.-M. Paek, J. K. Park, *ACS Appl. Mater. Interfaces* **2018**, *10*, 32102.
[257] J. Liu, P. Lyu, Y. Zhang, P. Nachtigall, Y. Xu, *Adv. Mater.* **2018**, *30*, 1705401.
[258] B. Chandra Patra, S. Kanti Das, A. Ghosh, A. Raj K, P. Moitra, M. Addicoat, S. Mitra, A. Bhaumik, S. Bhattacharya, A. Pradhan, *J. Mater. Chem. A* **2018**, *6*, 16655.
[259] R. van der Jagt, A. Vasileiadis, H. Veldhuizen, P. Shao, X. Feng, S. Ganapathy, N. C. Habisreutinger, M. A. van der Veen, C. Wang, M. Wagemaker, S. van der Zwaag, A. Nagai, *Chem. Mater.* **2021**, *33*, 818.
[260] M.-M. Hu, H. Huang, Q. Gao, Y. Tang, Y. Luo, Y. Deng, L. Zhang, *Energy Fuels* **2021**, *35*, 1851.
[261] H. Ha, S. Nam, S.-H. Jeong, S. Hyun, *J. Mech. Sci. Technol.* **2019**, *33*, 3865.
[262] R. Shi, L. Liu, Y. Lu, C. Wang, Y. Li, L. Li, Z. Yan, J. Chen, *Nat. Commun.* **2020**, *11*, 178.
[263] L. Zhang, R. Wang, Z. Liu, J. Wan, S. Zhang, S. Wang, K. Hua, X. Liu, X. Zhou, X. Luo, X. Zhang, M. Cao, H. Kang, C. Zhang, Z. Guo, *Adv. Mater.* **2023**, *35*, 2210082.
[264] S. Gu, S. Wu, L. Cao, M. Li, N. Qin, J. Zhu, Z. Wang, Y. Li, Z. Li, J. Chen, Z. Lu, *J. Am. Chem. Soc.* **2019**, *141*, 9623.
[265] Y. Zhang, Z. Gao, *Electrochim. Acta* **2019**, *301*, 23.
[266] J. Lee, H. Lim, J. Park, M.-S. Kim, J.-W. Jung, J. Kim, I.-D. Kim, *Adv. Energy Mater.* **2023**, *13*, 2300442.
[267] Q. Xu, Q. Li, Y. Guo, D. Luo, J. Qian, X. Li, Y. Wang, *Small Methods* **2020**, *4*, 2000159.
[268] X. Chen, H. Zhang, C. Ci, W. Sun, Y. Wang, *ACS Nano* **2019**, *13*, 3600.
[269] Y. Qiu, W. Li, W. Zhao, G. Li, Y. Hou, M. Liu, L. Zhou, F. Ye, H. Li, Z. Wei, S. Yang, W. Duan, Y. Ye, J. Guo, Y. Zhang, *Nano Lett.* **2014**, *14*, 4821.
[270] S. Feng, Z.-H. Fu, X. Chen, Q. Zhang, *InfoMat* **2022**, *4*, 12304.
[271] L. Yang, W. Wei, Y. Ma, Y. Xu, G. Chang, *J. Power Sources* **2020**, *449*, 227551.
[272] Y. Zu, Y. Xu, L. Ma, Q. Kang, H. Yao, J. Hou, *ACS Appl. Mater. Interfaces* **2020**, *12*, 18457.
[273] P. Jia, T. Hu, Q. He, X. Cao, J. Ma, J. Fan, Q. Chen, Y. Ding, J. Pyun, J. Geng, *ACS Appl. Mater. Interfaces* **2019**, *11*, 3087.
[274] B.-Y. Lu, Z.-Q. Wang, F.-Z. Cui, J.-Y. Li, X.-H. Han, Q.-Y. Qi, D.-L. Ma, G.-F. Jiang, X.-X. Zeng, X. Zhao, *ACS Appl. Mater. Interfaces* **2020**, *12*, 34990.
[275] R. Guan, L. Zhong, S. Wang, D. Han, M. Xiao, L. Sun, Y. Meng, *ACS Appl. Mater. Interfaces* **2020**, *12*, 8296.
[276] N. Deng, Y. Liu, W. Yu, J. Kang, Q. Li, H. Gao, L. Zhang, W. Kang, Y. Liu, B. Cheng, *Energy Storage Mater.* **2022**, *46*, 29.
[277] X. Song, F. Zhou, M. Yao, C. Hao, J. Qiu, *ACS Sustainable Chem. Eng.* **2020**, *8*, 10185.
[278] H. Shin, D. Kim, H. J. Kim, J. Kim, K. Char, C. T. Yavuz, J. W. Choi, *Chem. Mater.* **2019**, *31*, 7910.
[279] T. Zhang, F. Hu, C. Song, S. Li, W. Shao, S. Liu, H. Peng, S. Hu, X. Jian, *Chem. Eng. J.* **2021**, *407*, 127141.
[280] S. Royuela, J. Almarza, M. J. Mancheño, J. C. Pérez-Flores, E. G. Michel, M. M. Ramos, F. Zamora, P. Ocón, J. L. Segura, *Chemistry* **2019**, *25*, 12394.
[281] Z. Li, H.-Y. Zhou, F.-L. Zhao, T.-X. Wang, X. Ding, B.-H. Han, W. Feng, *Chin. J. Polym. Sci.* **2020**, *38*, 550.
[282] X.-F. Liu, H. Chen, R. Wang, S.-Q. Zang, T. C. W. Mak, *Small* **2020**, *16*, 2002932.
[283] Y. Ge, J. Li, Y. Meng, D. Xiao, *Nano Energy* **2023**, 108297.
[284] H. Liao, H. Ding, B. Li, X. Ai, C. Wang, *J. Mater. Chem. A* **2014**, *2*, 8854.
[285] H. Liao, H. Wang, H. Ding, X. Meng, H. Xu, B. Wang, X. Ai, C. Wang, *J. Mater. Chem. A* **2016**, *4*, 7416.
[286] Y. Meng, G. Lin, H. Ding, H. Liao, C. Wang, *J. Mater. Chem. A* **2018**, *6*, 17186.

[287] D.-G. Wang, N. Li, Y. Hu, S. Wan, M. Song, G. Yu, Y. Jin, W. Wei, K. Han, G.-C. Kuang, W. Zhang, *ACS Appl. Mater. Interfaces* **2018**, *10*, 42233.
[288] J. Kim, A. Elabd, S.-Y. Chung, A. Coskun, J. W. Choi, *Chem. Mater.* **2020**, *32*, 4185.
[289] X. Chen, Y. Xu, F.-H. Du, Y. Wang, *Small Methods* **2019**, *3*, 1900338.
[290] J. Wang, L. Si, Q. Wei, X. Hong, L. Lin, X. Li, J. Chen, P. Wen, Y. Cai, *J Energy Chem* **2019**, *28*, 54.
[291] R. Meng, Q. Deng, C. Peng, B. Chen, K. Liao, L. Li, Z. Yang, D. Yang, L. Zheng, C. Zhang, J. Yang, *Nano Today* **2020**, *35*, 100991.
[292] A. Khayum M, M. Ghosh, V. Vijayakumar, A. Halder, M. Nurhuda, S. Kumar, M. Addicoat, S. Kurungot, R. Banerjee, *Chem. Sci.* **2019**, *10*, 8889.
[293] D. Ma, H. Zhao, F. Cao, H. Zhao, J. Li, L. Wang, K. Liu, *Chem. Sci.* **2022**, *13*, 2385.
[294] H. Li, M. Cao, Z. Fu, Q. Ma, L. Zhang, R. Wang, F. Liang, T. Zhou, C. Zhang, *Chem. Sci.* **2024**.
[295] M. Yu, N. Chandrasekhar, R. K. M. Raghupathy, K. H. Ly, H. Zhang, E. Dmitrieva, C. Liang, X. Lu, T. D. Kühne, H. Mirhosseini, I. M. Weidinger, X. Feng, *J. Am. Chem. Soc.* **2020**, *142*, 19570.
[296] Y. Du, X. Gao, S. Li, L. Wang, B. Wang, *Chin. Chem. Lett.* **2020**, *31*, 609.
[297] B. Lu, W. Li, D. Cheng, B. Bhamwala, M. Ceja, W. Bao, C. Fang, Y. S. Meng, *Adv. Energy Mater.* **2022**, *12*, 2202012.
[298] Y. Zhao, K. Feng, Y. Yu, *Adv. Sci.* **2024**, *11*.
[299] G. Li, Z. Zhao, S. Zhang, L. Sun, M. Li, J. A. Yuwono, J. Mao, J. Hao, J. (Pimm) Vongsvivut, L. Xing, C.-X. Zhao, Z. Guo, *Nat. Commun.* **2023**, *14*, 6526.
[300] Z. Liu, G. Li, M. Xi, Y. Huang, H. Li, H. Jin, J. Ding, S. Zhang, C. Zhang, Z. Guo, *Angew. Chem. n/a*, 202319091.
[301] C. Li, R. Kingsbury, L. Zhou, A. Shyamsunder, K. A. Persson, L. F. Nazar, *ACS Energy Lett.* **2022**, *7*, 533.
[302] Y. Zhang, M. Zhu, G. Wang, F.-H. Du, F. Yu, K. Wu, M. Wu, S.-X. Dou, H.-K. Liu, C. Wu, *Small Methods* **2021**, *5*, 2100650.
[303] J. Wang, Y. Yang, Y. Zhang, Y. Li, R. Sun, Z. Wang, H. Wang, *Energy Storage Mater.* **2021**, *35*, 19.
[304] J. H. Park, M.-J. Kwak, C. Hwang, K.-N. Kang, N. Liu, J.-H. Jang, B. A. Grzybowski, *Adv. Mater.* **2021**, *33*, 2101726.
[305] G. Li, X. Wang, S. Lv, J. Wang, X. Dong, D. Liu, *Chem. Eng. J.* **2022**, *450*, 138116.
[306] C. Guo, J. Zhou, Y. Chen, H. Zhuang, Q. Li, J. Li, X. Tian, Y. Zhang, X. Yao, Y. Chen, S.-L. Li, Y.-Q. Lan, *Angew. Chem.* **2022**, *134*, 202210871.
[307] Q. Cao, L. Wan, Z. Xu, W. Kuang, H. Liu, X. Zhang, W. Zhang, Y. Lu, Y. Yao, B. Wang, K. Liu, *Adv. Mater. n/a*, 2210550.
[308] B.-Q. Li, S.-Y. Zhang, B. Wang, Z.-J. Xia, C. Tang, Q. Zhang, *Energy Environ. Sci.* **2018**, *11*, 1723.
[309] Y. Zhang, C. Wei, M.-X. Wu, Y. Wang, H. Jiang, G. Zhou, X. Tang, X. Liu, *Chem. Eng. J.* **2023**, *451*, 138915.
[310] R. Sun, S. Hou, C. Luo, X. Ji, L. Wang, L. Mai, C. Wang, *Nano Lett.* **2020**, *20*, 3880.
[311] S. Zhang, Y.-L. Zhu, S. Ren, C. Li, X.-B. Chen, Z. Li, Y. Han, Z. Shi, S. Feng, *J. Am. Chem. Soc.* **2023**, *145*, 17309.
[312] H. Lu, F. Ning, R. Jin, C. Teng, Y. Wang, K. Xi, D. Zhou, G. Xue, *ChemSusChem* **2020**, *13*, 3447.
[313] Y. Liu, Y. Lu, A. Hossain Khan, G. Wang, Y. Wang, A. Morag, Z. Wang, G. Chen, S. Huang, N. Chandrasekhar, D. Sabaghi, D. Li, P. Zhang, D. Ma, E. Brunner, M. Yu, X. Feng, *Angew. Chem., Int. Ed.* **2023**, *62*, 202306091.
[314] Q. Xu, K. Zhang, J. Qian, Y. Guo, X. Song, H. Pan, D. Wang, X. Li, *ACS Appl. Energy Mater.* **2019**, *2*, 5793.
[315] J. Wang, W. Qin, X. Zhu, Y. Teng, *Energy* **2020**, *199*, 117372.
[316] P. Li, H. Lv, Z. Li, X. Meng, Z. Lin, R. Wang, X. Li, *Adv. Mater.* **2021**, *33*, 2007803.
[317] Y. Wen, X. Wang, Y. Yang, M. Liu, W. Tu, M. Xu, G. Sun, S. Kawaguchi, G. Cao, W. Li, *J. Mater. Chem. A* **2019**, *7*, 26540.
[318] W. Sun, J. Zhang, M. Xie, D. Lu, Z. Zhao, Y. Li, Z. Cheng, S. Zhang, H. Chen, *Nano Lett.* **2020**, *20*, 8120.
[319] K. Zhang, X. Li, L. Ma, F. Chen, Z. Chen, Y. Yuan, Y. Zhao, J. Yang, J. Liu, K. Xie, K. P. Loh, *ACS Nano* **2023**, *17*, 2901.
[320] H. Wang, J. Jiang, T. Wan, Y. Luo, G. Liu, J. Li, *J. Colloid Interface Sci.* **2023**, *638*, 542.
[321] C. Zhan, T. Wu, J. Lu, K. Amine, *Energy Environ. Sci.* **2018**, *11*, 243.
[322] Y. Xu, Y. Zhou, T. Li, S. Jiang, X. Qian, Q. Yue, Y. Kang, *Energy Storage Mater.* **2020**, *25*, 334.
[323] S. Bian, G. Huang, Y. Xuan, B. He, J. Liu, B. Xu, G. Zhang, *J. Membr. Sci.* **2023**, *669*, 121268.
[324] V. Shrivastav, S. Sundriyal, A. Kaur, U. K. Tiwari, S. Mishra, A. Deep, *J. Alloys Compd.* **2020**, *843*, 155992.
[325] V. Shrivastav, S. Sundriyal, P. Goel, V. Shrivastav, U. K. Tiwari, A. Deep, *Electrochim. Acta* **2020**, *345*, 136194.
[326] S. Sundriyal, V. Shrivastav, A. Kaur, P. Dubey, S. Mishra, A. Deep, S. R. Dhakate, *IEEE Trans. Nanotechnol.* **2021**, *20*, 481.
[327] S. Sundriyal, V. Shrivastav, S. Mishra, A. Deep, *Int. J. Hydrog. Energy* **2020**, *45*, 30859.
[328] S.-Y. Lu, M. Jin, Y. Zhang, Y.-B. Niu, J.-C. Gao, C. M. Li, *Adv. Energy Mater.* **2018**, *8*, 1702545.
[329] S. Sundriyal, V. Shrivastav, A. Gupta, V. Shrivastav, A. Deep, S. R. Dhakate, *Mater. Res. Bull.* **2021**, *142*, 111396.
[330] S. Sundriyal, V. Shrivastav, S. K. Bhardwaj, S. Mishra, A. Deep, *Electrochim. Acta* **2021**, *380*, 138229.
[331] T. Li, X. Yan, Y. Liu, W.-D. Zhang, Q.-T. Fu, H. Zhu, Z. Li, Z.-G. Gu, *Polym. Chem.* **2020**, *11*, 47.
[332] N. An, Z. Guo, J. Xin, Y. He, K. Xie, D. Sun, X. Dong, Z. Hu, *J. Mater. Chem. A* **2021**, *9*, 16824.
[333] T. Li, W.-D. Zhang, Y. Liu, Y. Li, C. Cheng, H. Zhu, X. Yan, Z. Li, Z.-G. Gu, *J. Mater. Chem. A* **2019**, *7*, 19676.
[334] Y. Dong, X. Zhang, Y. Wang, L. Tang, Y. Yang, *J. Power Sources* **2023**, *564*, 232873.
[335] J. Zhang, Z. Zhang, X. Xing, X. Xu, X. Zhang, H. Liu, P. He, P. Ren, B. Zhang, *Dalton Trans.* **2023**, *53*, 223.
[336] B. C. Patra, S. Khilari, L. Satyanarayana, D. Pradhan, A. Bhaumik, *Chem. Commun.* **2016**, *52*, 7592.
[337] J. Xu, Y. He, S. Bi, M. Wang, P. Yang, D. Wu, J. Wang, F. Zhang, *Angew. Chem.* **2019**, *131*, 12193.
[338] X. Zhuang, W. Zhao, F. Zhang, Y. Cao, F. Liu, S. Bi, X. Feng, *Polym. Chem.* **2016**, *7*, 4176.
[339] L. Li, F. Lu, R. Xue, B. Ma, Q. Li, N. Wu, H. Liu, W. Yao, H. Guo, W. Yang, *ACS Appl. Mater. Interfaces* **2019**, *11*, 26355.
[340] L. Li, F. Lu, H. Guo, W. Yang, *Microporous Mesoporous Mater.* **2021**, *312*, 110766.
[341] P. Bhanja, S. K. Das, K. Bhunia, D. Pradhan, T. Hayashi, Y. Hijikata, S. Irle, A. Bhaumik, *ACS Sustainable Chem. Eng.* **2018**, *6*, 202.
[342] S. K. Das, K. Bhunia, A. Mallick, A. Pradhan, D. Pradhan, A. Bhaumik, *Microporous Mesoporous Mater.* **2018**, *266*, 109.
[343] S. Santi, S. Rossi, *Tetrahedron Lett.* **2019**, *60*, 151021.
[344] Y. Han, N. Hu, S. Liu, Z. Hou, J. Liu, X. Hua, Z. Yang, L. Wei, L. Wang, H. Wei, *Nanotechnology* **2017**, *28*, 33LT01.
[345] H. Shanavaz, B. P. Prasanna, S. Archana, M. K. Prashanth, F. A. Alharthi, R. Zhou, M. S. Raghu, B.-H. Jeon, K. Y. Kumar, *J. Energy Storage* **2023**, *67*, 107561.
[346] A. Roy, S. Mondal, A. Halder, A. Banerjee, D. Ghoshal, A. Paul, S. Malik, *Eur. Polym. J.* **2017**, *93*, 448.
[347] Y. Han, Q. Zhang, N. Hu, X. Zhang, Y. Mai, J. Liu, X. Hua, H. Wei, *Chin. Chem. Lett.* **2017**, *28*, 2269.
[348] T. K. Dutta, A. Patra, *Chem Asian J* **2021**, *16*, 158.
[349] R. Li, L. Xing, A. Chen, X. Zhang, A. Kong, Y. Shan, *Ionics* **2020**, *26*, 927.

[350] A. K. Mohammed, V. Vijayakumar, A. Halder, M. Ghosh, M. Addicoat, U. Bansode, S. Kurungot, R. Banerjee, *ACS Appl. Mater. Interfaces* **2019**, *11*, 30828.
[351] Y. Dong, Y. Wang, X. Zhang, Q. Lai, Y. Yang, *Chem. Eng. J.* **2022**, *449*, 137858.
[352] N. An, Z. Guo, C. Guo, M. Wei, D. Sun, Y. He, W. Li, L. Zhou, Z. Hu, X. Dong, *Chem. Eng. J.* **2023**, *458*, 141434.
[353] M. Yang, Z. Zhou, *Adv. Sci.* **2017**, *4*, 1600408.
[354] Y. Zhao, N. Bu, H. Shao, Q. Zhang, B. Feng, Y. Xu, G. Zheng, Y. Yuan, Z. Yan, L. Xia, *New J. Chem.* **2019**, *43*, 18158.
[355] G. Kim, J. Yang, N. Nakashima, T. Shiraki, *Chemistry* **2017**, *23*, 17504.
[356] Y. Li, S. Zheng, X. Liu, P. Li, L. Sun, R. Yang, S. Wang, Z.-S. Wu, X. Bao, W.-Q. Deng, *Angew. Chem.* **2018**, *130*, 8124.
[357] M. Chaudhary, A. K. Nayak, R. Muhammad, D. Pradhan, P. Mohanty, *ACS Sustainable Chem. Eng.* **2018**, *6*, 5895.
[358] H. Lavillunière, T.-N. Pham-Truong, T.-K.-L. Nguyen, C. Vancaeyzeele, P.-H. Aubert, *ACS Appl. Energy Mater.* **2024**.
[359] N. Deka, R. Patidar, S. Kasthuri, N. Venkatramaiah, G. K. Dutta, *Mater. Chem. Front.* **2019**, *3*, 680.
[360] D. Yan, Y. Wu, R. Kitaura, K. Awaga, *J. Mater. Chem. A* **2019**, *7*, 26829.
[361] Z. Zhou, X. Zhang, L. Xing, J. Liu, A. Kong, Y. Shan, *Electrochim. Acta* **2019**, *298*, 210.
[362] B. Tang, L. Zheng, X. Dai, H. Chen, *J. Energy Storage* **2019**, *26*, 100961.
[363] W. Ye, H. Wang, J. Shen, S. Khan, Y. Zhong, J. Ning, Y. Hu, *Chin. Chem. Lett.* **2023**, *34*, 107198.
[364] S. Gu, J. Chen, R. Hao, X. Chen, Z. Wang, I. Hussain, G. Liu, K. Liu, Q. Gan, Z. Li, H. Guo, Y. Li, H. Huang, K. Liao, K. Zhang, Z. Lu, *Chem. Eng. J.* **2023**, *454*, 139877.
[365] A. Chatterjee, J. Sun, K. S. Rawat, V. Van Speybroeck, P. Van Der Voort, *Small n/a*, 2303189.
[366] L. Liu, D. Cui, S. Zhang, W. Xie, C. Yao, N. Xu, Y. Xu, *Dalton Trans.* **2023**, *52*, 6138.
[367] B. Hu, J. Xu, Z. Fan, C. Xu, S. Han, J. Zhang, L. Ma, B. Ding, Z. Zhuang, Q. Kang, X. Zhang, *Adv. Energy Mater.* **2023**, *13*, 2203540.
[368] Y. Wang, M. Li, T. Wen, G. Gu, *Nanotechnology* **2023**, *34*, 375402.
[369] Y. Lin, H. Cui, C. Liu, R. Li, S. Wang, G. Qu, Z. Wei, Y. Yang, Y. Wang, Z. Tang, H. Li, H. Zhang, C. Zhi, H. Lv, *Angew. Chem.* **2023**, *135*, 202218745.
[370] S. K. Pati, D. Patra, S. Muduli, S. Mishra, S. Park, *Small* **2023**, *19*, 2300689.
[371] N. Sahiner, S. Demirci, *J. Porous Mater.* **2019**, *26*, 481.
[372] S. Haldar, D. Rase, P. Shekhar, C. Jain, C. P. Vinod, E. Zhang, L. Shupletsov, S. Kaskel, R. Vaidhyanathan, *Adv. Energy Mater.* **2022**, *12*, 2200754.
[373] N. M. Yousif, O. M. Gomaa, *Environ. Technol.* **2023**, *0*, 1.
[374] I. Hussain, M. Z. Ansari, C. Lamiel, T. Hussain, M. S. Javed, T. Kaewmaraya, M. Ahmad, N. Qin, K. Zhang, *ACS Energy Lett.* **2023**, *8*, 1887.
[375] E. Tylianakis, E. Klontzas, G. E. Froudakis, *Nanoscale* **2011**, *3*, 856.
[376] N. Yang, S. Yu, W. Zhang, H.-M. Cheng, P. Simon, X. Jiang, *Adv. Mater.* **2022**, *34*, 2202380.
[377] X. Song, X. Xu, J. Liu, *ChemNanoMat* **2023**, *9*, 202300246.

**Prashant Dubey** recently completed his Ph.D. in chemical sciences from the Academy of Scientific and Innovative Research (AcSIR-NPL), New Delhi, India in March 2024. His research interests include the synthesis of different bio-waste-derived activated carbon, conducting polymers, metal–organic frameworks, and their composites for supercapacitors. Also, he has a good hand in the preparation of free-standing carbon-based electrodes for supercapacitor applications. He has published more than 20 articles in reputed international journals. He is the winner of the prestigious Raman-Charpak visiting fellowship of France, and recently received an Early Career Postdoctoral Fellowship from the Indian Institute of Technology Gandhinagar, India.

**Vishal Shrivastav** is presently working as an assistant professor at the Institute of Physical Chemistry, Poland. He has completed his Ph.D. (physical sciences) in the area of hybrid electrochemical capacitors from the Academy of Scientific and Innovative Research (AcSIR-CSIO), Chandigarh, India. His research interests are the synthesis and characterization of Metal Organic Frameworks derived from nanoporous carbon and metal oxides and further their composites with transition metal dichalcogenides for hybrid electrochemical capacitor applications. He has published 24 articles in reputed international journals. He is the winner of the Marie-Curie cofounded PASIFIC fellowship of Poland and TÜBİTAK fellowship of Turkey.

**Tribani Boruah** is currently a Ph.D. candidate (School of Chemistry, Cardiff University, United Kingdom). After obtaining her master's (Delhi University), she joined the National Physical Laboratory, India, where she worked on the synthesis of nano-fibers through electrospinning. Then she worked at the Institute of Nano-Science and Technology, India, where she focused on single-atom catalysts for energy conversion. In 2023, she joined an industrial PhD program (Cardiff University) funded by TOK Japan Company, focusing on the synthesis of transition metal complexes for semiconductor applications and density functional theory. Additionally, she is working on the flow electrochemical organic transformation using microfluidics.

**Giorgio Zoppellaro** holds positions of senior researcher at RCPTM of the Czech Advanced Technology and Research Institute (CATRIN, Palacky University Olomouc, Czech Republic) and at VSB-Technical University of Ostrava. He obtained his Ph.D. degree in chemistry at The Johannes Gutenberg Universität in Mainz (Germany; 2004) and habilitation to associate professor of Chemistry in Italy (2017). His research focuses on the application of the electron paramagnetic resonance technique at the interface of material science/photo physics/biomedicine.

**Radek Zbořil** acts as the Scientific Director of the RCPTM division of the Czech Advanced Technology and Research Institute (CATRIN) at Palacky University in Olomouc and a head of the Materials-Envi Lab at VSB-Technical University Ostrava in the Czech Republic. He is an expert in nanotechnologies and the author of over 650 papers in prestigious journals including Nature Nanotechnology (4x) or Nature Catalysis. His publications have received over 68 000 citations and his H-index is 117 (Google Scholar, April 2024). Professor Zbořil has appeared several times on the list of Highly Cited Researchers announced by Clarivate Analytics.

**Aristides Bakandritsos** is the head of a research division in RCPTM of the Czech Advanced Technology and Research Institute (CATRIN, Palacky University Olomouc, Czech Republic) and senior researcher at VSB-Technical University of Ostrava. He received his PhD in Greece and he was a faculty member at the Department of Materials Science, University of Patras, before joining CATRIN-RCPTM. Research interests include the functionalization of nanomaterials and their application in energy storage, catalysis, and biomedicine. Results have been published in more than 120 articles (h-index 38, Scopus), and is the principal investigator in several European projects.

**Shashank Sundriyal** is a Marie Skłodowska-Curie Individual Postdoctoral Fellow in the Czech Advanced Technology and Research Institute (CATRIN, Palacky University Olomouc). He received his Ph.D. from the Academy of Scientific and Innovative Research (AcSIR-CSIO), Chandigarh in 2019. His research interests embrace the synthesis of metal–organic frameworks, graphene, biomass-derived carbons, and composites for energy storage applications. He has published more than 48 articles (2078 citations, h-index 22) in reputed international journals. He is the winner of several prestigious international fellowships and awards including Green Talents 2021 Germany, MSCA co-funded PASIFIC 2021 Poland, MSCAA-PF 2021, and Fulbright Nehru 2022 United States.